REPORT DOCUMENTATION PAGE

AFRL-SR-AR-TR-03-

0209

PLEASE DO NOT RETURN YOUR FORM TO THE ABOVE ADDRESS.

1. REPORT DATE (DD-MM-YYYY)	2. REPORT DATE	3. DATES COVERED (From - To)
28/04/2003	FINAL	Jan., 2000 – April, 2003

4. TITLE AND SUBTITLE
Active Control of Supersonic Impinging Jets Using Supersonic Microjets

5a. CONTRACT NUMBER

5b. GRANT NUMBER
F49620-00-1-0141

5c. PROGRAM ELEMENT NUMBER

6. AUTHOR(S)
Krothapalli, Anjaneyulu,
Alvi, Farrukh S.
Shih, Chiang
Annaswamy, Anu

5d. PROJECT NUMBER

5e. TASK NUMBER

5f. WORK UNIT NUMBER

7. PERFORMING ORGANIZATION NAME(S) AND ADDRESS(ES)
Florida Agricultural and Mechanical University
Division of Sponsored Research
400 Foote Hilyer Administration Center
Tallahassee, FL 32307

8. PERFORMING ORGANIZATION REPORT NUMBER
FMRL 03-03

9. SPONSORING/MONITORING AGENCY NAME(S) AND ADDRESS(ES)
Air Force Office of Scientific Research
801 N. Randolph St., Room 732
Arlington, VA 22203

10. SPONSOR/MONITOR'S ACRONYM(S)
AFOSR/NA

11. SPONSORING/MONITORING AGENCY REPORT NUMBER

12. DISTRIBUTION AVAILABILITY STATEMENT
Approved for Public Release; Distribution is unlimited

13. SUPPLEMENTARY NOTES

14. ABSTRACT

Supersonic impinging jet flows, such as those that occur in the next generation of STOVL aircraft, are highly unsteady due to the presence a feedback loop. This results in large dynamic loads on the nearby aircraft structures and surfaces and diminishes aircraft performance. In this study, a unique active control technique that utilizes arrays of supersonic microjets (≤ 400 μm) around the periphery of the main jet was examined. The efficacy of microjet control was explored over a large parametric range. This control approach was very successful and the activation of the microjets led to dramatic reductions in ground effect. The lift loss was reduced by up to 40%, while the unsteady loads were reduced by as much as 12 dB. These dramatic gains in performance were achieved with negligible microjet mass flux (less than 0.5%). A detailed study of this flow was conducted to better understand the governing flow physics. The velocity field data clearly indicates that the activation of microjets generates significant streamwise vorticity while reducing the azimuthal vorticity of the primary jet. It is proposed that the streamwise vorticity is mainly a result of the redirection of the azimuthal vorticity, which weakens the large-scale structures in the primary jet. This is considered to be a primary factor in the efficient disruption of the feedback loop. A new, POD-based, closed-loop control strategy, is also explored in order to achieve optimal and uniform control. The closed-loop control results led to an improvement in the control efficiency compared to the open-loop strategy in a number of cases.

15. SUBJECT TERMS
Supersonic Impinging Jets, Supersonic Microjets, Feedback, Active Control

16. SECURITY CLASSIFICATION OF:			17. LIMITATION OF ABSTRACT	18. NUMBER OF PAGES	19a. NAME OF RESPONSIBLE PERSON
a. REPORT	b. ABSTRACT	c. THIS PAGE			Dr. Farrukh Alvi
UU	UU	UU	SAR		19b. TELEPONE NUMBER (Include area code) (850)410-6336

Executive Summary

Supersonic impinging jets, such as those, which occur in the next generation of STOVL aircraft, generate a highly oscillatory flow with very high unsteady loads on the nearby aircraft structures and the landing surfaces. These high pressure and acoustic loads are also accompanied by a dramatic loss in lift while the aircraft is in hover. Studies of supersonic impinging jets have suggested that the highly oscillatory nature of the impinging jets is due to a feedback loop between the fluid and acoustic fields, which leads to these adverse effects – collectively referred to as ground effect. In this study, a unique active control technique was attempted with the aim of disrupting the feedback loop in order to diminish the flow unsteadiness with the ultimate aim of reducing the adverse effects of this flow. Flow control was implemented by placing arrays of supersonic microjets around the periphery of the main impinging jet. Various parametric effects, such as the number of microjets, microjet orientation and their penetration depth into the main jet shear layer, were explored, in order to determine their influence of control efficiency. In addition, these tests were conducted over a large range of operating conditions of the primary jet. Overall, this control approach was very successful in disrupting the feedback loop in that the activation of the microjets led to dramatic reductions in the ground effect. The lift loss was reduced by up to 40%), the unsteady pressure loads were reduced by up to 12 dB and nearfield noise by as much as 8 dB. These dramatic gains in performance were achieved with negligible mass flux through the microjets – less than 0.5% (less for many cases) of the primary jet mass flow.

The fundamental flow physics behind this technique was examined by detailed flow visualizations, mean and unsteady pressure measurements and whole-field velocity measurements using Particle Image Velocimetry (PIV). The velocity measurements provide valuable insight into this flow and reveal that the activation of microjets produces substantial streamwise vorticity in the form of well organized, counter-rotating pairs of streamwise vortices. The production of significantly higher streamwise vorticity due to microjets comes at the expense of the azimuthal vorticity in the shear layer thus diminishing the strength of the large-scale axisymmetric structures in the jet shear layer. The appearance of strong streamwise vortices in the shear layer near the nozzle exit due to microjets also weakens the spatial

coherence of the coupling between the acoustic waves and shear layer instability, while thickening the jet shear layer. All these effects are thought to be collectively responsible for the efficient disruption of the feedback loop using microjets.

Although very effective overall, the efficacy of microjet control is found to be dependant upon the operating conditions, such as nozzle to ground distance and the operating pressure of the primary impinging jet. In order to achieve optimal and uniform control, a novel closed-loop control strategy, which uses on-line pressure measurements near the nozzle exit to achieve optimal flow control irrespective of flow conditions, is explored. The closed-loop control strategy consisted of determining the dominant POD mode using pressure measurements at the nozzle exit and using a 'mode matched strategy' to determine the microjet pressure distribution along the nozzle. The results demonstrated a significant reduction in the unsteady pressure loads along with a consistent improvement compared to an open-loop control strategy where the microjet pressures were kept constant.

In summary, this study has conclusively demonstrated that the microjet-based control scheme proposed and developed under this research effort is very effective in disrupting the feedback loop and reducing the associated adverse effects such as the high dynamic loads in the hydrodynamic near-field, high noise levels and lift loss. The gains are substantial and dramatic with minimal mass flux requirement. Through a detailed examination of this flow, a better understanding of the flow physics with and without control has been obtained. A novel, POD-based control approach has been proposed and has the potential of further enhancing and providing more uniform performance gains with microjet control. This relatively simple and highly effective microjet control technique makes it a suitable candidate for implementation in practical aircraft systems

Table of Contents

1. INTRODUCTION

Besides being an important problem from a fundamental, fluid dynamics/aeroacoustics perspective, an understanding of the impinging jet flow field is also critical for the optimal design of Short Take-Off and Vertical Landing (STOVL) aircraft as they utilize downward-pointing jets to generate the lift force during hover. It is well known that when a high speed jet stream impinges on the ground, several flow-induced effects may emerge which can substantially diminish the performance of the aircraft. These include, but are not limited to, very high ambient noise levels dominated by discrete frequency tones – referred to as ***impingement tones*** – which may match the resonant frequencies of the aircraft panels, thus further exacerbating the sonic fatigue problem. In addition to adversely affecting the integrity of structural elements near the nozzle exhaust, such high OverAll Sound Pressure Levels (OASPL) associated with high speed impinging jets can pose also an environment pollution problem. Furthermore, a significant ***lift loss*** can be induced due to the flow entrainment by the lifting jets from the ambient environment in the proximity of the airframe.

Other adverse phenomena include severe ***ground erosion*** on the landing surface and ***Hot Gas Ingestion (HGI)*** into the engine inlets (Margason et al., 1997). These problems become more pronounced for supersonic impinging jets, the operating regime of the STOVL version of the future Joint Strike Fighter (JSF). In addition, the presence of multiple impinging jets can potentially further aggravate these effects due to the strong coupling between the jets and the emergence of an upward-moving fountain flow flowing opposite to the lift jets (Elavarasan, et al., 2000). A schematic of a generic STOVL aircraft with multiple lift/impinging jets is shown in Fig. 1 where various regions where these problems might occur have been indicated.

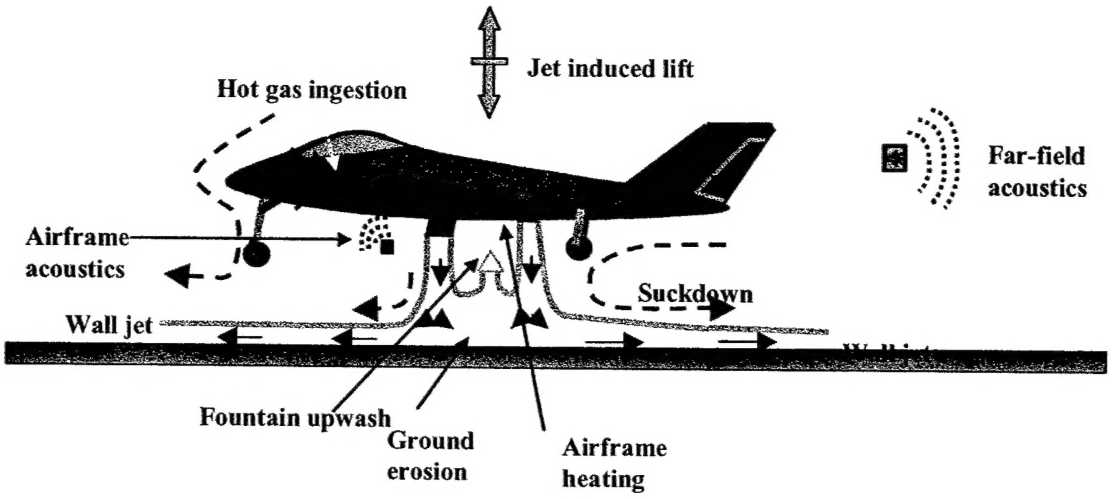

Fig. 1 - Flowfield created by the propulsion system around a STOVL aircraft.

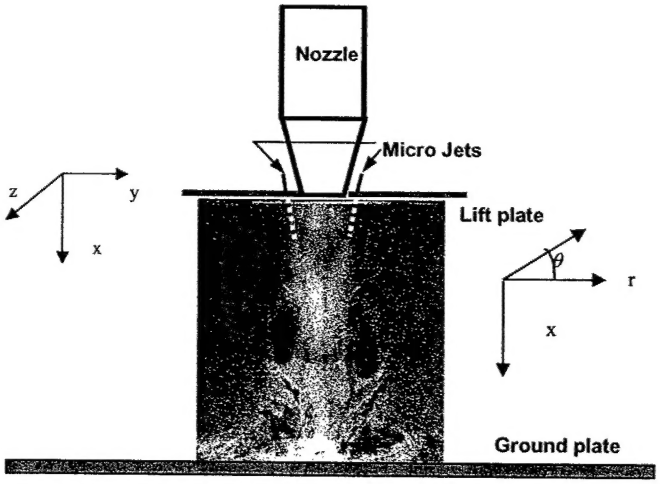

Fig. 2 - Schematic of the experimental arrangement for a single impinging jet.

A few years ago, an extensive study, in large part sponsored by the Air Force Office of Scientific research (AFOSR), was initiated at the Fluid Mechanics Research Laboratory (FMRL), in Tallahassee, Florida. Using relatively simple configurations, such as that shown in Fig. 2 – consisting of a single jet issuing through a planar, circular plate – the goal of this mainly experimental work is to provide a better fundamental understanding of the flow phenomena

involved. Based on a better understanding of the aeroacoustics governing this flow, we have implemented a unique flow control technique, which utilizes supersonic microjets and significantly alleviates the ground effect for single and dual impinging jets.

1.1 The Feedback Loop & Its Control

A host of studies on the aeroacoustics of impinging jets by Neuwarth (1974), Powell (1988), Tam and Ahuja (1990), and more recently Krothapalli *et al.* (1999) have clearly established that the self-sustained, highly unsteady behavior of the jet and the resulting impinging tones is governed by a feedback mechanism. This feedback occurs between the instability waves in the jet that originate at the nozzle and grow as they propagate downstream towards the impingement surface, and the acoustic waves that are produced upon impingement which then travel upstream and excite the nascent shear layer near the nozzle exit. The logical approach to controlling the adverse ground effect is to disrupt the feedback mechanism responsible for this behavior.

There are various potential approaches for disrupting the flow-acoustic coupling in the feedback loop. For example, one could: (1) Intercept the upstream propagating acoustic waves so that they can not complete the feedback loop, and/or (2) Manipulate the shear layer (for example, increase its thickness) near the nozzle lip hence reducing its receptivity to the acoustic disturbances and/or (3) Disrupt the coherent interaction between the flow instabilities and the acoustic field by 'tickling' the nozzle shear layer using a disturbance at or very near the nozzle exit. The source of these disturbances could in principal be passive, such as those generated by 'tabs' at the nozzle exit or, they could be active in nature, such as the use of high energy acoustic and/or fluidic sources near the nozzle exit. A brief summary of some the past attempts can be is presented next.

1.2 Previous Attempts of Feedback Loop Control

A number of attempts have been made in the past to suppress the feedback mechanism. For instance, Karamcheti et al (1969) successfully suppressed edge tones in low speed flows, which are governed by a similar feedback mechanism, by placing two plates normal to the centerline of the jet. Motivated by their work, Elavarasan et al (2001) employed a similar technique to attenuate the feedback loop in an impinging jet flow by introducing a control plate near the

nozzle exit. Using this approach, they were able to intercept the upstream propagating acoustic waves thus disrupting the feedback loop. As anticipated, attenuation of the loop led to a measurable weakening of the large-scale structures in the jet flow. For selected cases, this passive control approach resulted in a maximum recovery of about 16% of the lift loss relative to an uncontrolled impinging jet. Similarly for a few cases, Elavarasan et al. also reported a reduction of about 6-7 dB in the near-field OASPL. Glass (1968) and Poldervaart et al (1976) used similar passive control techniques with limited success. In a series of experiments reported by Samimy et al. (1993) and Zaman et al. (1994), the effect of passive 'tabs' on the aeroacoustic properties of supersonic jets was also investigated. Although the tabs were able to attenuate the screech tones, significant reduction in the OASPL was achieved by using multiple tabs which also resulted in significant thrust loss, as high as 12% (Zaman et al., 1994).

Consequently, although passive control techniques have been able to weaken the feedback mechanism, gains are usually accompanied by a significant cost, such as thrust loss (Samimy et al., 1993; Zaman et al., 1994). In addition, any significant performance gains are confined to a limited range of operating conditions, especially for impinging jets. This is because relatively small changes in the nozzle-to-ground separation (h/d) can lead to significant changes in the magnitude and frequency of the tones responsible for the flow unsteadiness, changes to which passive techniques cannot readily respond. Consequently, any efficient control technique aimed at suppressing the feedback loop must be 'active' and capable of adapting to the shift in frequencies/wavelengths of the modes that lock on to the feedback loop.

In a more recent study, Sheplak and Spina (1994) used high-speed co-flow to shield the main jet from the near field acoustic disturbances. For a suitable ratio of the main jet and co-flow exit velocity, they measured a reduction of greater than 10 dB in the near-field broadband noise level. In addition to noise reduction, the impinging tones were also significantly suppressed using this approach. Although effective, the high mass flow rates of the co-flowing jet required to achieve this noise reduction— around 20%-25% of the main jet mass flux — limits the practical applicability of this coflow approach. Shih et al (1999) used a counterflowing stream near the nozzle exit to successfully suppress screech-tones of non-ideally expanded jets. They were also able to obtain modest reductions in OASPL, approximately 3-4 dB while enhancing the mixing of the primary jet. However, these active control schemes require additional design

modifications and/or high operating power rendering them often impractical for implementation in aircraft.

1.3 Present Approach to Active Flow Control

In the current program, we are proposing the implementation of a control-on-demand strategy using microactuators in the form of supersonic microjets. These microjets are extremely small and require very low mass flux. Although further details of these microjets are discussed later, we simply note that one of the most significant advantages of using microactuators is that their extremely small size allows these systems to be operated in places where traditional systems cannot work due to either space limitation or a lack of system response.

In principal, by populating the appropriate region on the lift plate, in the vicinity of the nozzle exit for the present case, one could develop a system where the most appropriate microjets would be strategically turned on and off to provide optimal control. The proposed control system would have the advantage that, depending upon the operating and local flow conditions; optimal flow control can be achieved by activating the pertinent supersonic microjets with the appropriate magnitude and frequency (if possible) and at the desired time. In contrast to the traditional passive control methods, the proposed control-on-demand system can be switched on and off strategically. As reported later in this report (section on *closed-loop control*), we are presently in the initial stages of implementing the adaptive portion of this technique, i.e. the ability to selectively activate appropriate microjets operating at the appropriate amplitudes (pressures). The initial results demonstrate the considerable promise for implementing adaptive flow control using microjets. Such a system should not measurably influence the operational performance of the aircraft when it is not needed. The very small size of the hardware and the minimal mass flow rates require minimal power consumption and is expected to result in negligible, if any, thrust loss of the primary jet.

In the present study, microjets were made using 400 μm diameter stainless tubes and which were distributed around the periphery of the nozzle in the nozzle exit plane. A sketch of the microjet arrangement can be seen in Fig. 4a. A more detailed description of the microjet hardware is

2. EXPERIMENTAL DETAILS

2.1 Test Configurations and Facility

The experiments were carried out at the STOVL supersonic jet facility of the Fluid Mechanics Research Laboratory (FMRL) located at the Florida State University. A schematic of the test geometry with a single impinging jet is shown in Fig.2 and picture of this facility if shown in Fig. 3. This facility is used primarily to study jet-induced phenomenon on STOVL aircraft hovering in and out of ground effect. Further details can be found in Krothapalli *et al.* (1999).

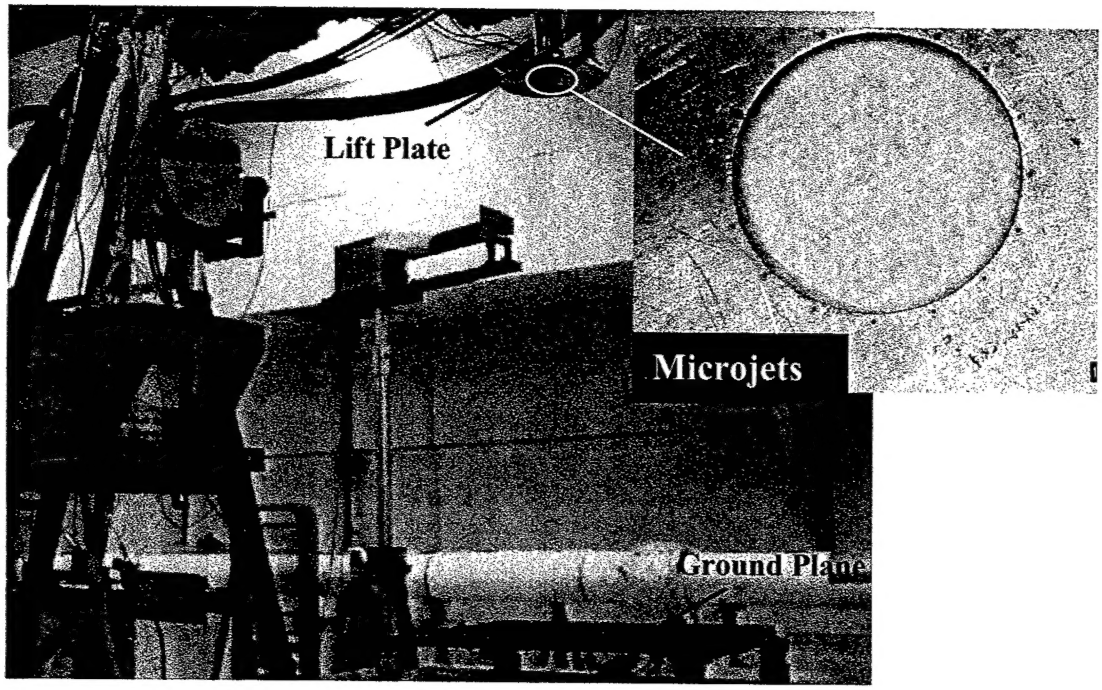

Fig. 3 – STOVL test facility with a close-up view of the Lift Plate with Microjets.

The measurements were conducted using an axisymmetric, convergent-divergent (**C-D**) nozzle with a design Mach number of 1.5. The throat and exit diameters (**d, d_e**) of the nozzle are 2.54cm and 2.75cm (see Fig. 4a). The divergent part of the nozzle is a straight-walled conic section with a 3° divergence angle from the throat to the nozzle exit. Although tests were conducted over a range of Nozzle Pressure Ratios (NPR, where NPR = stagnation pressure/ambient pressure), the results discussed in the present paper are limited to NPR = 3.7 and 5. NPR = 3.7 corresponds to an ideally expanded Mach 1.5 jet, while NPR = 5 produces a moderately under-expanded jet. A circular plate of diameter D (25.4 cm ~10d) was flush mounted with the nozzle exit. The circular

plate, henceforth referred to as the 'lift plate', represents a generic aircraft planform and has a central hole, equal to the nozzle exit diameter, through which the jet is issued. A 1m x 1m x 25 mm aluminum plate serves as the ground plane and is mounted directly under the nozzle on a hydraulic lift (see Figs. 2 & 3).

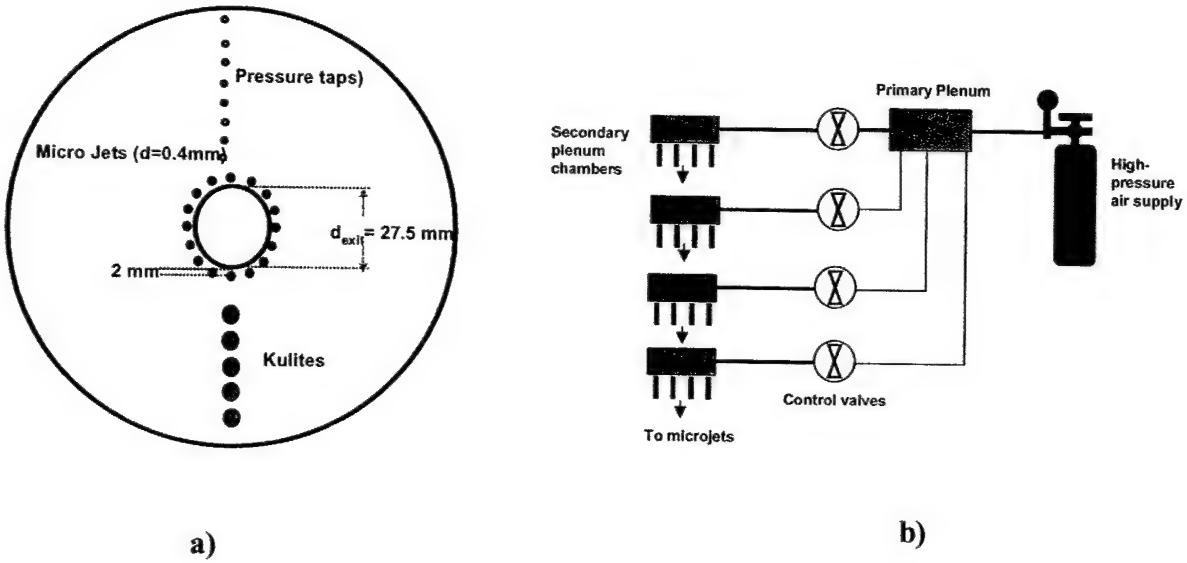

a) b)

Fig. 4 – STOVL test facility with a close-up view of the Lift Plate with Microjets.
a) Geometry of the lift plate and microjets; b) Microjets supply assembly.

Active flow control was implemented using array of sixteen microjets, flush mounted circumferentially around the main jet as shown in Fig. 4a. The jets were fabricated using 400 μm diameter stainless tubes; the effect of microjet injection angle was examined by testing microjets at two angles, 20° and 90° with respect to the main jet axis. The supply for the microjets was provided from compressed Nitrogen cylinders through a main and four secondary plenum chambers. In this manner, the supply pressures to each bank of microjets could be independently controlled. The discussion in the controls portion of this report (§ 5) will illustrate why independent control of the microjet banks is an important requirement. The microjets were operated over a range of NPR = 5 to 7 where the combined mass flow rate from all the microjets was less than 0.5% of the primary jet mass flux.

As discussed in the introduction section, tabs have been used successfully in reducing supersonic jet noises and enhancing mixing in the jet shear layer (Sammimy et al., 1993; Zaman et al., 1994). Previous studies have suggested that the generation of counter-rotating streamwise vortex pairs around the tabs is responsible for the improvement of performance. In light of this, 'micro-tabs' were made by inserting a thin stainless wire (400 μm in dia.) into the 90° micro-nozzles. The wire tabs extends 2.5 mm (approximately 10% of the primary jet diameter) outward from the micro-nozzle into the primary jet. This allows us to compare the effectiveness of the 90° microtabs with the 90° microjets, thus providing insight into the role of microjets in the present control scheme. More details of the facility and hardware can be found in Alvi *et al.*, 2000 (attached as *Appendix A1*). and Shih *et al., 2001* (attached as *Appendix A2*).

2.2 Pressure and Acoustic Measurements

The unsteady loads generated by the impinging jet flow were measured using Kulite™ transducers on the lift plate and the ground plate. In addition, near-field noise was measured using B&K™ microphones placed approximately 25 cm away from the jet. In order to minimize sound reflections during the near-field acoustic measurements, near-by exposed metal surfaces were covered with 10 cm thick acoustic foam. As discussed in § 5, in order to implement closed loop control, the azimuthal distribution of the unsteady loads on the lift plate was needed. Up to six high frequency response miniature Kulite ™ pressure transducers, placed symmetrically around the nozzle periphery plate, at r/d =1.3 from the nozzle centerline, were used to obtain this distribution (Fig. 2). The transducer outputs were conditioned and simultaneously sampled using National Instruments digital data acquisition cards and LabView ™ software. Standard statistical analysis techniques were used to obtain the spectral content and the Overall Sound Pressure Level (OASPL) from these measurements.

2.3 Flow Visualization Methods

The primary flow was visualized using a conventional single-pass shadowgraph arrangement. A stroboscopic white-light flash unit with variable pulse frequency of up to 1 kHz was used as a light source. Cross flow shear layer characteristics were qualitatively examined by using a Planar Laser Scattering (PLS) visualization technique where a laser sheet cuts diametrically (Cross-stream) across the jet. The shear layer at the jet periphery is made visible due to the scattering of the laser light by the water droplets or ice crystals which condense as the cold jet flow entrains the relatively moist ambient air. The laser sheet was generated by a Spectra Physics Nd-YAG pulsed laser. Light scattered by the condensed water droplets in the mixing region was recorded by a CCD camera. These condensed droplets were formed when warm, humid air from outside come into contact with the cold air in the jet. It is worth noting that the flow visualization images can also be used to measure the level of mixing inside the shear layer.

The supersonic microjets used as actuators were also visualized using a specialized micro-schlieren system, which was specifically designed to clearly visualize flows at the very small scales associated with these microjets. The main factors, which have to be controlled for optimal visualization, are *magnification, resolution, field of view* and *sensitivity*. In the present case, diffraction effects, not generally an issue in conventional 'macro-scale' schlieren systems, also become important. The micro-schlieren was designed to provide very high magnifications, capable of resolving features as small 5μm, and very high sensitivity. Details of this system can be found in Phalnikar et al. 2001 (attached as *Appendix A3*)

2.4 Particle Image Velocimetry

Particle Image Velocimetry was used to obtain whole-field velocity data at various jet cross-sectional planes. The primary jet was seeded with small (~0.3μm) oil droplets generated using a modified Wright Nebulizer. The ambient air was seeded with smoke particles (~1-5μm) produced by a Rosco 1600 fog generator. A schematic of the experimental arrangement of the PIV system is shown in Fig. 5. where a double-pulsed Nd:YAG laser (Spectra-Physics, 400 mJ) was used to illuminate the flow field. A light sheet, about 1.5 mm thick, was created using a combination of spherical and cylindrical lenses. The images were recorded by a cross-correlation CCD camera (Kodak ES 1.0) with a 1k x 1k resolution. The PIV images were acquired at a rate

of 15 image pairs per second. Although it was possible to cover a larger area, the present measurements were limited to approximately 60 x 60 mm square cross section. The time between pulses was optimized at 1.2 μs. The double-pulsed images were acquired through an Imaging Technologies ICPCI board, which resides on a single slot of the PCI bus of a personal computer.

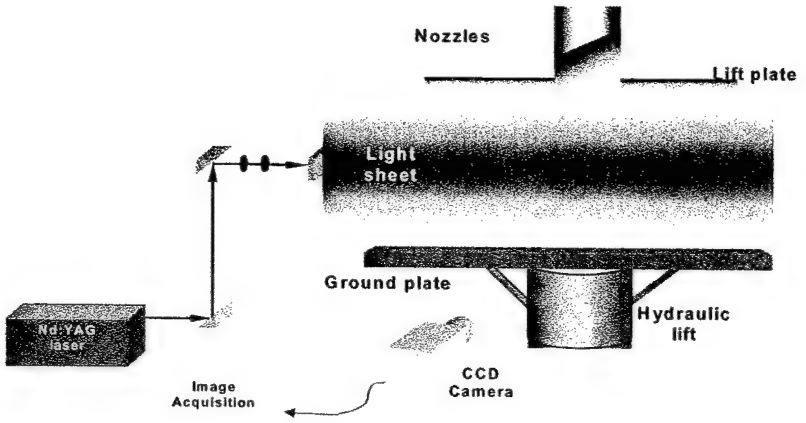

Fig 5 - Schematic of the experimental arrangement of the PIV system.

An image matching approach was used for the digital processing of the image pairs to produce the displacement field. To achieve velocity data with high spatial resolution, a novel processing scheme was used. Details of this technique are described in Lourenco *et al.* (1998). We simply note that a principal advantage of this approach is that velocity field is obtained with second-order accuracy, hence the spatial derivatives are computed with a higher precision.

The main controlling parameters in these experiments are the Nozzle Pressure Ratio (NPR, where NPR = stagnation pressure/ambient pressure) and the ground plane height. Experiments were conducted at NPR=2.5, 3.7 and 5, which corresponds to an over-expanded, ideally expanded and under-expanded primary jet flow, respectively. However, the emphasis of this study was on ideally expanded and under-expanded jets and the results discussed herein will be limited to those two conditions. For most of the experiments, the ground plane height was varied between **2d** and **10d** (d = nozzle throat diameters) since ground effect become almost negligible beyond this distance.

3. SUMMARY OF VISUAL AND ACOUSTIC RESULTS

3.1 Impinging Jet Without Control

Fig. 6 shows instantaneous shadowgraph images of the impinging jet flowfield at h/d = 4 with and without control. Although both cases are shown here, a discussion of the effect of control is delayed until the next sub-section. The uncontrolled case, i.e. microjets off, in Fig. 6a clearly shows the presence of multiple, strong, acoustic waves. These waves signify the presence of impinging tones and, as seen in the image, they impinge and reflect from nearby surfaces – represented by the lift plate in the present case. Concomitant with the appearance of the acoustic waves is the emergence of large-scale structures in the jet shear layer, an example of which has been marked in Fig. 6a. As discussed in the introduction, such large-scale structures, not normally observed in high-speed jets, significantly increase jet entrainment velocities (Elavarasan et al., 2000) leading to significant lift loss (see Fig. 8).

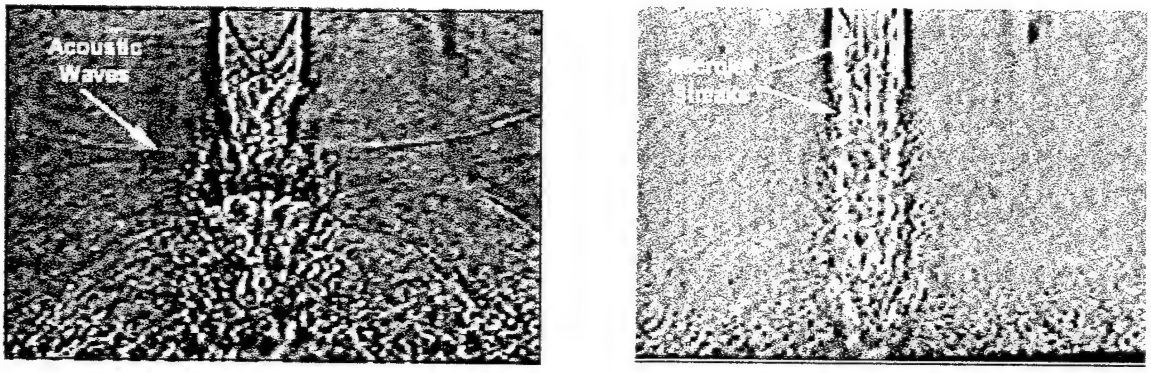

Fig. 6 – Instantaneous shadowgraph images of an ideally-expanded, NPR = 3.7, supersonic impinging jets without (a, left) and with control (b, right) at h/d = 4.

Narrowband spectra for the ground plane unsteady pressures and near-field microphone measurements are shown in Figs. 7a and 7b, respectively. In these, as in all subsequent similar plots, the fluctuating pressures have been expressed in decibels, dB, using a 20 μPa reference. The red spectra in both plots corresponds to the uncontrolled case while the blue spectra shows the effect of microjet control. One of the most significant features in both plots is the presence of discrete, high amplitudes, multiple peaks that are indicative of impingement tones due to the feedback loop. An examination of the ground plane and near-field noise spectral data for a fixed height reveals that the resonant tones occur at identical frequencies for both locations. In fact,

the unsteady pressures on the lift plate, not shown here (see Appendix A1), show an almost identical trend, with tones occurring at identical frequencies at corresponding h/d. This clearly indicates the global nature of the flow unsteadiness generated by the feedback loop. A comparison of spectra for different heights (see Alvi et al., 2000, Appendix A1) shows that the frequencies at which these tones occur changes with nozzle height; a similar shift in frequencies is also observed with respect to NPR (Alvi and Iyer, 1999). The change in the tonal nature of the unsteady flowfield suggests that an efficient control technique must be able to *adapt* to the changes in the feedback loop for effective control. The intensity of the unsteady pressure fluctuations (P_{rms}) and the nearfield noise can be obtained by integrating the total energy under the spectra such as those shown in Fig. 7. Such a comparison reveals that rms pressure levels on the ground plane are the highest in magnitude, in the 180 to 190 dB range, followed by significant unsteady loads on the lift plate, in the 160-165 dB range.

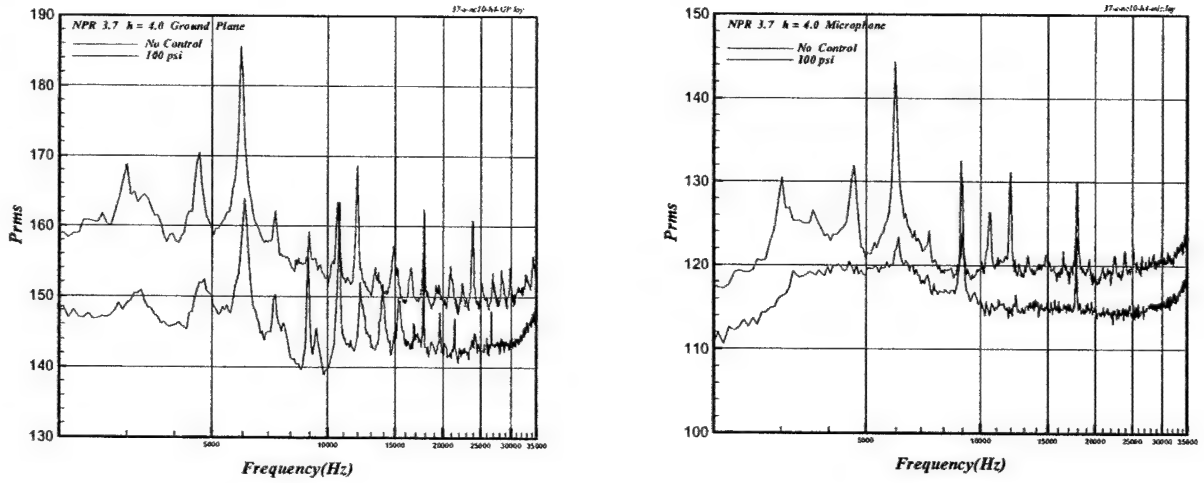

(a) Ground plane (b) Microphone

Fig. 7 - Unsteady surface pressure and microphone spectra for NPR = 3.7, h/d = 4.0; (a) Ground plane, (b) Microphone.

The high entrainment rates due to the presence of large scale structures, such as those visible in Fig. 6, lead to low pressures on the lift plate surface resulting in a suckdown force or lift loss. The lift loss variation with height can be seen in Fig. 8 for the present case. This figure shows the lift loss behavior without (filled symbols) and with (open symbols) microjet control, where the negative lift force has been normalized by the primary jet thrust. This plot illustrates the

dramatic lift loss for the uncontrolled case, as high 60% or more for small heights, which can occur due to jet impingement. The plot also shows that, at least in terms of lift loss, ground effect become negligible for h/d > 9. A more detailed discussion of the uncontrolled impinging jet can be found in Krothapalli et al (1999) and Alvi et al. (1999).

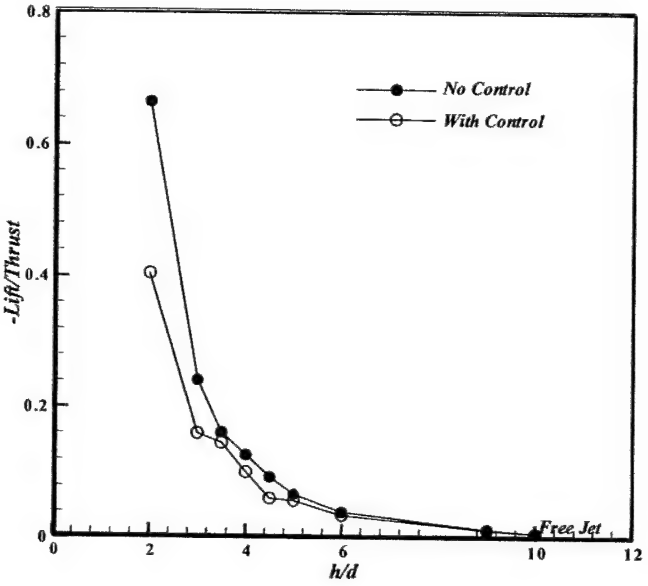

Fig. 8 – Lift loss variation with h/d, with and without microjet control for the ideally expanded jet at NPR = 3.7.

3.2 Impinging Jet with Microjet Control

In light of the detrimental effects of the feedback loop, which leads to a globally unsteady flowfield, an attempt to disrupt this feedback was made by activating the supersonic microjets, described in §2, which are located at the nozzle exit. It was anticipated that the penetration of the microjets into the primary jet shear layer at the nozzle exit would sufficiently modify the shear layer stability characteristics to disrupt the feedback loop and lead to reduction in the related ground effect. In addition, the interruption of the feedback loop could also occur due to the disruption of the spatial coherence of the interaction between the acoustic and instability waves as well as through a modification of the stability characteristics of the primary jet shear layer itself. Although a range of microjets conditions and configurations, i.e. microjet pressures, angle and number were examined in this study, in this section we will limit the discussion of the

results to sixteen 20° microjets operating at ~ 100 psia. The effect of microjet parameters is presented in § 3.2.

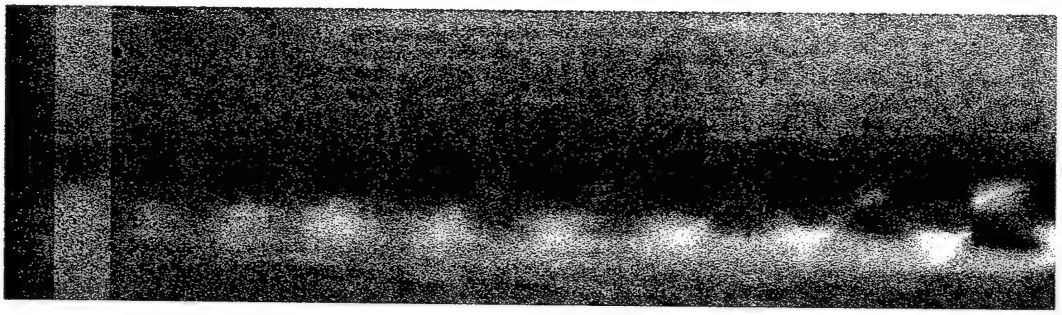

Fig. 9 - Schlieren image of a supersonic microjet issuing from a 400 micron nozzle, $P_0 \sim 100$ psi.

We begin by showing, in Fig. 9, a representative schlieren image of one of the 400μm microjets used to control the feedback loop. The microjet is operating at a pressure of approximately 100 psia and the flow is clearly supersonic as demonstrated by the characteristic periodic shock-cell structure usually observed in much larger supersonic jets. Judging from the presence of the shock cells, the supersonic core of the jet appears to extend at least 10-12 jet diameters downstream of the nozzle exit. Given the high momentum associated with the supersonic microjets and the large supersonic core length, it is anticipated that they will serve as effective 'actuators' capable of penetrating the primary jet shear layer and modifying its properties. A more detailed description of the supersonic microjets, their behavior and the technique used for visualizing may be found in Phalnikar et al. (2001, also attached as Appendix A3).

A comparison of the instantaneous shadowgraphs without control, Fig. 6a, to that with control, Fig. 6b, shows the dramatic effect of activating the microjets. First, the strong acoustic waves present for the uncontrolled case have been eliminated when the microjets are activated. Furthermore, the large-scale shear-layer structures readily visible in Fig. 6a have also been significantly reduced, if not entirely eliminated, in Fig. 6b. As anticipated, the elimination of the large-scale structures is accompanied by a reduction in the jet spreading rate and a narrowing of the jet column as seen in Fig. 6b. Also visible in this figure are the 'streaks' generated by the supersonic microjets. Such streaks are very similar to those generated by tabs (Zaman et al.,

1994) and tape elements on the nozzle surface (Krothapalli et al., 1998); they have been used as indication of the presence of substantial streamwise vorticity. It is worth noting that the presence of such tabs and the concomitant generation of streamwise vorticity have led to a suppression of screech tones (Samimy et al., 1993; Krothapalli et al., 1998) this aspect will be very briefly discussed later in this report.

Given the striking effect of the microjets observed in the shadowgraphs, one expects the unsteady flow properties to be similarly influenced. This is indeed the case as seen in the near field narrow band frequency spectra in Fig. 7. Upon comparing the control data (blue lines) to the uncontrolled case (red lines), one observes that the distinct tones present in the uncontrolled impinging jet are either eliminated or significantly diminished by the activation of microjets. In addition, and perhaps more significantly, the attenuation in the discrete tones is accompanied by a broadband reduction in the spectral amplitudes. This broadband reduction is observed at *all locations*, i.e. on the lift and ground plates and in near-field noise, and are due to lower acoustic and hydrostatic fluctuations, which suggests a *global* decline in the unsteady behavior of this flow.

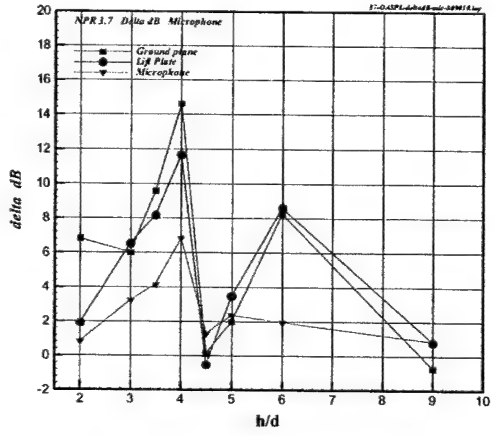

Fig. 10 - Reductions in fluctuating pressure intensities as a function of h/d, NPR=3.7 (microjet angle = 20°, pressure 100 psi).

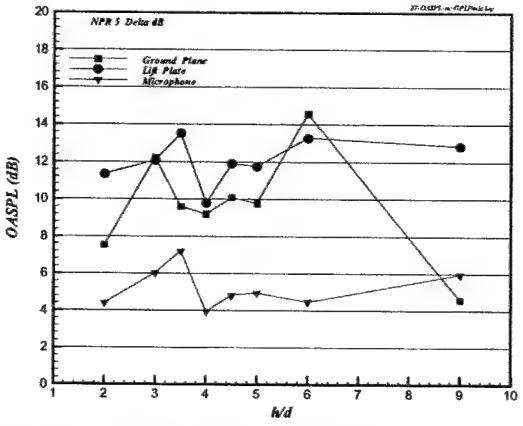

Fig. 11 - Reductions in fluctuating pressure intensities as a function of h/d, NPR=5 (microjet angle = 20°, pressure 100 psi).

Plots summarizing the overall reduction in the unsteady pressure levels (P_{rms}) on the lift plate, the ground plane, and in the nearfield noise are shown in Figs. 10 and 11 for NPR = 3.7 and 5,

respectively. Although a range of microjet pressures were tested, the data shown in these plots correspond to the microjets operating at ~ 100 psia. The trends observed here are very similar to those obtained at other microjet pressures. These plots clearly show that the fluctuating loads are significantly reduced at all three measurement locations for both NPR's, at almost all heights. However, the magnitude of reduction is strongly dependent upon the ground plane distance (h/d) and to a lesser degree on the nozzle pressure (NPR). Whereas a very substantial reduction of more than 10 dB is achieved at h/d = 4, the unsteady loads is only reduced by 2 dB or so at h/d = 4.5. The non-uniform reductions illustrate that the control technique is not equally efficient at all heights, presumably because it does not track changes in the feedback loop due to a variation in h/d. However, notably, the overall trends for at all three measurement locations are very similar with the greatest reductions achieved at h/d = 3 and 4.5. In general, the microjets are more effective for the under-expanded jet (NPR=5) where the lift and ground plate pressures are reduced by 10-14 dB and the nearfield noise by 5-6 dB. The reason for greater control efficiency for the underexpanded case is discussed later in this report. (Also see Shih et al., 2001 and Lou et al., 2002; Appendix A2 and A4, respectively)

The substantial effect of microjets on the lift loss behavior can be surmised from the lift loss plot shown in Fig. 8. Since the loss in lift is due to the low pressures created on the underside of the airframe—the lift plate in this study—due to flow entrainment by the large-scale structure, it is logical to assume that elimination or reduction of these structures should also result in a reduction in lift loss. Measurements of the mean static pressures on the lift plate surface show that the activation of supersonic microjets leads to an increase in the surface pressures, i.e. to lower vacuum/suction pressures on the lower surfaces of the airframe. This reduction in the vacuum pressures on the lift plate translates to a reduction in lift loss as seen in Fig. 8. A comparison of the open symbols (with control) to filled symbols (no control) in Fig. 8 shows that the activation of microjets leads to a significant reduction in lift loss. The maximum lift loss recovery occurs for small heights, e.g. the lift loss is reduced by more than 40% at h/d = 2, with the influence becoming less significant for larger heights. This behavior is expected and desirable since the largest losses in lift also occur for small separations. The reduction in lift loss behaves in a manner similar to the trends observed in Figs. 10 and 11 in that that the gains in

lift are non-monotonic with respect to h/d. This further substantiates the fact that the lift loss associated with impinging jets is directly related to the feedback loop.

These results clearly demonstrate that the unsteady properties of feedback loop of the uncontrolled jet, such as the amplitude and frequency of the impingement tones and the dominant instability modes in the flow, are highly sensitive to operating conditions. It is also worth noting that, due to the sensitivity of the feedback loop on the *exact* operating conditions, the effect of microjet control can vary even if all parameters are unchanged. As an example, as discussed in § 5, although the height at which the microjets are minimally effective is h/d = 4.5 for the conditions in Fig. 10, it can on occasion shift to h/d = 4 or 5 during a particular test. Hence, an efficient control scheme should be able to *adapt* to the changes in the local flow conditions, in real time, to provide optimal control over the entire operating range. Such a control strategy was explored and the results are described in § 5.

3.3 Microjet Parametric Effects

A wide range of permutations in the operating parameters of microjets, such as microjet angle/orientation, pressure and number were examined in order to better understand the physical mechanisms behind microjet control and to devise an optimum control strategy. A brief overview of the effect of some of these parametric variations is discussed next, a more detailed discussion can be found in Shih et al. (2001).

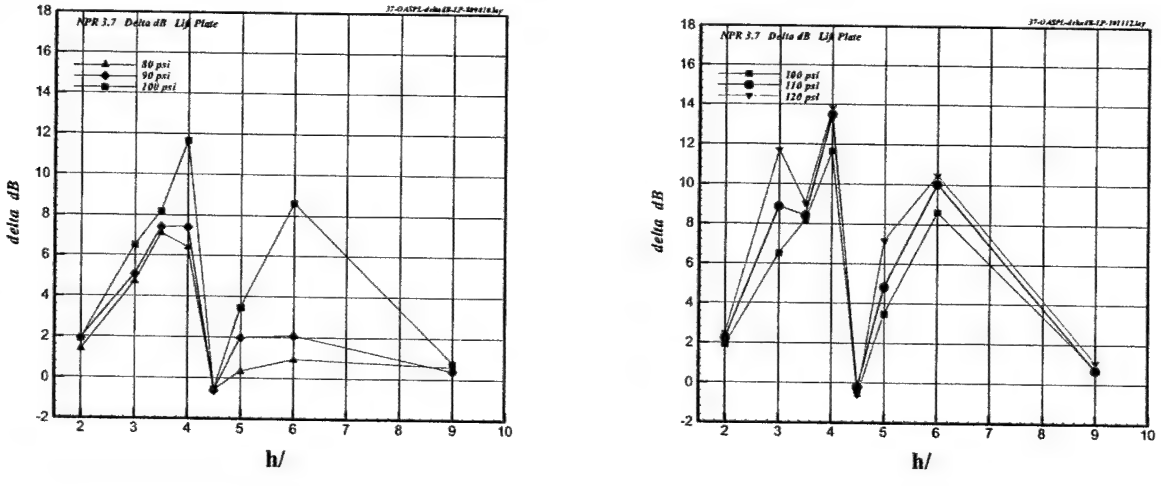

(a) (b)

Fig. 12 Reductions of fluctuating ground plane pressure intensities for different microjet operating pressure; (a) 80 to 100 Psi, (b) 100 to 120 psi. NPR=3.7.

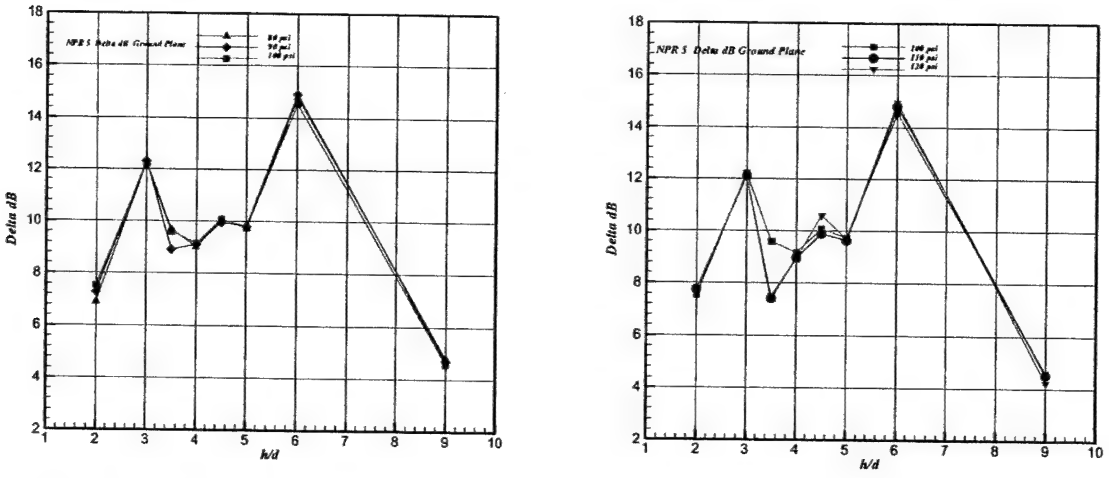

(a) (b)

Fig. 13 Reductions of fluctuating ground plane pressure intensities for different microjet operating pressure; (a) 80 to 100 Psi, (b) 100 to 120 psi. NPR= 5.

3.3.1 Microjet Pressure

The first parameter we explore is the operating pressure of the microjets. For these tests, the microjets with a 20° angle were used. The effect of microjet pressure on the reduction of unsteady flow fluctuations for different h/d is shown in Figs. 12 and 13, for NPR = 3.7 and 5, respectively. The microjet pressure is gradually increased from 80 psi to 120 psi with an increment of 10 psi. For the ideally expanded case, shown in Fig. 12, the reductions of the pressure fluctuations increase relatively faster with increasing microjet pressure up to 100 psi. Beyond this value, the gains become incrementally smaller. In addition, the increasing microjet pressure seems to have minimal effect at three ground plane positions: h/d=2, 4.5, and 9. These are also the positions where the microjet control is found to be the least effective. However, the variation of microjet pressure has a negligible effect when the primary jet is operating under an under-expanded condition. In general, the overall reductions of pressure fluctuations of the under-expanded jet are much higher for all h/d, in the order of 10 to 14 dB. The least effective ground plate distance for microjet control has shifted from h/d=4.5 to h/d=4, nevertheless, the non-monotonic or 'staging' behavior of the control effectiveness still exists for the under-expanded case.

Another factor contributing to the ineffectiveness of the microjet operating under ideally and over-expanded conditions might be the relatively short "penetration depth" of the control jet

under these conditions. The penetration depth can be loosely defined as the extent the control microjets can penetrate into the primary jet with sufficient momentum to modify the shear layer instability. It is expected that the effective penetration depth is longer for the under-expanded case since the jet boundary expands outward in order to compensate the difference between the higher pressure at the nozzle exit and the ambient pressure. On the other hand, the jet boundary expansion is more moderate for the ideally-expanded case. Shorter penetration depth means less influence on the jet flowfield for over- and ideally- expanded cases. The opposite is true for the under-expanded case.

Using the isentropic flow assumption, the expansion angle is estimated to be about 6° between the ideally-expanded and the under-expanded cases and it is not a significant value. From our study[16], the supersonic length for a 400μm jet is about 4 mm (10 jet diameters) at an operating pressure of 80 psi. This means that the microjet should be able to penetrate the shear layer with a speed exceeding the local speed of sound even at this lowest pressure used. Therefore, penetration depth may not be a substantial enough factor to account for the significant difference of the control effectiveness for ideally-expanded and the under-expanded cases. Nevertheless, this issue will be examined more in the next section when we place all microjets at a 90° angle with respect to the primary jet. In this configuration, the control jets are aligned flushed against the outer edge of the nozzle so that penetration depth is no longer a factor.

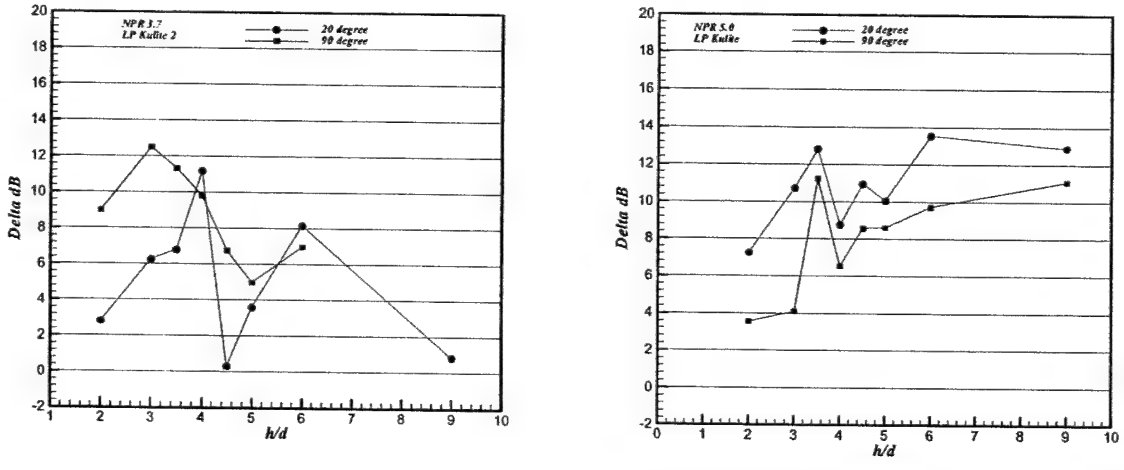

(a) (b)

Fig. 14 Reductions in fluctuating pressure intensities on the lift plate, 20° verse 90° microjet control. (a) NPR = 3.7 (b) NPR = 5.

3.3.2 Microjet Angle

The overall pressure fluctuations for microjet control angles of 20° and 90° are compared in Figs. 14 for NPR = 3.7 and 5. Although only lift plate pressures are shown, the same trends are observed for the ground plane and near-field noise (see Shih et al., 2001). For the ideally-expanded case (NPR=3.7), control becomes more effective, i.e. larger reductions are obtained, for almost all h/d when the angle is changed from 20° to 90°. This increase in control efficacy is especially impressive for short ground plate distance cases (h/d <3.5) such that the unsteady pressure loads on both the lift and ground planes (not shown here) decrease by an additional 6-9 dB compared to the 20° jet angle cases. The only exception is the h/d=4 case when the reduction is a maximum for 20° microjets. At this ground plane distance, there is no further reduction of the flow unsteadiness by placing the microjets right next to the primary jet shear layer. This suggests that the improvement of control effectiveness might not solely due to the increase of penetration depth. The increased reduction at h/d=4.5 is a promising sign since it implies that a more uniform control for all h/d is possible if an adaptive control scheme could be identified and implemented.

Surprisingly the reductions actually either decrease slightly or remain the same for the under-expanded case (Fig. 14b). The decrease seems to be more severe for short (h/d<3.5) and long (h/d>6) ground plane distance cases. For example, a 6 dB decrease can be found in the ground pressure fluctuations for h/d=3. This again indicates that an adaptive control scheme is critical since the flowfield responds in a notably different way when the control configuration changes. This also suggests that, at least for the range of cases examined here, the proximity of the microjets to the primary jet shear layer provides no significant advantage for an under-expanded impinging jet. We believe that this will be the case, as long as the microjet penetration depth exceeds a minimum threshold. This means that the physical mechanism for the effective control might be different for the ideally-expanded and under-expanded cases. This observation is supported by direct velocity measurements, to be presented in §4. The effect replacing the microjets with micro-tabs, discussed in the following section, also supports this hypothesis.

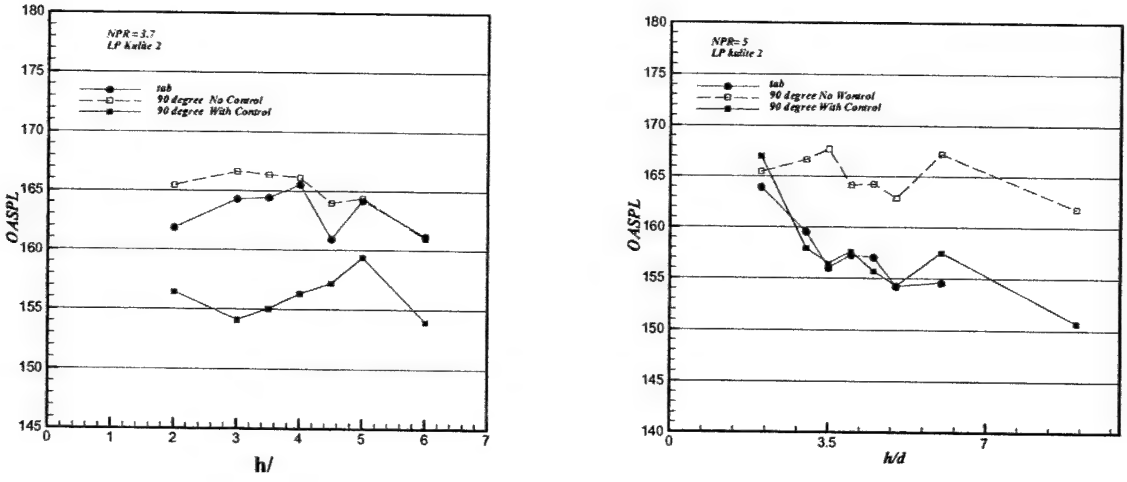

(a) (b)

Fig. 15 Reductions in fluctuating pressure intensities on the lift plate, microtabs vs. 90° microjets. (a) NPR = 3.7 (b) NPR = 5.

3.3.3 Effect of Micro-tabs

As mentioned earlier, tabs have been used successfully in reducing supersonic jet noise and for enhancing mixing in jet shear layers (Samimy et al., 1993; Ibrahim and Nakamura, 2001). It has been demonstrated that the generation of counter-rotating streamwise vortex pairs around the tabs is responsible for the improvement of performance. One can argue that the 90° supersonic microjets may play a role similar to tabs. This was investigated by placing micro-tabs, which were made by inserting a thin stainless wire (400 μm in dia.) into the microjet nozzle, at the nozzle exit plane. The wire tabs extend 2.5 mm (approximately 10% of the primary jet diameter) outward from the micro nozzle into the primary jet. Comparisons of the effect of micro-tabs vs. microjets are presented in Fig. 15a and Fig. 15b for both ideally- and under-expanded cases, respectively. For the under-expanded case (Fig. 15b), the micro-tab control produces almost identical effect as compared to the microjet control. This supports the notion that the generation of counter-rotating, streamwise vortex pair is responsible for the reductions of flow unsteadiness when microjets are used in an under-expanded jet. However, relatively little effect in control can be found when the micro-tabs are used in the ideally-expanded case (Fig. 15a). Most interestingly, the micro-tab control seems to have the least effect at h/d=4 while it is most effective in h/d=4.5, while the outcome is exactly the opposite when 20° microjet control is used

(Fig. 5). This once again indicates that different flow physics are responsible for the flow control at different h/d.

3.4 Planar Laser Scattering (PLS) Visualization

Before obtaining quantitative velocity field measurements, discussed in § 4, the flow field was qualitatively examined using the PLS technique. The aim of these visualizations was to further elucidate the role of streamwise vorticity in microjet control. Figs. 16 shows representative time-averaged PLS images for the underexpanded, NPR = 5, case where the laser sheet cuts diametrically (Cross-stream) across the jet. The shear layer is visible due to the scattering of the laser light by the water droplets or ice crystals which condense as the cold jet flow entrains the relatively moist ambient air. For the images shown in Fig. 16, the laser sheet is placed one diameter downstream of the nozzle exit for both cases. For flow without control, Fig. 16a, very few, weak indentations are observed in the shear layer periphery. More clearly defined 'corrugations' emerge when the microjets are turned on and one can identify a total of 16 of these modulations inside the ring in Fig. 16b, where the azimuthal locations of these indentations correspond to the microjet position around the nozzle periphery. In the past, similar shear layer indentations have been considered as evidence of significant streamwise vorticity in other flows (Alvi, et al., 1996; Krothapalli et al., 1998)

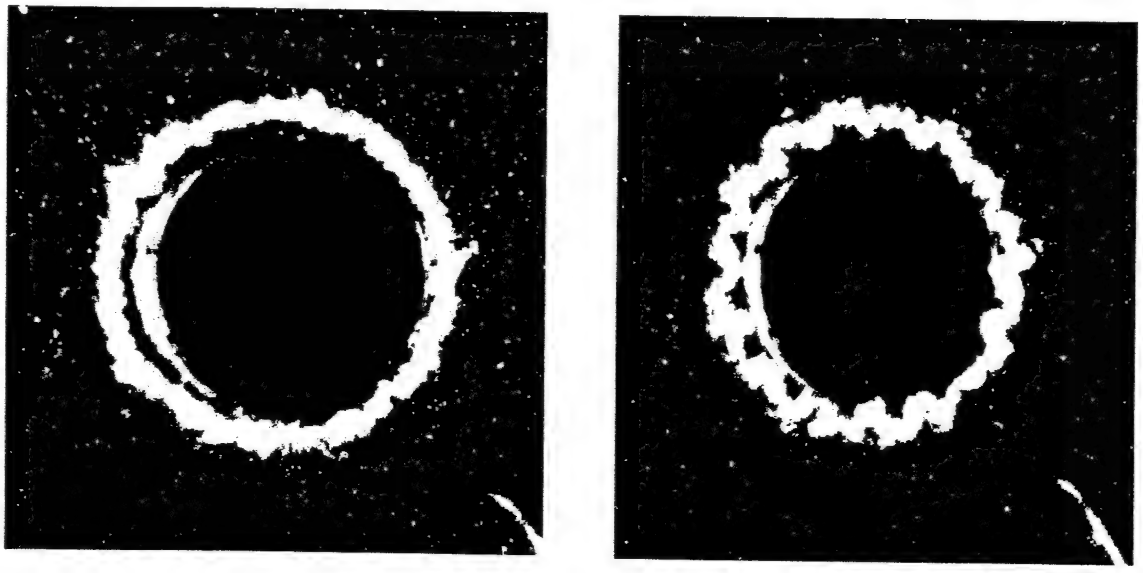

Fig 16 - Time-averaged PLS images, one diameter downstream (x/d=1) of the nozzle, NPR=5, h/d=4; (a) No Control, (b) With control using 20° microjets.

4. VELOCITY FIELD MEASUREMENTS

4.1 Properties of the Vorticity Field

Based on the corrugated shear layer shown in Fig. 16b together with the presence of streamwise streaks observed in the shadowgraphs (Fig. 6b) and their marked similarity to the streaks observed in other studies (Samimy *et al.*, 1993 & Krothapalli, *et al.*, 1999), it was anticipated that the microjets introduce significant streamwise vorticity into the shear layer of the main jet. It was further expected that this streamwise vorticity plays a primary role in the efficacy of this technique.

Prompted by the visual evidence, the role of microjets on the impinging jet flow was quantitatively examined by obtaining whole flowfield measurements using the PIV technique. The PIV results discussed here correspond to the 20° microjets operated at 100 psi for the control cases. All the measurements shown here were made in cross-sectional planes normal to the jet axis, one diameter downstream of the nozzle exit. (More detailed velocity/vorticity-field results can be found in Lou et al, 2002). The instantaneous vorticity contour distributions, shown in Fig. 17 and 18, correspond to flow with and without microjet control, respectively. Similarly, *ensemble-averaged* vorticity contour distributions, for the same conditions are shown in Figs. 19 and 20 where each ensemble average represents an average of 100 instantaneous PIV samples. The vorticity contours in all these plots have been extracted from the velocity-field data. Also, note that the streamwise vorticity shown in Figs 17 through 20 corresponds to the out-of-plane component that has been normalized by (Uj/d) where Uj is the fully-expanded jet velocity.

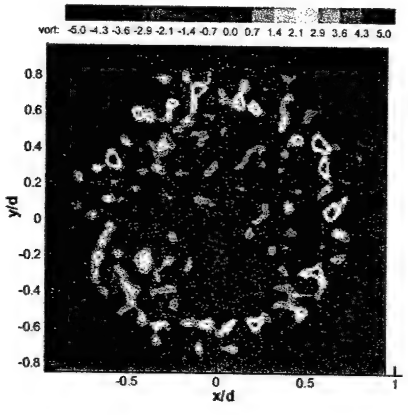

Fig 17 – Instantaneous vorticity distribution at x/d = 1. NPR=5, h/d=4; No Control

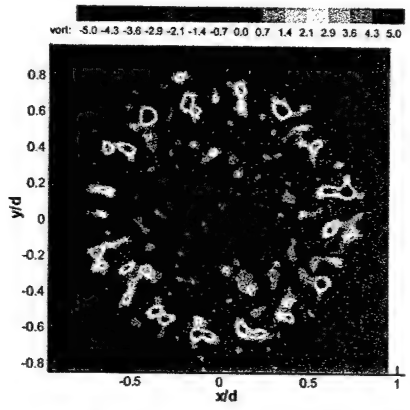

Fig 18 – Instantaneous vorticity distribution at x/d = 1. NPR=5, h/d=4; Microjet control using 20° microjets.

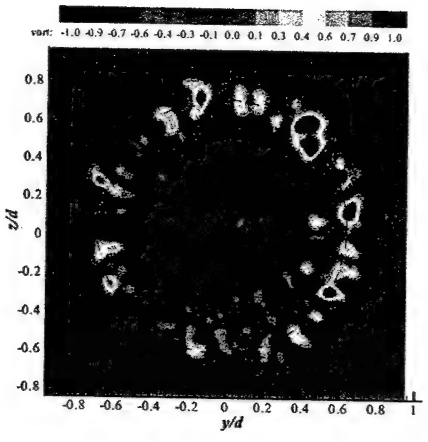

Fig 19 – Ensemble-averaged vorticity distribution at x/d = 1. NPR=5, h/d=4; No Control

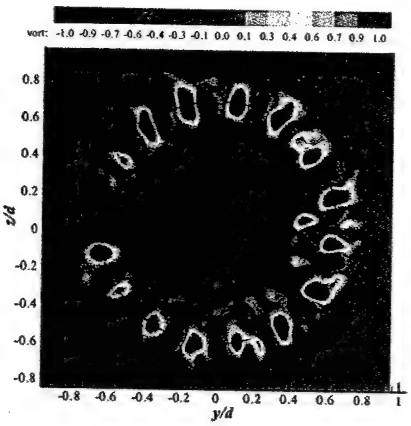

Fig 20 - Ensemble-averaged vorticity distribution at x/d = 1. NPR=5, h/d=4; Microjet control using 20° microjets.

An examination of the instantaneous vorticity distributions shown in Figs. 17 and 18, show the presence of scattered, weak vortical structures in the no control case in Fig. 17. In contrast, much stronger, and somewhat more organized vortical structures are seen in Fig. 18, when the microjets are turned on. The difference in streamwise vorticity due to microjets is much more dramatically revealed in the corresponding *ensemble-averaged* vorticity contour plots shown in Fig. 19 and 20. In Fig. 20, the presence of distinct and organized pairs of counter-rotating vortical structures is clearly visible, where the number of counter rotating vortex pairs corresponds to the number of microjets in Fig. 20. Note that only fifteen streamwise vortex pairs are observed in Fig. 20 because one of the microjets was not functional during these PIV experiments.

A comparison of the no-control to the microjet control data, in Figs. 17 through 20, leaves little doubt that the activation of microjets introduces significant, spatially coherent, streamwise vorticity in the jet shear layer. Similar measurements were also made for the ideally-expanded jet operating at NPR = 3.7 (see Lou at al., 2002). These measurements further revealed that the magnitude of the streamwise vorticity generated by the microjets is appreciably larger for the underexpanded jet compared to the ideally expanded case. Since the shear layer curvature in an underexpanded jet is likely to enhance the amplification rates of disturbances due to a Taylor-

Görtler instability, the stronger streamwise vorticity measured at NPR = 5 is not entirely unexpected. Recalling the earlier results (§3.2) that the microjets were more effective in reducing the impinging jet noise levels at NPR =5, it is reasonable to surmise that there is a direct correlation between the strength of streamwise vorticity and the efficacy of microjet control. Although not shown here (Lou at al., 2002), a closer examination of the velocity field near the counter-rotating vortices, such as those seen in Figs. 20, reveals that relatively high induction velocities exist in areas between these vortices. This increased flow entrainment due to these well-organized streamwise structures can significantly enhance the radial mixing rate in the jet shear layer. This can result in two possible effects: First, it can lead to a weakening of the primary shear layer structures, as seen in the shadowgraphs (see Fig. 6b) and the emergence of a stronger three-dimensionality in the flow. Second, the increased entrainment can lead to a local thickening of the primary jet shear layer near the nozzle exit, making it less receptive to the acoustic disturbances propagating upstream from the ground plane. The combined effect will result in a weaker interaction between the acoustic waves and the shear layer and a reduction in the growth of the shear layer instabilities leading to a weaker feedback loop and a more stable flowfield, as observed.

Further insight can be gained by examining the streamwise vorticity distribution as a function of the azimuthal angle, as shown in Fig. 21. The vorticity values, shown on the ordinate in these plots, were extracted from the corresponding mean vorticity contours (Figs. 19 and 20) along a fixed radial position roughly in the middle of the shear layer. The dotted circles in Figs. 19 and 20, show the approximate location at which the vorticity values were extracted. Taking advantage of the flow symmetry, data for only half of the jet periphery is shown. In each plot, the solid line corresponds to the microjet control case, while the dashed line corresponds to no control. The organized, counter-rotating vorticity pairs due to microjets observed in Fig. 20 are revealed as adjacent pairs of large-amplitude, vorticity peaks and valleys in Fig. 21. In contrast, the no control distribution the vorticity is less organized with significantly lower amplitudes.

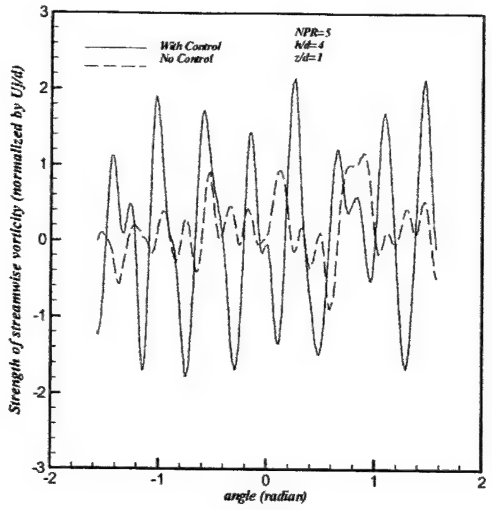

Fig. 21 - Ensemble-averaged streamwise vorticity distribution along the azimuthal direction for NPR=5, h/d=4; extracted from Figs. 19 and 20.

4.2 Streamwise Vorticity: Its Source and Properties

Having demonstrated that the microjets introduce significant streamwise vorticity, we now briefly explore the source of this vorticity and its role in attenuating the feedback loop. The most logical and direct source of streamwise vorticity are the microjets themselves. However, using an order of magnitude analysis, it is easily shown that total streamwise vorticity due to all sixteen microjets is less than 10% of the additional streamwise vorticity measured in the main jet when microjets are turned on. This suggests that a significant portion of the streamwise vorticity has to come from a different source — the shear layer of the primary jet appears to be the next most logical candidate, as follows.

The presence of large scale structures in the shear layer of the uncontrolled impinging jet (see Fig. 2 and 6a) implies that the uncontrolled jet possesses substantial azimuthal vorticity, ω_θ (see Fig. 2 for the coordinate system). Conversely, the lack of such structures with microjet control, concomitant with the appearance of substantial streamwise vorticity suggests that the additional streamwise vorticity, ω_x comes at the expense of the azimuthal vorticity. In Figs 16-21, it has been clearly demonstrated the appearance of streamwise vorticity with the activation of microjets. Azimuthal vorticity distributions were obtained from PIV measurements made in the centerline plane along the axial direction to verify this hypothesis. A comparison of the microjet control to the uncontrolled case shows that the azimuthal vorticity is appreciably reduced when the microjets are activated.

More detailed measurements of the velocity and vorticity field are currently underway for a larger range of operating parameters. However, based on the results presented above, there is strong evidence that the streamwise vorticity appears as a result of the redirection of the azimuthal vorticity in the primary jet. This redirection mainly occurs through the 'tilting' and 'stretching' of the azimuthal vorticity by the microjets. A more detailed discussion of this proposed vorticity redistribution mechanism for the present flowfield can be found in Shih et al. (2001) where the vorticity transport equation is examined in the present context. Suffice it to say the 'drainage' of azimuthal vorticity into streamwise direction can also be thought of as a weakening of the large-scale axisymmetric structures in the jet shear layer. Consequently, the weaker vortical structures produce weaker acoustic waves when they impinge on the ground plane, thus further attenuating the feedback loop.

5. ACTIVE CLOSED-LOOP CONTROL OF IMPINGEMENT TONES

The motivation for considering active control comes from the behavior of the flow-field in the presence of the supersonic microjets. As can be seen in Figs. 10 and 11 the microjets disrupt the feedback loop thereby reducing the OASPL. This reduction, however, is non-uniform with respect to the height and varies with flow conditions. Furthermore, the reduction is unpredictable and can vary even for the same nominal conditions as shown in Fig. 22. In order to obtain a uniform and guaranteed reduction over a range of operating conditions in a reliable manner, closed-loop control that uses on-line measurements and active-adaptive algorithms is an appropriate methodology that can be employed.

5.1 A Reduced-Order Model of Impingement Tones

Much of feedback control consists of designing suitable external actuators that introduce a control input so as to alter, typically, the dynamic characteristics of the process being controlled. In many of these problems, the control method begins with a description of the process in the form of a differential equation

$$\dot{x} = f(x,u)$$

where x denotes the process state, and u denotes the control input-source. The control strategy then consists of determining a feedback signal according to the rule

$$u = g(x)$$

where $g(.)$ is to be determined so as to realize the desired objective in the process.

The reduced-order model adopted for the control of impingement tones is based on the vortex-sheet jet model of Tam [1]. Within a short distance ($\sim 0.01R_j$) downstream from the nozzle exit, the jet can be idealized as a uniform stream of velocity U_j and radius R_j bounded by a vortex sheet. Small-amplitude disturbances are superimposed on the vortex sheet (see Figure 1). By starting from the linearized equation of motion of a compressible flow, it can be shown that the governing equations for the problem are:

$$\frac{1}{a_\infty^2}\frac{\partial^2 p_+}{\partial t^2} = \nabla^2 p_+ \qquad (r \in \Omega_2)$$

$$\frac{1}{a_j^2}\left(\frac{\partial}{\partial t} + U_j \frac{\partial}{\partial z}\right)^2 p_- = \nabla^2 p_- \qquad (r \in \Omega_1) \tag{1}$$

where $p_+(r,\theta,t)$ and $p_-(r,\theta,t)$ be the pressures associated with the disturbances outside and inside the jet, denoted respectively by domains Ω_2 and Ω_1 where Ω_1 denotes jet-core which extends from z = -∞ to z = +∞, Ω_2 denotes the domain outside the jet-core and (r,θ,t) are the cylindrical coordinates, a_∞ and a_j are the speed of sound outside and inside the jet and U_j is the main jet speed. The aim here is to choose u, the microjet velocity such that the pressure p is reduced in magnitude. In order to extract as much information possible about the state of the system, we adopt the Principal Decomposition Method (POD). The Proper Orthogonal Decomposition (POD) is a tool used to systematically extract the most energetic modes from a set of realizations from the underlying system.

By separation of variables, we can write for the outer area Ω_2

$$p_+(r,\theta,z,t) = \sum_{i=1}^{L} X_i(t)\Phi_i(r,\theta,z) \tag{2}$$

where X_i is the state variable, and $\{\Phi_i\}$ are the POD modes. Using the wave equation, the equality conditions, the effect of the microjets, and the flow condition on the lift plate, we can obtain a model of the form

$$\ddot{X}_j(t) = a_\infty^2 \sum_{i=1}^{L} \left(\nabla^2 \Phi_i, \Phi_j\right) X_i(t) \qquad j = 1, \ldots, L \tag{3}$$

where $\{\Phi_i\}$ is a function of microjet velocity. Eq. (3) will be suitably used for future control designs. The POD modes can be obtained as the solution of an optimization problem

$$\underset{\Psi}{Min}\, J_m(\bar{\phi}_1, \ldots, \bar{\phi}_l) = \sum_{j=1}^{m} \left\| \; Y_j - \sum_{k=1}^{l} \left(Y_j^T \bar{\phi}_k\right) \bar{\phi}_k \; \right\|^2$$

subjected to: $\bar{\phi}_i^T \bar{\phi}_j = \delta_{i,j}, \;\; 1 \le i, j \le l, \;\; \Psi = \left[\bar{\phi}_1, \ldots, \bar{\phi}_l\right]$ (4)

where $Y_j \in \Re^n$ is the vector of flow data F at time $t = t_j$ (see Holmes et al., 1996 for further details).

It can be seen from Equation (2) that in order to find the POD modes of the system, the calculation of pressure at all flow points is needed. This is not feasible either experimentally or computationally due to obvious constraints. However, our main goal is to model the impingement tones and it is worth noting that the key ingredients that contribute to their formation such as the initiation of the shear layer instability waves and their interaction with the acoustic waves appear to be localized at the jet nozzle. Therefore, we derive the impingement tones model by focusing only on the POD of the pressure field close to the nozzle. That is, we derive the control strategy using the expansion:

$$p_+(r = R_s, \theta, z = z_{nozzle}, t) \equiv p(\theta, t) = \sum_{i=1}^{l} T_i(t) \phi_i(\theta) \tag{5}$$

where R_s is the radial position of the sensors on the lift plate. Note that ϕ_i's in Equation (5) are, quite likely, a subset of Φ_i's in Equation (2) which are the modes of the entire flow field. The state space equation corresponding to these reduced set of modes are given by:

$$\ddot{T}_j(t) = a_\infty^2 \sum_{i=1}^{L} \left(\nabla^2 \phi_i, \phi_j\right) T_i(t) \qquad j = 1, \ldots, L \tag{6}$$

with the inner product suitably defined. In vector form, this becomes:

$$\dot{T}(t) = \breve{A}(p_\mu)T(t) \tag{7}$$

Once the mode shapes are determined, we simply choose the control strategy as:

$$p_\mu(\theta) = k\phi_1(\theta) \tag{8}$$

where ϕ_1 is the most energetic mode in Equation (5) and k is a calibration gain. The complete closed-loop procedure therefore consists of collecting pressure measurements $p(\theta,t)$, expanding them using POD modes as in Equation (5), determining the dominant mode ϕ_1, and matching the control input - which is the microjet pressure distribution along the nozzle - to this dominant mode as in Equation (8).

The closed-loop control approach used here is distinctly different from the traditional feedback control paradigm where the control input is typically required to be modulated at the natural frequencies of the system. The latter, in turn, mandates that the external actuator have the necessary bandwidth for operating at the natural frequencies. In the problem under consideration, the edge tones associated with the flow-field are typically a few kilohertz. Given the current valve technology, modulating the microjets at the system frequencies is a near impossibility. The approach presented above overcomes this hurdle by modulating the control input, u, at a slow time-scale, so that it behaves like a parameter. If this control input is chosen judiciously, then even small and slow changes in this "parameter" can lead to large changes in the process dynamics, as is shown below.

5.2 Experimental Results

The closed-loop control strategy described above was implemented at the STOVL supersonic jet facility of the Fluid Mechanics Research Laboratory, shown in Figs. 2 and 3. As discussed earlier, four banks of microjets were distributed around the nozzle exit, while pressure fluctuations were sensed using six Kulite™ transducers placed symmetrically around the nozzle periphery plate, at r/d = 1.3, from the nozzle centerline where d is the nozzle throat diameter. The control experiment was performed for a range of heights (of the nozzle above ground).

At each height, in addition to the mode-matched control, active control was also implemented by supplying all the microjets with a uniform pressure, the results of this uniform forcing have already been described in §3 and §4. The latter case, where the spatial distribution of microjet pressure around the nozzle exit was kept uniform, can be viewed as an open-loop control procedure. To ensure a fair comparison between the two control methods, the main nozzle was forced to operate under constant condition throughout the whole process. The calibration constant k in Equation (8) was chosen such that the minimum and maximum values of the POD mode over θ correspond to 70psi and 120psi, respectively, which ensured maximum effectiveness of the actuator. Figure 2(a) shows the shape of the first mode and the suggested microjet bank pressure distribution for several heights and Figure 23 (b) shows a block diagram of the active closed-loop control method. Figure 3 shows the results for the closed loop control strategy, which indicates better performance throughout all operational conditions, with a large improvement at heights h/D = 4, 4.5 and 5. The reason for this increased pressure reduction can be attributed to the percentage of energy contained in the dominant mode, which is used in the control strategy. At heights 4 to 5, the energy content of the first mode is above 86 %. In contrast, at heights 2 and 3, the energy level drops to about 50 % and hence the corresponding improvement in the closed-loop strategy also drops to about half the db-value at heights 2 and 3 compared to at heights 4 and 5.

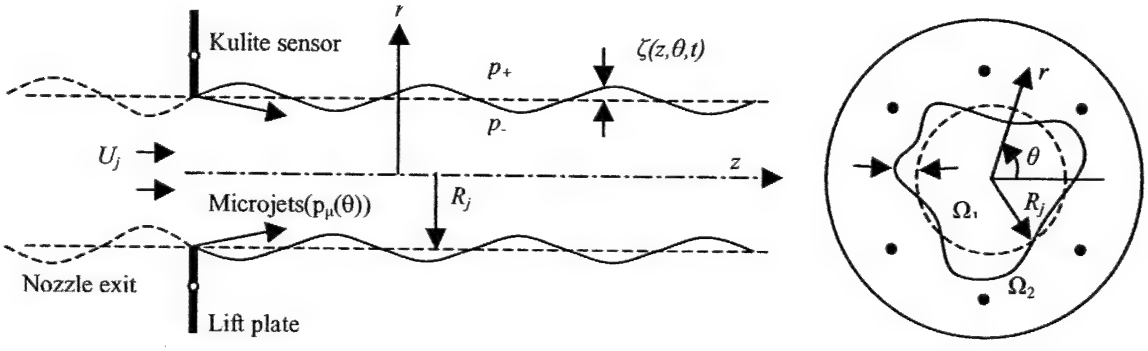

Fig. 22 - Vortex-sheet jet model for the impingement tones control problem. Location of microjets and pressure sensors are also shown.

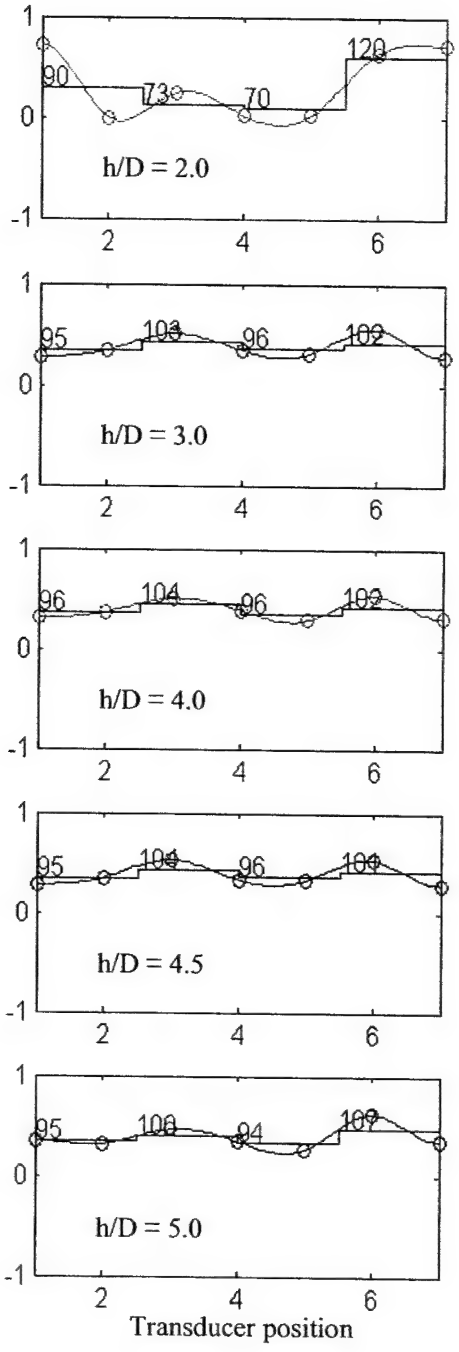

Fig. 23 - (a) The first mode shape and suggested microjet pressure distribution for each height. *h* is the height of the lift-plate from ground and *D* is the diameter of the lift-plate.

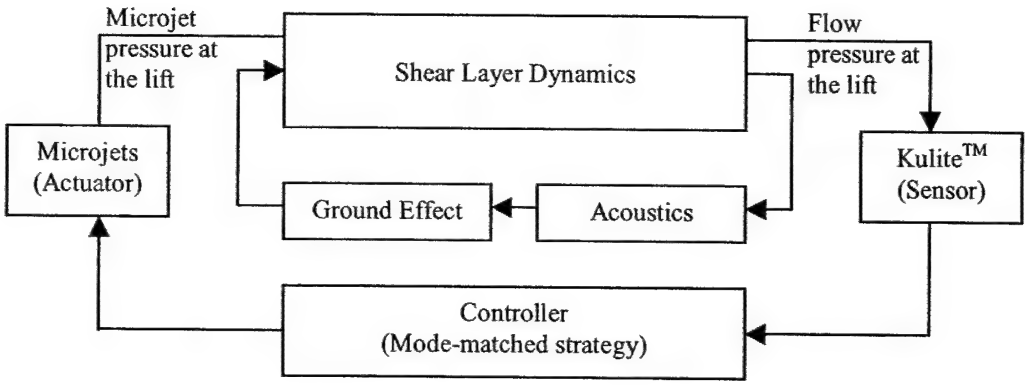

b)

Fig. 23 - (b) Block diagram of the closed-loop control program of impingement tones.

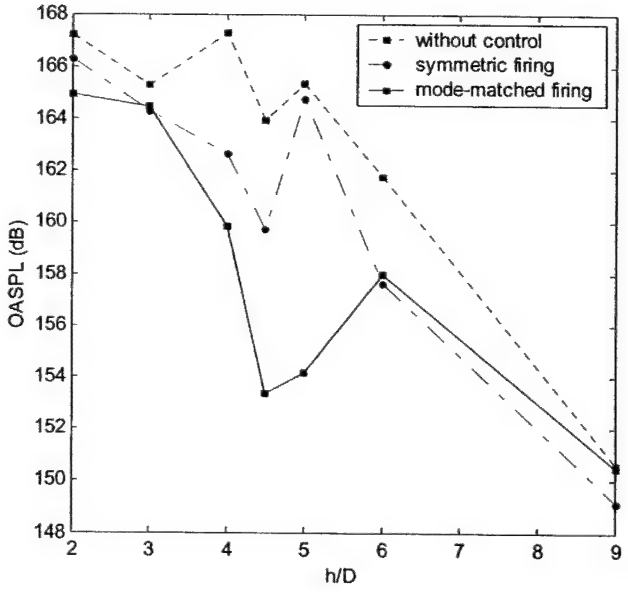

Fig. 24: Overall sound pressure levels (OASPL) for different control (NPR=3.7).

6. SUMMARY

This report describes the results of a three-year effort with the aim of *understanding* the properties of supersonic impinging jets and *controlling* the adverse effect of associated with such flows, such has very high noise levels and discrete tones. The flowfield of impinging jets were examined in detail in this experimental study using conventional techniques such as flow visualization and acoustic measurements, as well as advanced diagnostics such as Particle Image Velocimetry. A novel approach was used to establish flow control by using an array of supersonic microjets positioned around the nozzle exit of the primary jet. Supersonic microjets were found to be very effective in controlling impinging jet flows by disrupting the feedback mechanism inherent this flowfield. This control strategy results in significant performance gains relative to the uncontrolled case. Lift loss, overall noise levels, and the fluctuating pressure loads on the lift and ground surfaces all experienced substantial reductions. However, the performance enhancements due to microjet control were not uniform over the entire parametric space. An on-line, closed-loop control strategy was explored with the aim of producing optimal performance gains over the entire operating regime and the initial results of this approach are very promising. Based on the detailed measurements obtained in this study, not only a better understanding of the impinging jet flowfield has been achieved, some insight has also been gained into the physical mechanisms behind the effectiveness of microjet control. The efficacy of this control technique, together with ease of implementation and minimal mass flow requirements, make this a potentially promising candidate for implementation in future propulsion systems of STOVL aircraft. Some specific, significant outcomes of this study are listed below.

- The ground effect associated with impinging jets, such as lift loss, high dynamic loads in the near-field, high noise levels and discrete tones, are all a result of the feedback loop inherent in such flows which makes it globally unstable.
- A novel control technique utilizing *supersonic microjets* was explored in order to disrupt the feedback mechanism in supersonic impinging jet flows. The technique proved to be very successful, where the activation of microjets resulted in significant performance gains, including:
    - Substantial reductions in lift loss, by as much as 40%.

- 10-12 dB reductions in the fluctuating pressure loads on the lift and ground surfaces for certain conditions.
- Significant reductions in overall near-field noise levels, up to 6-8 dB, were also achieved.

- The performance gains were achieved with minimal mass flow requirements, which was below 0.5% of the main jet mass flux for all cases and substantially less than that for a majority of cases examined.
- Although the performance gains were substantial, they were found to be non-uniform over the operating parametric range with respect to NPR and nozzle height above ground.
- A closed-loop control strategy was explored to obtain more uniform gains over the operating range of interest. This approach is based on determining the dominant POD mode using pressure measurements at the nozzle exit and using a 'mode matched strategy' to determine the microjet pressure distribution along the nozzle. The results demonstrated a significant reduction in the unsteady pressure loads along with a consistent improvement compared to an open-loop control strategy where the microjet pressure was kept at a constant.
- The velocity/vorticity field data clearly reveal the appearance of well-organized, strong, streamwise vortices with the activation of microjets where the magnitude of the streamwise vorticity is significantly higher with microjet control. Based on these results to date, this stronger streamwise vorticity appears to primarily come from through the redirection of the vorticity in the primary shear layer by vorticity tilting and stretching mechanisms. The weakening of the azimuthal vorticity by the generation of streamwise vorticity is thought to be a primary factor behind the disruption of the feedback loop.

7. REFERENCES

1. Alvi, F. S., Krothapalli, A., Washington D., and King, C. J. "Aeroacoustic Properties of a Supersonic Diamond-Shaped Jet," AIAA Journal, Vol. 34, No. 8, August 1996, pp. 1562-1569.
2. Alvi, F S. and Iyer, K. G., "Mean and Unsteady Flowfield Properties Of Supersonic Impinging Jets with Lift Plates", AIAA Paper 99-1829, presented at the 5th AIAA/CEAS Aeroacoustics Conference, May 1999.
3. Alvi, F. S., Elavarsan R., Shih, C., Garg G., and Krothapalli, A., " Control of supersonic impinging jet flows using Microjets," *AIAA Paper* 2000-2236, to appear in the *AIAA Journal*, August 2003.
4. Glass, D.R., "Effect of acoustic feedback on the spread and decay of supersonic jets," *AIAA Journal*, Vol.6, No.6, 1968, pp1890-1897.
5. Elavarasan, R., Krothapalli, A., Venkatakrishnan, L., and Lourenco, L., "Suppression of Self-Sustained Oscillations in a Supersonic Impinging Jet", *AIAA Journal*, **39** (12), 2001, 2366-2373.
6. Holmes, P. J., Lumley, J. L., and Berkooz, G. "Turbulence, Coherent Structures, Dynamical Systems and Symmetry," Cambridge University Press, 1996.
7. Ibrahim, M.K and Nakamura, Y., "Effects of Rotating Tabs on Flow and Acoustic Fields of Supersonic Jet," AIAA Journal, Vol. 39, No. 4, pp745-748, 2001
8. Karamcheti, K., Bauer, A.B., Shields, W.L., Stegen, G.R., and Woolley, J.P., "Some Features of an Edge Tone Flow Field", NASA SP 207, 1969, pp. 275-304.
9. Krothapalli A., Strykowski P. J. and King C. J., "Origin of Streamwise Vortices in Supersonic Jets," *AIAA Journal*, Vol. 36: No. 5, 1998, pp. 869-872.
10. Krothapalli, A., Rajakuperan, E., Alvi, F., and Lourenco, L., "Flow Field and Noise Characteristics of a Supersonic Impinging Jet", *J. Fluid Mechanics*, **392**, 1999, pp. 155-181.
11. Lourenco, L.M. and Krothapalli, A., "Mesh-Free Second Order Accurate Algorithm for PIV Processing," Proceedings of the International Conference on Optical Technology and Image Processing in Fluid, Thermal and Combustion Flows, Yokohama Japan, Dec. 1998, pp. 224.
12. Margason, R., Arledge, T.K., Wardwell, D. A., Hange, C and Naumowicz. T., "Jet Efflux Characteristics and their Influence on STOVL Aircraft Propulsion-Induced Effects", Proceedings of International Powered Lift Conference, SAE P-306, March 1997, pp. 3-10.

13. Neuwerth, G.," Acoustic Feedback of a subsonic and Supersonic Free Jet which Impinges on an Obstacle", NASA TT F-15719, 1974.
14. Powell, A., "The Sound-Producing Oscillations of Round Underexpanded Jets Impinging on Normal Plates", *J. Acoust. Soc. Am.*, 83 (2), 1988, 515-533
15. Poldervaart, L.J., Wijnands, A.P.J., vanMoll, L.H.A.M., and vanVoorthuisen, E.J., "Modes of vibration", *J. Fluid Mech*, Vol. 78, 1976, pp.859-862.
16. Samimy, M. Zaman, K. B. M.Q. and Reeder, M. F., "Effect of Tabs on the Flow and Noise Field of an Axisymmetric Jets," *AIAA Journal*, Vol.31, No.4, 1993, pp. 609-619.
17. Sheplak, M. and Spina, E.F., "Control of high-speed impinging-jet resonance", *AIAA Journal*, Vol.32, No.8, 1994, pp. 1583-1588.
18. Shih, C., Alvi, F.S., Lou, H., Garg G., and Krothapalli, A., " Adaptive Control of Supersonic Impinging Jets," *AIAA Paper* 2001-3027, July 2.
19. Shih, C., Alvi, F. S., and Washington, D., "Effects of Counterflow on the Aeroacoustic Properties of a Supersonic Jet," *AIAA Journal of Aircraft*, Vol. 36, No. 2, March/April 1999, pp. 451-457
20. Tam, C.K.W., and Ahuja, K.K., "Theoretical model of discrete tone generation by impinging jets", *J. Fluid Mech.*, Vol. 214, 1990, pp 67-87.
21. Wardwell, D. A., Hange, C., Kuhn, R. E., and Stewart, V.R., "Jet-Induced Ground Effects on a Parametric Flat-Plate Model in Hover", NASA TM 104001, 1993.
22. Zaman, K. B. M.Q., Reeder, M. F. and Samimy, M. "Control of an Axisymmetric Jet Using Vortex Generators," *Physics of Fluids*, Vol. 6, No. 2, February 1994, pp. 778-793.

8. PERSONNEL SUPPORTED

Faculty

Prof. *A. Krothapalli* (Ph.D., Stanford) is the principal investigator; Profs. *F. Alvi* (Ph.D., Penn State) and *C. Shih* (Ph.D., USC) are co-investigators at Florida A & M University-Florida State University (FAMU-FSU). Dr. *A. M. Annaswamy* (Ph.D., Yale), at MIT, is also a co-PI on this project.

Students

FAMU-FSU: Mr. K. Phalnikar and G. Garg have been supported by this program and received their M.S. degrees from FAMU-FSU College of Engineering in 2001. A third M. S. student, Ms. C. Davy is expected to complete her degree in summer 2003. A Ph. D. candidate, Mr. H. Lou, is expected to complete his doctoral dissertation by Spring 2004.

MIT: Mr. J. Choi, an M. S. student supported by this grant at MIT is expected to complete his degree in summer, 2003.

9. PUBLICATIONS & INTERACTIONS

9.1 Related Archival Publications By Investigators (published, submitted & in preparation)

1. Krothapalli, A., Rajakuperan, E. Alvi, F. S. and Lourenco, L., "Flow field and Noise Characteristics of a Supersonic Impinging Jet," *Journal of Fluid Mechanics*, Vol. 392, August 1999, pp. 155-181.
2. Elavarasan, R., Venkatakrishnan, L., Krothapalli, A., and Lourenco, L., "A PIV Study of a Supersonic Impinging Jet", *Journal of Visualization*, Vol. 2 (3/4), 2000, pp 213-221.
3. Alvi, F. S., Ladd, J. A. and Bower, W. W. "Experimental & Computational Investigation of Supersonic Impinging Jets," *AIAA Journal*, Vol. 40, No. 4, April 2002.
4. Alvi, F. S., Shih, C., Elavarasan, R., Garg, G, and Krothapalli, A., "Control of Supersonic Impinging Jet Flows Using Supersonic Microjets", to appear in the *AIAA Journal*, anticipated publication date, July 2003.
5. Naugthon, J. W., Davy, C. and Alvi, F. S. "Skin Friction Measurements for Supersonic Impinging Microjets," to be submitted to *Experiments in Fluids*, anticipated submission date: May, 2003.

6. Phalnikar, K., Alvi, F. S. and, C. Shih "Visualizations and Measurements in Supersonic Microjets," to be submitted to *Experiments in Fluids*, anticipated submission date: May, 2003.
7. Alvi, F. S. and Phalnikar, K., "Properties and Structure of Supersonic Microjets," to be submitted to *Physics of Fluids*, anticipated submission date: June 2003.

9.2 Presentations and Conference Publications (00-02)

1. Alvi, F. S., Elavarasan, R., Shih, C., Garg, G, and Krothapalli, A., "Active control of Supersonic Impinging Jets using Micro Jets", AIAA 2000-2236, to appear in the *AIAA Journal* (accepted).
2. Alvi, F.S., Shih, C. and Krothapalli, A., "Active Control Of The Feedback Loop in High-Speed Jets," AIAA Paper 2001-0373
3. Alvi, F. S. Ladd, J. A. and Bower, W. W. "Experimental & Computational Investigation of Supersonic Impinging Jets," AIAA Paper 2000-2236.
4. "Use of Microjets for Active Control Of Resonance in High-Speed Jets," Forum on High Speed Jet Flows, 2001 ASME Fluids Engineering Summer Meeting, New Orleans, June, 2001. *(Invited Talk)*
5. Elavarasan, R.,Venkatakrishnan, L., Krothapalli, A. and Lourenco, L., "Supersonic Twin Impinging Jets", AIAA-2000-0812.
6. Phalnikar, K.A., Alvi, F. S., and Shih, C., "Behavior of Free and Impinging Supersonic Microjets, " AIAA Paper 2001-3047.
7. Shih, C., Alvi, F. S., Lou, H. and Garg. G., "Adaptive Flow Control of Supersonic Impinging Jets," AIAA Paper 2001-3027.
8. Lou, H., Alvi, F. S., Shih, C., Choi, J. and Annaswamy, A., "Active Control of Supersonic Impinging Jets: Flowfield Properties and Closed-Loop Control Strategies," AIAA Paper 2002-2728.

9.3 Technology Transition

We are a primary Boeing partner in a DARPA project on Micro Adaptive Flow Control (MAFC) where supersonic microjets are being used for active control of cavity flows at supersonic speeds. To date, the results have been very promising and microjets are the most effective actuator that also meet the overall system requirements. Further testing for cavity flow control is rapidly proceeding at Boeing, Long Beach. Full-scale tests using supersonic microjets are scheduled to take place in 2005 under Phase III of the DARPA project. The microjets are also one of the primary actuators in an AFRL sponsored project for cavity flow control for the Long Range Strike Aircraft (LRSA). Microjets have also been used very successfully in reducing jet noise emanating cold and hot supersonic jets under work sponsored by the Office of Naval Research; this research shows considerable promise for transition to an aircraft platform. In research sponsored by NASA Langley under the Ultra Efficient Engine Technology (UEET) initiative, supersonic microjets are also being evaluated for separation control in adverse pressure gradients, such those which occur in inlet diffusers and S-ducts. The results to date have been very encouraging in that microjets have been shown to eliminate or delay separation over a range of conditions.

9.4 New Discoveries, Inventions or Patent Disclosures Related to this Work

- A patent disclosure was filed for the use of microjets for controlling supersonic impinging jets; a provisional patent has been granted.
- We are in the process of filing a patent application for the use of microjets in cavity flow control.
- Microjets have also been successfully used for reducing supersonic jet noise and a patent disclosure is also being filed.

Appendix A1

AIAA-2000-2236

To appear in
AIAA Journal (July/August 2003)

Appendix A1

Control of Supersonic Impinging Jet Flows Using Supersonic Microjets

F.S. Alvi, C. Shih, R. Elavarasan, G. Garg and A. Krothapalli
Department of Mechanical Engineering
Florida A & M University and Florida State University
Tallahassee, FL

Control of Supersonic Impinging Jet Flows Using Supersonic Microjets

F. S. Alvi[§], C. Shih[†], R. Elavarasan[*], G. Garg[¶] and A. Krothapalli[‡]

Department of Mechanical Engineering
2525 Pottsdamer Street
Florida A&M University and Florida State University
Tallahassee, FL 32310

Supersonic impinging jets, such as those occurring in the next generation of STOVL aircraft, generate a highly oscillatory flow with very high unsteady loads on the nearby aircraft structures and the landing surfaces. These high pressure and acoustic loads are also accompanied by a dramatic loss in lift during hover. Previous studies of supersonic impinging jets suggest that the highly unsteady behavior of the impinging jets is due to a feedback loop between the fluid and acoustic fields, which leads to these adverse effects. In this paper, a unique active control technique was attempted with the aim of disrupting the feedback loop, diminishing the flow unsteadiness and ultimately reducing the adverse effects of this flow. Flow control was implemented by placing a circular array of 400-micron diameter supersonic microjets around the periphery of the main jet. This control approach was very successful in disrupting the feedback loop in that the activation of the microjets led to dramatic reductions in the lift loss (40%), unsteady pressure loads (11 dB) and nearfield noise (8 dB). This relatively simple and highly effective control technique makes it a suitable candidate for implementation in practical aircraft systems.

1. INTRODUCTION

An understanding of the impinging jet flowfield is necessary for the design of efficient Short Take-off and Vertical Landing (STOVL) aircraft. When such STOVL aircraft are operating in hover mode, i.e. in close proximity to the ground, the downward-pointing lift jets produce high-speed, hot flow that impinges on the landing surface and generates the direct lift force. It is well known that in this configuration several flow-induced effects can emerge, which substantially diminish the performance of the aircraft. In particular, a significant lift loss can be induced due to flow entrainment by the lifting jets from the ambient environment in the vicinity

---

§Associate Professor, Senior Member AIAA
† Professor, Chairman, Associate,Fellow AIAA
*Post-doctoral Research Associate, Member AIAA
¶Graduate Research Assistant, Student Member AIAA
‡ Don Fuqua Eminent Professor, Associate Fellow AIAA

of the airframe. Other adverse phenomena include severe ground erosion on the landing surface and Hot Gas Ingestion (HGI) into the engine inlets. In addition, the impinging flow field usually generates significantly higher noise levels relative to that of a free jet operating under similar conditions. Increased OverAll Sound Pressure Levels (OASPL) associated with the high speed impinging jets can pose an environment pollution problem and adversely affect the integrity of structural elements in the vicinity of the nozzle exhaust due to acoustic loading. Moreover, the noise and the highly unsteady pressure field are frequently dominated by high-amplitude discrete tones, which may match the resonant frequencies of the aircraft panels, thus further exacerbating the sonic fatigue problem.

These problems become more pronounced when the impinging jets are supersonic, the operating regime of the STOVL version of the future Joint Strike Fighter (JSF). In addition, the presence of multiple impinging jets can potentially further aggravate these effects due to the strong coupling between the jets and the emergence of an upward-moving fountain flow flowing opposite to the lift jets[1]. A schematic of a generic STOVL aircraft with multiple lift/impinging jets is shown in Fig. 1 where various regions where these problems might occur have been indicated.

1. 1 The Feedback Loop

In order to minimize their adverse influence on aircraft performance, it is evident that the undesirable effects of supersonic impinging jets need to be controlled. However, before one can devise an effective control scheme to eliminate these detrimental characteristics one must have a fundamental understanding of the principal physical mechanisms governing these flows. The acoustic properties of single supersonic impinging jet flow field have been investigated by a

number of researchers, including Powell[2], Neuwerth[3] and Tam[4]. These studies conclusively demonstrated that the unsteady properties of impinging jet flows are dominated by the presence of discrete impingement tones. These high-amplitude tones are generated by highly coherent instability waves due to the emergence of a self-sustained feedback loop. For a detailed discussion of the feedback mechanism, the reader is referred to the above articles. Very briefly, large-scale vortical structures in the jet shear layer impingeme on the wall and generate coherent pressure fluctuations, which result in acoustic waves of significant intensity. These acoustic waves travel through the ambient medium and, upon reaching the nozzle (a region of high receptivity), excite the shear layer of the jet. This leads to the generation of a new set of enhanced instability waves, which rapidly evolve into large-scale vortical structures, thus closing the feedback loop. A similar feedback mechanism is also responsible for the production of discrete tones such as *screech tones* which are conspicuously present in non-ideally expanded (i.e. over or under-expanded) and *edge tones* generated due to the presence of an 'edge' in the jet hydrodynamic field . In fact, the feedback mechanism responsible for discrete tones was first clearly articulated by Powell in classic papers on jet noise[5] and on the feedback loop responsible for edge tones[6].

Flow properties of high speed impinging jets have also been examined by a number of investigators including Donaldson & Snedeker[7], Carling & Hunt[8] and Lamont and Hunt[9], among others. These studies mainly emphasized the mean properties of this flow with most of the measurements limited to mean surface properties, such as the pressure distributions on the impingement surface. Recently, Krothapalli et al.[10] conducted an extensive investigation to obtain a better understanding of the physics governing some of the mean and unsteady properties of such flows. One of the main findings of their work was the intimate connection between the

discrete impinging tones and the highly unsteady, oscillatory behavior of the impinging jet column. They demonstrated that, through the generation of large-scale structures in the jet shear layer, the feedback phenomenon might also be responsible for lift loss on the surfaces in the vicinity of the nozzle. These structures induce higher entrainment velocities that lead to lower pressures on surfaces in the jet vicinity and, consequently, a significant loss in lift.

In a companion study, Alvi & Iyer[11] noted the emergence of discrete peaks in the spectra of the unsteady surface pressures, which match the impinging tone frequencies in the near-field acoustic measurements. This suggests that these feedback loop-driven flow instabilities are also responsible for the unsteady loads on the ground plane. In some cases these measured unsteady loads were extremely high, as high as 190 dB. When coupled with the high temperatures associated with lifting jets, such high loads can severely aggravate the ground erosion problem.

1. 2 Control of the Feedback Loop - Prior Attempts

Based on the above discussion, it is apparent that, to effectively eliminate these unwanted effects of impinging jet flows, one must reduce the highly unsteady behavior of the impinging flow by weakening the feedback loop. There are various potential approaches for disrupting the feedback loop and achieving a measure of control of the unsteady properties of this flow. For example, one could: (1) Intercept the upstream propagating acoustic waves so that they can not complete the feedback loop, and/or (2) Manipulate the shear layer (for example, increase its thickness) near the nozzle lip hence reducing its receptivity to the acoustic disturbances and/or (3)Disrupt the coherent interaction between the flow instabilities and the acoustic field by 'tickling' the nozzle shear layer using a disturbance at or very near the nozzle exit. The source of these disturbances could in principal be passive, such as those generated by 'tabs' at the nozzle

exit or, they could be active in nature, such as the use of high energy acoustic and/or fluidic sources near the nozzle exit..

Based on these concepts, a number of attempts have been made in the past to suppress the feedback mechanism. For instance, Karamcheti et al.[12] successfully suppressed edge tones in low speed flows, which are governed by a similar feedback mechanism, by placing two plates normal to the centerline of the jet. Motivated by their work, Elavarasan et al.[13] employed a similar technique to attenuate the feedback loop in an impinging jet flow by introducing a control plate near the nozzle exit. Using this approach, they were able to intercept the upstream propagating acoustic waves thus disrupting the feedback loop. As anticipated, attenuation of the loop led to a measurable weakening of the large-scale structures in the jet flow. For selected cases, this passive control approach resulted in a maximum recovery of about 16% of the lift loss relative to an uncontrolled impinging jet. Similarly for a few cases, Elavarasan et al.[13]also reported a reduction of about 6-7 dB in the near-field OASPL. Glass[14] and Poldervaart et al.[15] used similar passive control techniques with limited success. In a series of experiments reported by Samimy et al. [16] and Zaman et al. [17], the effect of passive 'tabs' on the aeroacoustic properties of supersonic jets was also investigated. Although the tabs were able to attenuate the screech tones, significant reduction in the OASPL was achieved by using multiple tabs[16] which also resulted in significant thrust loss, as high as 12%[17].

Consequently, although passive control techniques have been able to weaken the feedback mechanism, gains are usually accompanied by a significant cost, such as thrust loss.[16,17] In addition, any significant performance gains are confined to a limited range of operating conditions, especially for impinging jets. This is due to the fact that relatively small changes in the nozzle-to-ground separation (h/d) can lead to significant changes in the magnitude and

frequency of the tones responsible for the flow unsteadiness[11], changes to which passive techniques cannot readily respond. Consequently, any efficient control technique aimed at suppressing the feedback loop must be 'active' and capable of adapting to the shift in frequencies/wavelengths of the modes that lock on to the feedback loop.

In a recent study, Sheplak and Spina[18] used high-speed co-flow to shield the main jet from the near field acoustic disturbances. For a suitable ratio of the main jet and co-flow exit velocity, they measured a reduction of greater than 10 dB in the near-field broadband noise level. In addition to noise reduction, the impinging tones were also significantly suppressed using this approach. Although effective, the high mass flow rates of the co-flowing jet required to achieve this noise reduction— around 20%-25% of the main jet mass flux — limits the practical applicability of this coflow approach. Shih et al.[19] used a counterflowing stream near the nozzle exit to successfully suppress screech-tones of non-ideally expanded jets. They were also able to obtain modest reductions in OASPL, approximately 3-4 dB while enhancing the mixing of the primary jet. However, these active control schemes require additional design modifications and/or high operating power rendering them often impractical for implementation in aircraft.

1.3 Present Approach for Flow Control

In the current program, we are proposing the implementation of a control-on-demand strategy using microactuators in the form of supersonic microjets. These microjets are extremely small and require very low mass flux. Although further details of these microjets are discussed later, we simply note that one of the most significant advantages of using microactuators is that their extremely small size allows these systems to be operated in places where traditional systems cannot work due to either space limitation or a lack of system response.

In principal, by populating the appropriate region on the lift plate, in the vicinity of the nozzle exit for the present case, one could develop a system where the most appropriate microjets would be strategically turned on and off to provide optimal control. The proposed control system would have the advantage that, depending upon the operating and local flow conditions, optimal flow control can be achieved by activating the pertinent supersonic microjets with the appropriate magnitude and frequency (if possible) and at the desired time. In contrast to the traditional passive control methods, the proposed control-on-demand system can be switched on and off strategically. We are presently in the initial stages of implementing the adaptive portion of this technique, i.e. the ability to selectively activate appropriate microjets. Although still preliminary in nature, the results demonstrate considerable promise for implementing adaptive flow control using microjets. The interested reader is referred to Lou et al.[20] for these results. Such a system should not measurably influence the operational performance of the aircraft when it is not needed. The very small size of the hardware and the minimal mass flow rates require minimal power consumption and is expected to result in negligible, if any, thrust loss of the primary jet.

In the present experiments, microjets were made using 400 μm diameter stainless tubes and 16 supersonic microjets were distributed around the nozzle exit (Fig. 3a). Based on the earlier discussion of the feedback loop, it is evident that the presence of these supersonic micro-flow streams can be effective in weakening the loop in a number of ways. First, the microjet streams may play a role in the interception of the upstream propagating acoustic disturbances. Second, these high momentum jets can provide spatial/temporal distortions to the coherent shear-layer instabilities thus disrupting their interactions with the acoustic field. A more detailed description of the microjet hardware is provided in § 2, the experimental methods section.

Finally, it should be noted that the purpose of this study is not to perform a systematic, exhaustive investigation of the microjet system necessary to achieve optimal control over a large parametric space. Rather, in this proof-of-concept study, our aim is to examine the feasibility and potential benefits of using microjets to alleviate the adverse effects of the supersonic impinging jet flowfield. The influence of this control strategy on the flow behavior was studied using flow visualization, microphone measurements and mean and unsteady surface pressure measurements. As the results presented in this paper illustrate, there is convincing evidence that the proposed control strategy is very promising as a means of effectively controlling supersonic impinging jet flow fields.

2. EXPERIMENTAL HARDWARE & TECHNIQUES

The experiments were carried out at the STOVL supersonic jet facility of the Fluid Mechanics Research Laboratory (FMRL) located at the Florida State University. A schematic of the facility with a single impinging jet is shown in Fig. 2. This facility is used primarily to study jet-induced phenomenon on STOVL aircraft hovering in and out of ground effect. Facility details can be found in Wardwell[21] and Krothapalli et al.[10]; only a very brief description is provided here.

The measurements were carried using a shock free, nearly ideally expanded jet issuing from a convergent-divergent (C-D) axisymmetric nozzle. The throat and exit diameters ($\mathbf{d}$, $\mathbf{d_e}$) of the nozzle are 2.54cm and 2.75cm, respectively. The divergent part of the nozzle is a straight-walled conic section with a 3° divergence angle from the throat to the nozzle exit. The nozzle was designed for an exit Mach number of 1.5 and operated at a Nozzle Pressure Ratio (NPR, where NPR = stagnation pressure/ambient pressure) of 3.7 to produce a nominally, ideally

expanded impinging jet. The primary reason for running an ideally expanded jet was to isolate the effect of the impingement tones from screech tones, since the latter only occur in jets operating at off-design conditions. A circular plate of diameter 25.4 cm (~10**d**) was flush mounted with the nozzle exit. The circular plate, henceforth referred to as the 'lift plate', represents a generic aircraft planform and has a central hole, equal to the nozzle exit diameter, through which the jet is issued. A 1m x 1m x 25mm aluminum plate serves as the ground plane; it is mounted directly under the nozzle on a hydraulic lift (see Fig. 2).

The flow induced lift forces were estimated by measuring the mean pressure distribution on the lift plate. This was accomplished by using an array of pressure taps arranged along a radial line on the lift plate. The pressure measurements were obtained by scanning the static pressure ports using a Scanivalve™ system connected to a Validyne™ strain gauge transducer. In addition, high frequency response miniature Kulite™ pressure transducers were also mounted on the lift plate along a radial line, as shown in Fig. 3a and were used to measure the unsteady pressure loads on the lift plate. The lift plate data shown in this paper is obtained from a single Kulite located approximately 35 mm from the nozzle lip. . The unsteady pressure field created by the jet impingement on the ground plane was measured with two additional high frequency 100psi, Kulite™ pressure transducers (model-XCQ-062-100), one at the impingement point on the jet centerline and the other 25mm away from the centerline. The near field acoustic measurements were made using a 0.635cm diameter B&K microphone placed 25 cm away from the nozzle exit oriented 90° to the jet axis. In order to minimize sound reflections during the near-field acoustic measurements, near-by exposed metal surfaces were covered with thick acoustic foam. The flow was visualized using a conventional, single-pass shadowgraph

arrangement where a stroboscopic white-light flash unit with variable pulse frequency of up to 1 kHz was used as a light source.

The microphone and the lift plate surface pressure signals were acquired through National Instruments digital data acquisition cards using LabView™ software. For unsteady measurements, i.e. microphone and Kulite data, 100k points were recorded for each signal. Standard statistical analysis techniques were used to obtain the spectral content and the OverAll Sound Pressure Level (OASPL) from these measurements. The spectral content of the unsteady signals was obtained by segmenting each data record into 100 subgroups with 1k points each and an FFT with a frequency resolution of 68.4Hz was computed for each segment. The 100 FFT's thus obtained were averaged to obtain a statistically reliable estimate of the narrow-band noise spectra. The estimated uncertainty associated with the unsteady lift plate pressure, P_{rms}, is $\pm$ 0.02 psi while the rms intensities of the ground plane pressures was estimated to be accurate within $\pm$ 0.2 psi. Note that when the unsteady pressures are expressed in dB, a fixed error in psi translates into different errors in dB, depending upon the overall value of P_{rms}. The P_{rms} values on the lift plate are around 160dB (see Fig. 8) for the cases of interest, which results in an uncertainty of approximately 0.6dB. Similarly, the dynamic pressure levels on the ground plane are in the range of 180dB, which also translates into an uncertainty of approximately 0.6dB. The microphone signal was measured with an estimated uncertainty of $\pm$ 1 dB.

The main controlling parameter in the experiment was the ground plate height h with respect to the nozzle exit, which was varied from 2**d** to 60**d**. As stated earlier, the experiments discussed here were conducted at NPR=3.7, which corresponds to a nearly ideally expanded primary jet flow. The jet stagnation temperature was maintained at 20°C $\pm$ 2°C. The nominal

exit Reynolds number at exit of the nozzle was $7x10^5$ (based on exit velocity and nozzle diameter).

Active flow control was implemented using sixteen microjets, flush mounted circumferentially around the main jet as shown in the Fig. 3a. The jets were produced using 400 μm diameter stainless tubes, mounted on the lift plate with an inclination of approximately 20° with respect to the primary jet axis. The supply for the micro jets was provided from a compressed air cylinder through a main and four secondary plenum chambers (Fig. 3b). The high-pressure air was passed through a micron-sized filter to prevent the micronozzles from becoming clogged. The secondary plenum chambers ensured that the flow coming out of the micro jets were relatively free of unsteadiness. The microjets were connected to the secondary plenum chamber through four solenoid-controlled valves in such a way that any four microjets can be controlled (on/off) individually. The microjets were operated at an NPR of approximately 7. At this operating condition, the combined mass flow rate of all sixteen microjets was well below 0.5 % of the primary jet mass flux.

3. DISCUSSION OF RESULTS

3.1 Impinging Jet Without Control

Fig. 4 shows instantaneous shadowgraph images of the impinging jet flowfield at h/d = 4.5 with and without control while Fig. 5 shows phase-averaged images under the same conditions. (Note that all linear dimensions in this paper are non-dimensionalized by the nozzle throat diameter, **d**) Although both cases – with and without control – are shown here, a discussion of the effect of control is delayed until the next sub-section. The instantaneous shadowgraph for the uncontrolled case, i.e. microjets off, in Fig. 4a clearly shows the presence of

multiple, strong, acoustic waves. These waves signify the presence of impinging tones and, as seen in the image, they impinge and reflect from nearby surfaces – represented by the lift plate in the present case. Concomitant with the appearance of the acoustic waves is the emergence of large-scale structures in the jet shear layer. Such structures can be clearly seen in both the instantaneous and phase-averaged, shadowgraphs in Figs. 4a and 5a where they have also been marked for clarity. The phase-averaged image was obtained by triggering the light source at a sub-harmonic of the dominant impinging tone frequency such that 15-16 pulses are averaged per frame to produce the phase-averaged image. As discussed in the introduction, such large-scale structures, not normally observed in high-speed jets, significantly increase jet entrainment velocities[10,13] leading to lift loss. Furthermore, the presence of such distinct, stationary structures in the phase-averaged images visually indicates that, in addition to the acoustic field, the unsteady flow properties are also dominated by periodic, discrete frequency disturbances, a fact confirmed by the quantitative measurements discussed next.

The spectral content of the unsteady fluid and acoustic properties is examined via the narrowband spectra of the nearfield microphone, unsteady lift plate and ground plane pressures shown in Figs. 6 and 7 for h/d = 3 and 4.5 in, respectively. (In these, as in all subsequent similar plots, the fluctuating pressures have been expressed in decibels, dB, using a 20 μPa reference). Although data for the ground plane is only shown for the Kulite transducer located on the impinging jet centerline, the behavior of the unsteady ground plane pressures at other transducer locations is very similar. One of the most significant features in both plots is the presence of discrete, high amplitude, multiple peaks that are indicative of impingement tones due to the feedback loop. An examination of the microphone and unsteady pressure data for a fixed height reveals that the resonant tones occur at identical frequencies for all three transducer locations.

This supports our earlier observation based on the visual evidence in Fig. 5a and further confirms the global nature of the flow oscillations generated by the feedback loop. A comparison of spectra for h/d = 3 with h/d = 4.5 in Fig. 6 and Fig. 7, respectively, shows that the frequencies at which these tones occur change with nozzle height. Although not shown here, a similar shift in frequencies is also observed with respect to NPR[11]. Furthermore, since the unsteady properties of this flowfield – as is the case for most flows governed by a feedback loop – are extremely sensitive to local boundary conditions, experiments conducted at the same facility, under the same nominal conditions[20], can display some variations in the unsteady properties, such as a shift in the tone frequencies and amplitudes. The strong dependence of the unsteady flowfield on the operating conditions, suggests that an efficient control technique must be able to adapt to such changes in the feedback loop for optimal control.

The intensities of the unsteady pressure fluctuations (P_{rms}) on the lift and ground planes as well as the nearfield noise are shown in Fig. 8 as a function of the ground plane height. The rms pressure levels on the ground plane have the highest magnitude, in the 180–190 dB range (corresponding to $P_{rms} \approx 3$ to 9 psi), which is to be expected since the primary jet flow directly impinges on the ground plane. Such high unsteady loads on the ground plane can cause significant ground erosion of the landing surface, especially when combined with the thermal loads generated by the impingement of hot lift jets of STOVL aircraft. The unsteady pressure loads on the lift plate, in the 160-165 dB range in the present case (loads as high as 175-180 dB have been measured for other conditions) are also significant and can lead to structural fatigue of nearby aircraft surfaces.

The high entrainment rates due to the presence of large scale structures, such as those visible in Figs. 4a and 5a, lead to low pressures on the lift plate surface resulting in a suckdown

force or lift loss. The lift loss variation with height can be seen in Fig. 9 for the present case. This figure shows the lift loss behavior with (open symbols) and without (filled symbols) microjet control, where the negative lift force has been normalized by the primary jet thrust. This plot illustrates the dramatic lift loss for the uncontrolled case, as high 60% or more for small heights, which can occur due to jet impingement. The plot also shows that, at least in terms of lift loss, ground effect become negligible for $h/d > 9$.

3.2 Impinging Jet With Microjet Control

In light of the detrimental effects of the feedback loop, an attempt to disrupt this feedback was made with the hope of alleviating some of these undesirable properties. In this study, flow control was applied by simply activating the supersonic microjets placed at the nozzle exit. It was anticipated that the penetration of the microjets into the primary jet shear layer at the nozzle exit would sufficiently modify the shear layer properties, including perhaps its stability characteristics, to disrupt this loop. .

Fig. 10 shows a representative schlieren image of one of the 400μm microjets used to control the feedback loop. The microjet is operating at a pressure of approximately 100 psia and the flow is clearly supersonic as demonstrated by the characteristic periodic shock-cell structure usually observed in much larger supersonic jets. Judging from the presence of the shock cells, the supersonic core of the jet appears to extend at least 10-12 jet diameters downstream of the nozzle exit. A more detailed description of the supersonic microjets, their behavior and the technique used for visualizing may be found in Phalnikar et al[22]. Given the high momentum associated with the supersonic microjets and the large supersonic core length, it is anticipated that they will serve as effective 'actuators' capable of penetrating the primary jet shear layer and modifying its properties. Before discussing the results of microjet flow control, we note that no

attempt was made in the present study to actively modulate or manipulate the microjets in response to the local flow conditions. The results presented here only compare the relevant properties with and without the microjets.

A comparison of the instantaneous shadowgraphs without control, Fig. 4a, to that with control, Fig. 4b, shows the dramatic effect of activating the microjets. First, the strong acoustic waves present for the uncontrolled case have been eliminated when the microjets are activated. Furthermore, the large-scale shear-layer structures readily visible in Fig. 4a and Fig. 5a have also been significantly reduced, if not entirely eliminated, in Figs. 4b and 5b. As anticipated, the elimination of the large-scale structures is accompanied by a reduction in the jet spreading rate and a narrowing of the jet column as seen in Fig. 5b. Also visible in Fig. 5b are the 'streaks' generated by the supersonic microjets. Such streaks are very similar to those generated by tabs[16-17] and tape elements on the nozzle surface[24]; they have been used as indication of the presence of substantial streamwise vorticity. It is worth noting that the presence of such tabs and the concomitant generation of streamwise vorticity have led to a suppression of screech tones[16, 23]; this aspect will be very briefly discussed later in this paper.

Given the striking effect of the microjets observed in the shadowgraphs, one expects the unsteady flow properties to be similarly influenced. This is indeed the case as seen in the near field narrow band frequency spectra for h/d = 4.5 in Fig. 11. Here Fig. 11a and 11b show the ground and lift plate unsteady pressures, respectively while Fig. 11c shows the nearfield microphone spectrum. Upon comparing the control data (solid lines) to the uncontrolled case (broken lines), one observes that the distinct tones present in the uncontrolled impinging jet are either eliminated or significantly diminished by the activation of microjets. In addition, and perhaps more significantly, the attenuation in the discrete tones is accompanied by a broadband

reduction in the spectral amplitudes. This broadband reduction is observed for all three plots due to lower acoustic and hydrostatic fluctuations, which suggests a *global* decline in the unsteady behavior of this flow.

A plot of the overall unsteady pressure levels (P_{rms}) on the lift plate at different heights and the influence of microjet control at each location are shown in Fig. 12. Note that the error bars shown at selected data points are representative of the errors over the range of conditions shown here. This figure plainly shows that the fluctuating loads on the lift plate are reduced with the activation of microjet control. However, the magnitude of reduction is strongly dependent upon h/d, the ground plane distance. Whereas a very substantial reduction of more than 10 dB is achieved at h/d = 4.5, the unsteady load is only reduced by 2 dB or so at h/d = 3.5. The non-uniform reductions illustrate that the control technique is not equally efficient at all heights, presumably because it does not track changes in the feedback loop due to a variation in h/d. The reductions in the overall unsteady pressure and acoustic intensities on the lift and ground planes and for the nearfield microphone measurements are summarized in Fig. 13. Similar to the behavior observed in Fig. 12, the reductions in flow unsteadiness due to microjet control are strongly dependent on the ground plane height. However, notably, the overall trends for all three measurements are very similar with the greatest reductions achieved at h/d = 3 and 4.5. Once again, the non-monotonic influence of control suggests that efficient control of this flow requires an adaptive control approach where the microjets can be actively manipulated to provide optimal control at all heights.

As observed earlier in this paper, the unsteady behavior of the impinging jet, including the hydrodynamic and acoustic loads generated by this flowfield, is highly sensitive to the local boundary conditions. Hence, these properties are not only a function of the operating conditions,

such as h/d or NPR as shown in Figs. 8 and 13, but can also change somewhat when an experiment is repeated under the same conditions. Consequently, the efficacy of the control technique, e.g. it's variation with h/d (see Fig. 13) can also vary between experiments, even if there are very minor changes in the flow conditions. However, upon repeating these experiments a number of times, our results consistently show that although minor shifts in the performance (with h/d) can occur due to minor changes in the flow properties, the changes are global in nature, i.e. they occurs at all measurement locations – the lift plate, ground plane and the near-field acoustics. The error bars shown on Fig. 13 roughly span the extent of such variations observed for the present study. This dependence once again emphasizes the need for adaptive control (see reference 20 for further discussion).

Finally, we present the effect of microjets on the lift loss behavior of this flow. Since the loss in lift is due to the low pressures created on the underside of the airframe—the lift plate in this study—due to flow entrainment by the large-scale structure, it is logical to assume that elimination or reduction of these structures should also result in a reduction in lift loss. Measurements of the mean static pressures on the lift plate surface show that the activation of supersonic microjets leads to an increase in the surface pressures, i.e. to lower vacuum/suction pressures on the lower surfaces of the airframe. This reduction in the vacuum pressures on the lift plate translates to a reduction in lift loss as seen in Fig. 9. A comparison of the open symbols (with control) to filled symbols (no control) in Fig. 9 shows that the activation of microjets leads to a significant reduction in lift loss. The maximum lift loss recovery occurs for small heights, e.g. the lift loss is reduced by more than 40% at h/d = 2, with the influence becoming less significant for larger heights. This behavior is expected and desirable since the largest losses in lift also occur for small separations. Fig. 14 summarizes the lift loss reduction variation with

h/d. The reduction in lift loss in this plot behaves in a manner similar to the trends observed in Fig. 13 on the influence of microjets on unsteady pressures and noise; this plot confirms that control effectiveness varies non-uniformly with h/d. Moreover, a comparison of Fig. 14 to the reduction in P_{rms} on the lift plate shown in Fig. 13 shows the similarity between the two plots where the local minima and maxima in lift loss recovery occurs at roughly the same heights as the local minima and maxima in the reduction in the fluctuating pressures (Fig. 13). This again suggests a strong correlation between the strength of the acoustic waves impinging on the lift plate (see Fig. 4a), which are expected to be the primary source of unsteady loads on the lift plate, and the large scale structures, which lead to lift loss. Given the global nature of the unsteady properties such a connection is expected.

The non-uniform behavior in the reductions in lift loss, fluctuating pressures and noise, reinforces the notion that an adaptive control strategy is necessary to achieve *optimal* performance at all operating conditions. Nevertheless, even without adaptive control, microjets are a rather effective control tool at most heights where they result in notable reductions in unsteady loads in the range of 4 to 10 dB and a lift loss recovery of 20 % or higher for small h/d.

3.3 Physical Mechanisms Behind Microjet Control

Before concluding, we very briefly discuss the possible physical mechanisms that may be responsible for the efficient disruption of the feedback loop by microjets. As mentioned earlier, there are many potential ways by which one can disrupt the feedback loop. The interception of the upstream propagating acoustic waves before reaching the shear layer at the nozzles exit was one of the possible ways the feedback may be interrupted. However, we believe that the although the microjets may provide some shielding of the shear layer at the nozzle exit, given the

extremely small size of the microjets, the shielding effect will not be significant. The disruption of the spatial coherence of the interaction between the acoustic waves and the shear layer at the nozzle exit is another such possible mechanism. Our results suggests that the spatial extent of the disruption by the microjets does play some role in reducing the efficacy of the feedback mechanism, in that when the number of microjets were reduced beyond a certain threshold, the feedback loop was minimally disrupted. However reducing the number of microjets also reduces the amount of streamwise vorticity introduced into the primary jet, which as discussed next, may be the significant mechanism behind the success of this technique. Hence, at present, it is difficult to quantify the exact extent to which the disruption of the spatial coherence plays a role except to say that it does play *some* role in attenuation of the feedback.

We believe that the most significant reason for the weakening of the feedback is due to the redirection of some of the significant azimuthal vorticity – manifested as large-scale structures in the shear layer – into streamwise vorticity as a result of microjet injection. This hypothesis is supported by preliminary measurements of the streamwise vorticity in the shear layer, which revealed that the activation of microjets leads to the generation of significant streamwise vorticity. The streamwise vorticity —manifested in the form of pairs of counter-rotating vortices corresponding to the microjet locations — is generated at the expense of the azimuthal vorticity thereby weakening the large-scale structures, hence the feedback loop. In order to shed some light on the role of microjets relative to more traditional approaches such as the use of tabs, a limited number of experiments were conducted using sixteen 'microtabs' instead of microjets. These microtabs were made by using stainless wires of the same diameter as the microjets, placed at the nozzle exit, protruding five (microjet) diameters into the jet shear layer. These

microtabs produced almost no reduction for the ideally-expanded impinging jet, suggesting that the flow physics behind the present technique is different.

Although many questions remain unanswered at present, it is clear from the results presented here that microjet control is a very effective and potentially useful control approach for impinging jets. It is also likely that more than one mechanism, e.g. redirection of the azimuthal vorticity, disruption of the spatial coherence of the interaction, among others, may play a role in the physics behind this method. Presently, we are conducting experiments that are more detailed in order to better understand some of these physical mechanisms and their relative influence.

4. CONCLUDING REMARKS

Previous investigators have unequivocally established the intimate connection between the fluid dynamic and acoustic properties of the impinging jet flowfield, an interaction that occurs through a feedback loop. The occurrence of this feedback loop was also hypothesized to be responsible for a number of performance diminishing effects for STOVL aircraft[10].

The objective of this research program is to develop a practical control strategy to enhance the STOVL aircraft performance under realistic operating conditions by taking advantage of our understanding of the aeroacoustic properties of this flow. In this paper, we explored a novel control technique utilizing supersonic microjets to disrupt the feedback mechanism in supersonic impinging jet flows. The disruption of this feedback mechanism through this control technique resulted in significant performance gains relative to the uncontrolled case. Lift loss was substantially reduced, by as much as 40%, accompanied by a 10-11 dB reduction in the fluctuating pressure loads on the lift and ground surfaces for certain conditions. Similarly, the

overall noise levels were substantially reduced and the discrete, high-amplitude impinging tones ubiquitous in such flows were either eliminated or significantly attenuated.

However, the performance enhancements due to microjet control were not uniform over the entire parametric space. We believe this is due to the fact that the microjets are presently used in a 'passive' mode. Due to the dynamic nature of this flow, the properties of the flow-acoustic interactions change with operating conditions. Hence, an optimal control technique must be able to adapt to these changes. We are presently exploring ways of actively manipulating the supersonic microjets to respond to the changing environment. We are also developing on-demand control methods using integrated sensors and supersonic microjet actuators. In future studies, we expect to implement these control techniques in more realistic planform geometries utilizing single and dual supersonic impinging jets.

5. ACKNOWLEDGEMENTS

Our research program on STOVL aircraft jet induced effects is supported by NASA Ames Research Center (Technical monitor - Mr. Doug Wardwell), Air Force Office of Scientific Research (Technical Monitor – present: Dr. John Schmisseur; previous, Dr. Steven Walker) and The Boeing Corporation. We also thank the students and staff at FMRL for their help in conducting these experiments, especially Mr. K. Phalnikar for characterizing the supersonic microjets and Mr. H. Lou for editing some of the figures.

6. REFERENCES

1. Elavarasan, R., Ventkatakrishnan, L., Krothapalli, A. and Lourenco, L, " Supersonic Twin Impinging Jets," AIAA Paper 2000-0812, presented at the 38th AIAA Aerospace Sciences Meeting and Exhibit, Reno, NV, Jan. 10-13, 2000.
2. Powell, A., "The Sound-Producing Oscillations of Round Underexpanded Jets Impinging on Normal Plates", *J. Acoust. Soc. Am.*, 83 (2), 1988, 515-533.
3. Neuwerth, G.," Acoustic Feedback of a subsonic and Supersonic Free Jet which Impinges on an Obstacle", NASA TT F-15719, 1974.
4. Tam, C.K.W., and Ahuja, K.K., "Theoretical model of discrete tone generation by impinging jets", *J. Fluid Mech.*, Vol. 214, 1990, pp 67-87.Powell, A., "On the Mechanism of Choked Jet Noise", *Proc. Phys .Soc. London*, Section B66, 1953, pp. 1039-1057.
5. Powell, A., "On the Mechanism of Choked Jet Noise", *Proc. Phys .Soc. London*, Section B66, 1953, pp. 1039-1057.
6. Powell, A., "On Edge tones and Associated Phenomena", *Acoustica*, **3**, 1953, pp. 233-243.
7. Donaldson, C. DuP. and Snedeker, R.S., "A Study of Free Jet Impingement. Part 1. Mean Properties of Free and Impinging Jets", *J. Fluid Mech.*, 45, 1971, 281-319.
8. Carling, J. C. and Hunt, B.L., "The Near Wall Jet of a Normally Impinging, Uniform, Axisymmetric, Supersonic," *J. Fluid Mech.*, 66, 1974, 159-176.
9. Lamont, P.J., and Hunt, B.L., "The Impingement of Underexpanded Axisymmetric Jets on Perpendicular and Inclined Flat Plates," *Journal of Fluid Mechanics*, Vol. 100, 1980, 471-511.
10. Krothapalli, A., Rajakuperan, E. Alvi, F. S. and Lourenco, L., "Flow field and Noise Characteristics of a Supersonic Impinging Jet," *Journal of Fluid Mechanics,* Vol. 392, August 1999, pp. 155-181.

11. Alvi, F S. and Iyer, K. G., "Mean and Unsteady Flowfield Properties Of Supersonic Impinging Jets With Lift Plates", AIAA Paper 99-1829, presented at the 5th AIAA/CEAS Aeroacoustics Conference, May 1999.

12. Karamcheti, K., Bauer, A.B., Shields, W.L., Stegen, G.R., And Woolley, J.P., "Some Features of an Edge Tone Flow Field", NASA SP 207, 1969, pp275-304.

13. Elavarasan, R., Krothapalli, A., Venkatakrishnan, L. and Lourenco, L., " Suppression of self-sustained oscillations in a supersonic impinging jet", *AIAA Journal*, Vol. 39, No. 12, 2001, pp. 2366-2373 Also see, Elavarasan R., Venkatakrishnan, L., Krothapalli, A. and Lourenco, L., "A PIV study of a supersonic impinging jet," *Journal of Visualization*, Vol. 2, No.3/4, 213-222, 2000.

14. Glass, D.R., "Effect of acoustic feedback on the spread and decay of supersonic jets," *AIAA Journal*, Vol.6, No.6, 1968, pp1890-1897.

15. Poldervaart, L.J., Wijnands, A.P.J., vanMoll, L.H.A.M., and vanVoorthuisen, E.J., "Modes of vibration", *J. Fluid Mech*, Vol. 78, 1976, pp.859-862.

16. Samimy, M. Zaman, K. B. M.Q. and Reeder, M. F., "Effect of Tabs on the Flow and Noise Field of an Axisymmetric Jets," *AIAA Journal*, Vol.31, No.4, 1993, pp. 609-619.

17. Zaman, K. B. M.Q., Reeder, M. F. and Samimy, M. "Control of an Axisymmetric Jet Using Vortex Generators," *Physics of Fluids*, Vol. 6, No. 2, February 1994, pp. 778-793.

18. Sheplak, M. and Spina, E.F., "Control of high-speed impinging-jet resonance", *AIAA Journal*, Vol.32, No.8, 1994, pp1583-1588.

19. Shih, C., Alvi, F. S., and Washington, D., "Effects of Counterflow on the Aeroacoustic Properties of a Supersonic Jet," *AIAA Journal of Aircraft*, Vol. 36, No. 2, March/April 1999, pp. 451-457.

20. Lou, H., Alvi, F. S., Shih, C., Choi, J. and Annaswamy, A., "Active Control of Supersonic Impinging Jets: Flowfield Properties and Closed-loop Strategies" AIAA Paper 2002-2728, 1st AIAA flow Control conference and Exhibit, St. Louis, MO, June 2002.

21. Wardwell, D. A., Hange, C., Kuhn, R. E., and Stewart, V.R., "Jet-Induced Ground Effects on a Parametric Flat-Plate Model in Hover", NASA TM 104001, 1993.

22. Phalnikar, K., Alvi, F. S., and Shih, C., "Behavior of Free and Impinging Supersonic Microjets," AIAA Paper 2001-3047, Anaheim, CA, June 2001.

23. Krothapalli A., Strykowski P. J. and King C. J., "Origin of Streamwise Vortices in Supersonic Jets," *AIAA Journal*, Vol. 36: No. 5, 1998, pp. 869-872.

24. Tanna, H. K. "An Experimental Study of Jet Noise, Part II, Shock Associated Noise," *Journal of Sound and Vibration*, Vo. 50, No. 3, 1977, pp. 429-444.

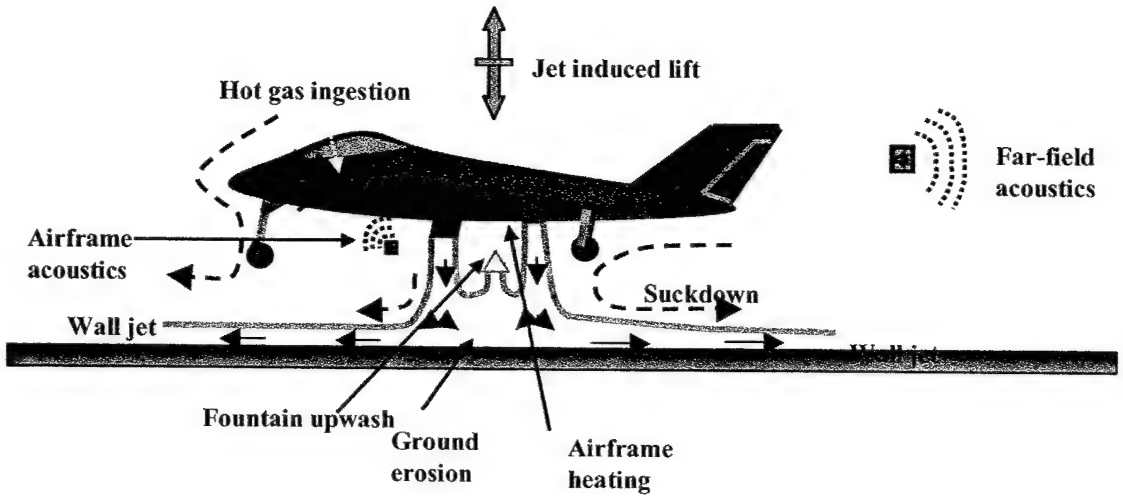

Fig. 1 - Flowfield created by the propulsion system around a STOVL aircraft.

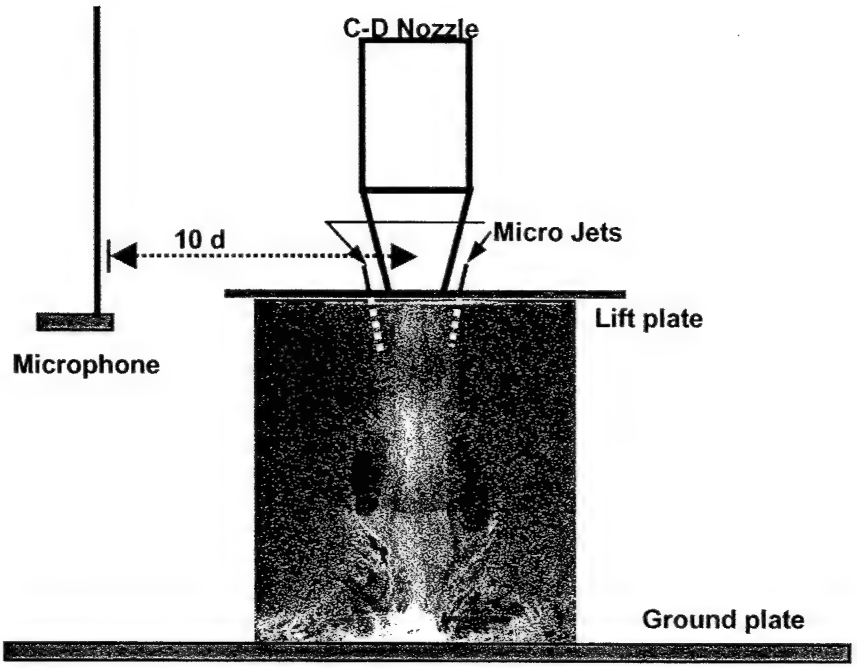

Fig. 2 - Schematic of the experimental arrangement.

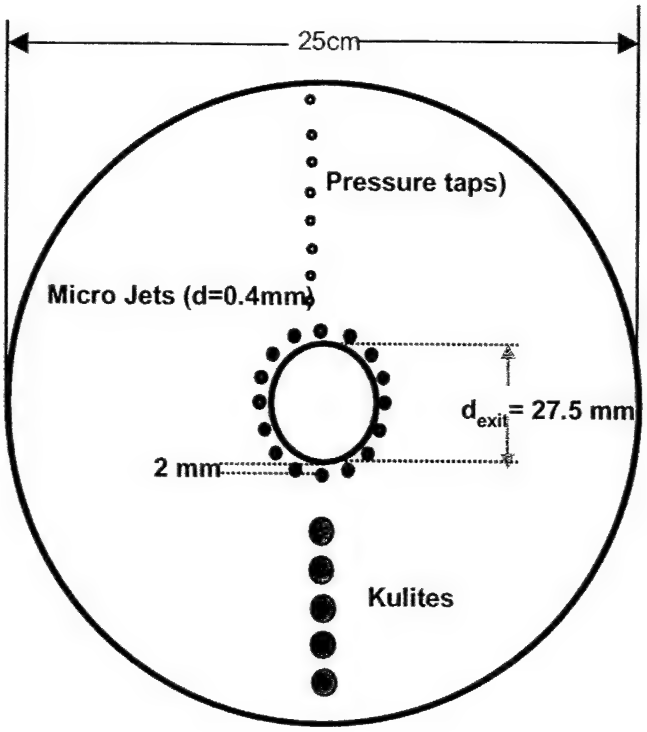

Fig. 3a - Geometry of the lift plate and microjets.

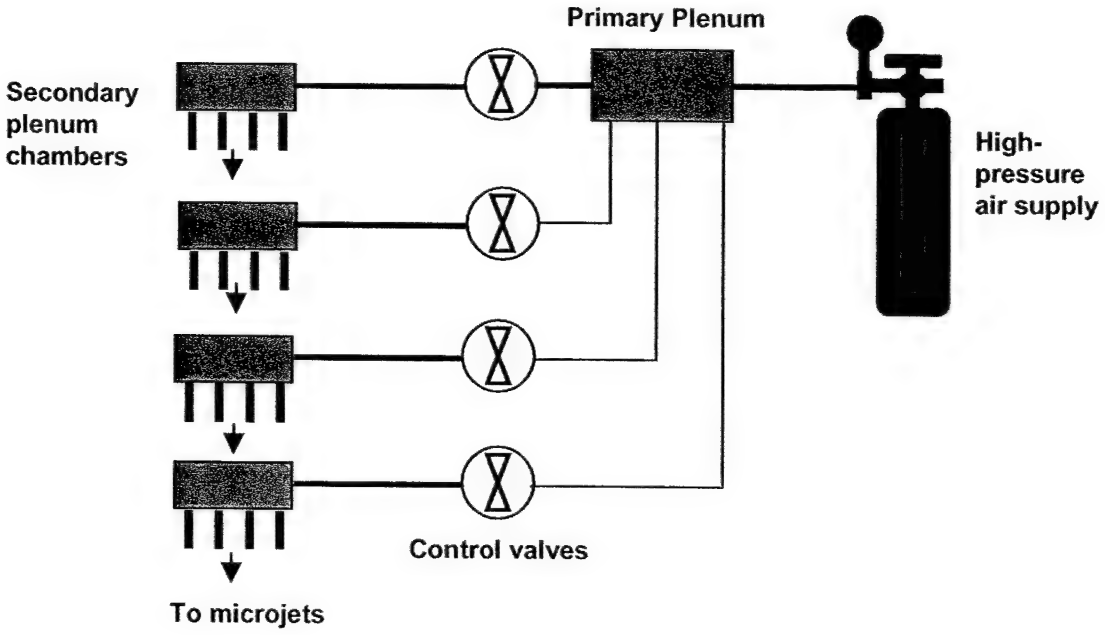

Fig. 3b - Microjets supply assembly.

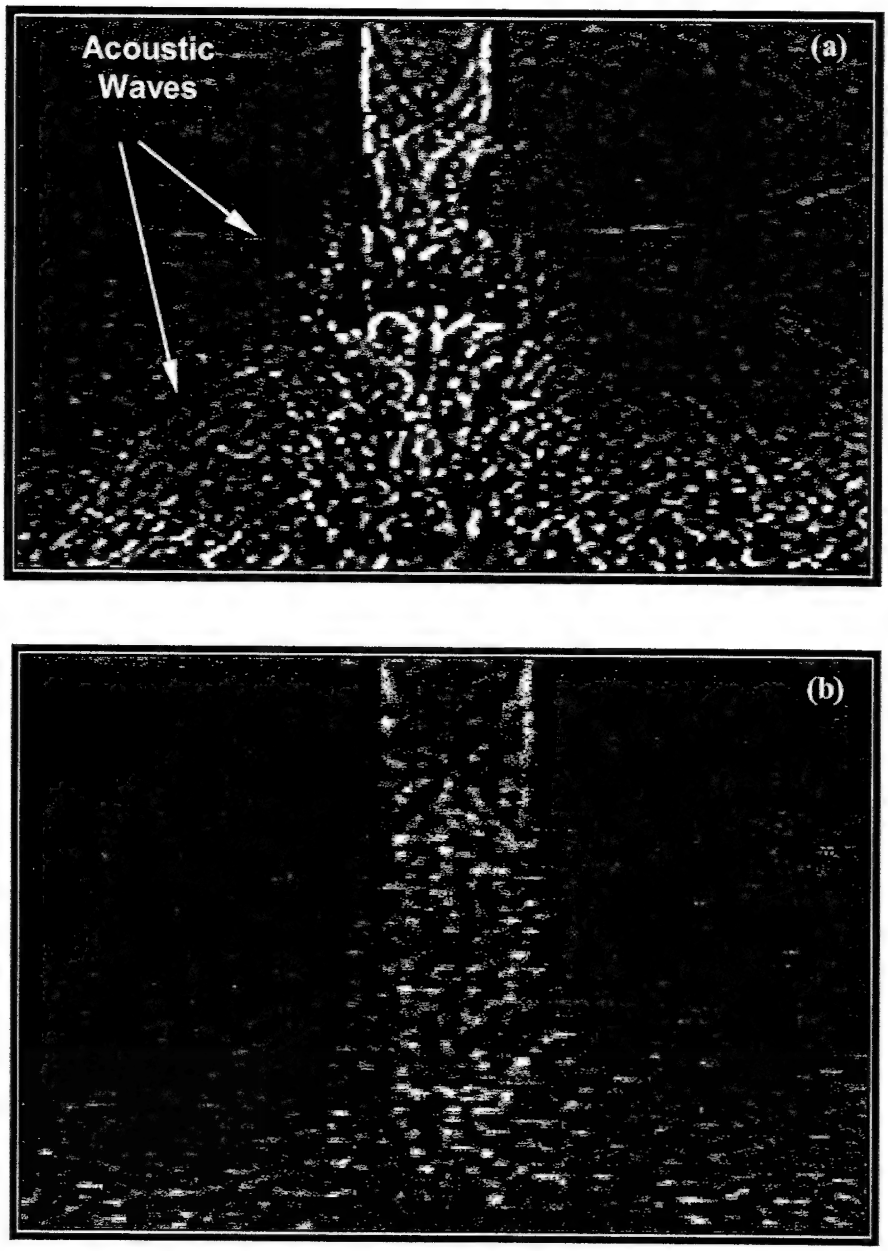

Fig. 4 - Instantaneous shadowgraph images, NPR = 3.7, h/d = 4.5.
a) No control; b) With microjet control.

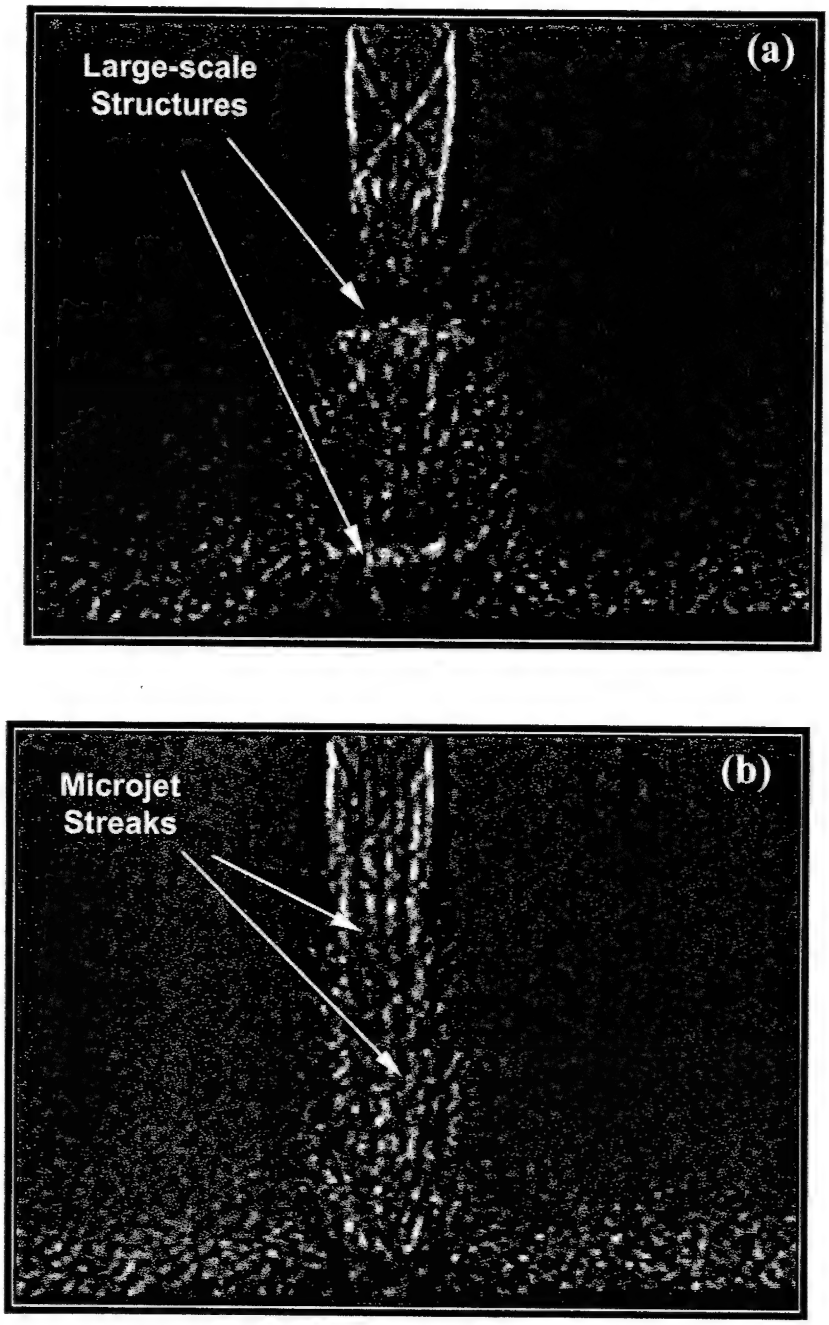

Fig. 5 – Phase-averaged shadowgraph images, NPR = 3.7, h/d = 4.5.
a) No control; b) With microjet control.

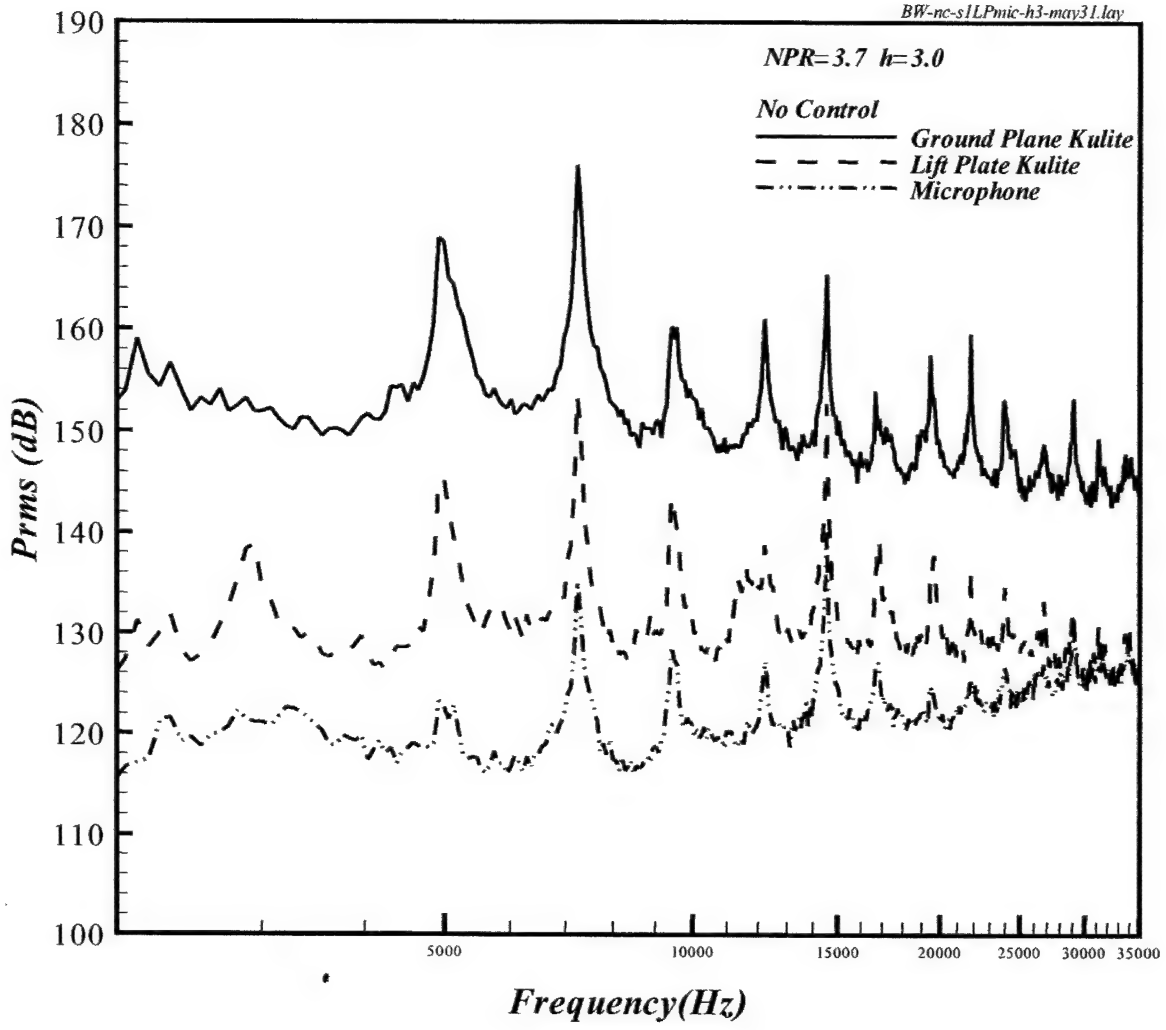

Fig. 6 - Unsteady surface pressure and microphone spectra for NPR = 3.7, h/d = 3.

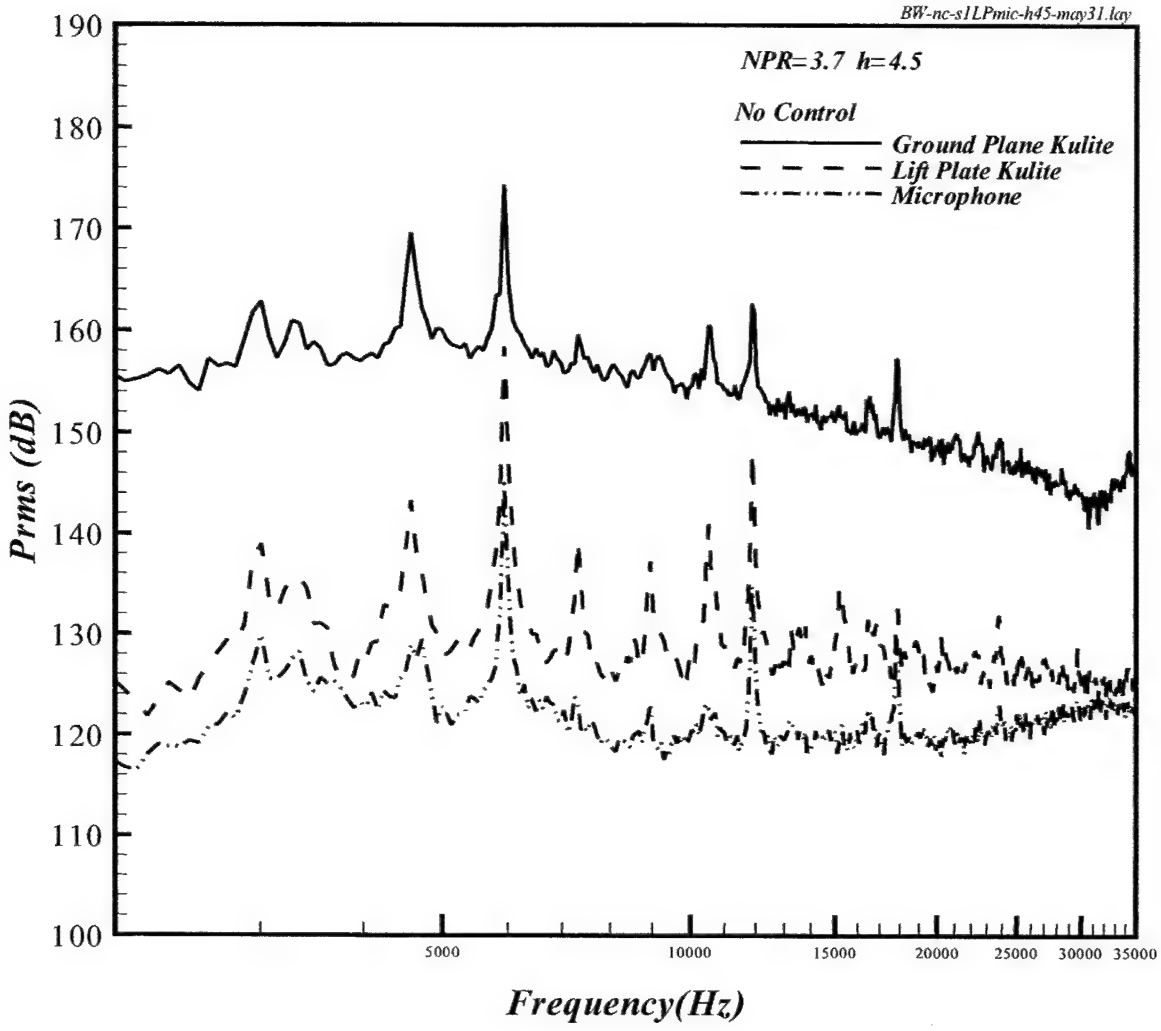

Fig. 7 - Unsteady surface pressure and microphone spectra for NPR = 3.7, h/d = 4.5.

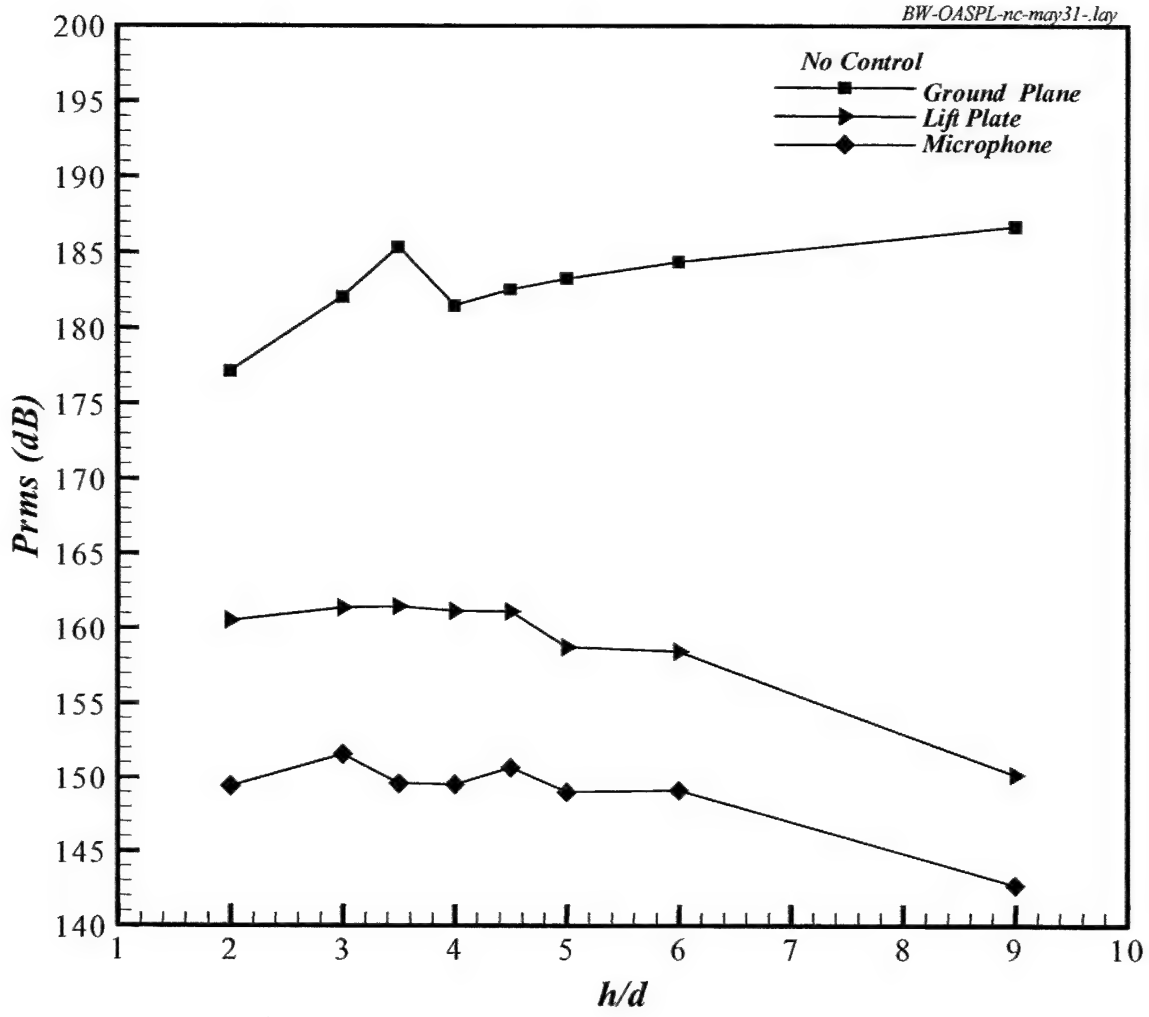

Fig. 8 – Fluctuating pressure intensities for NPR = 3.7, h/d=3.5

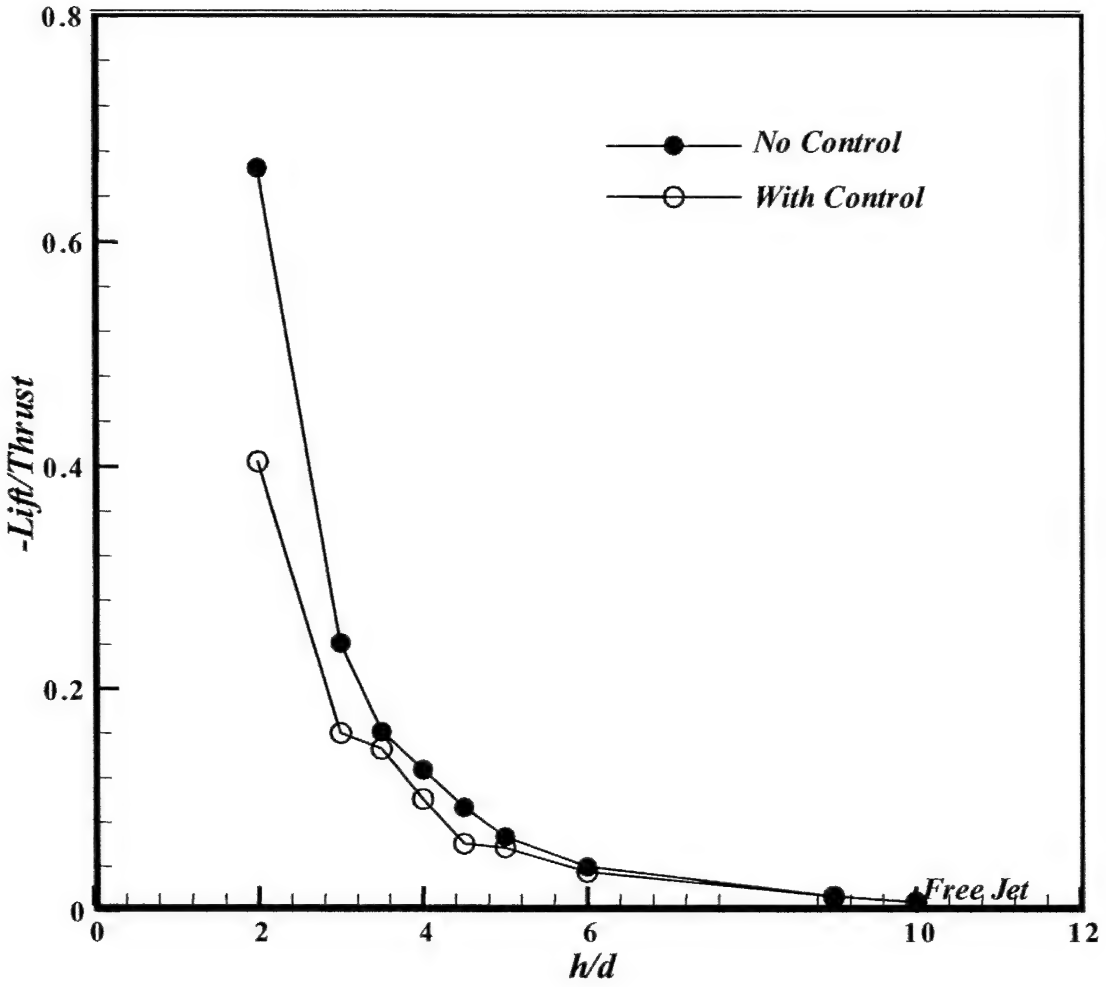

Fig. 9 - Lift loss variation with ground plane distance, with and without control; NPR=3.7.

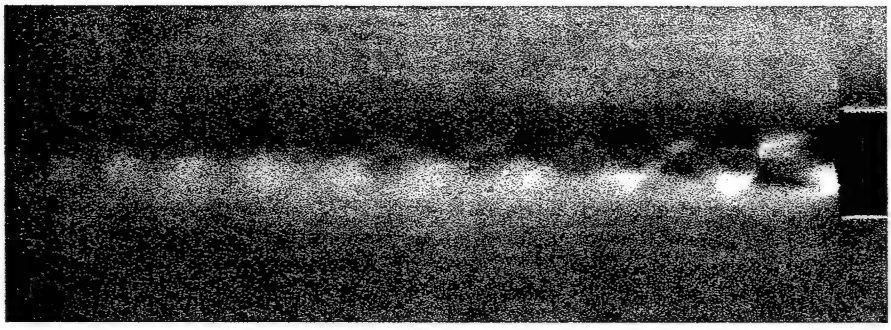

Fig. 10 - Schlieren image of a supersonic microjet issuing from a 400 micron nozzle, $P_0 \sim 110$ Psia.

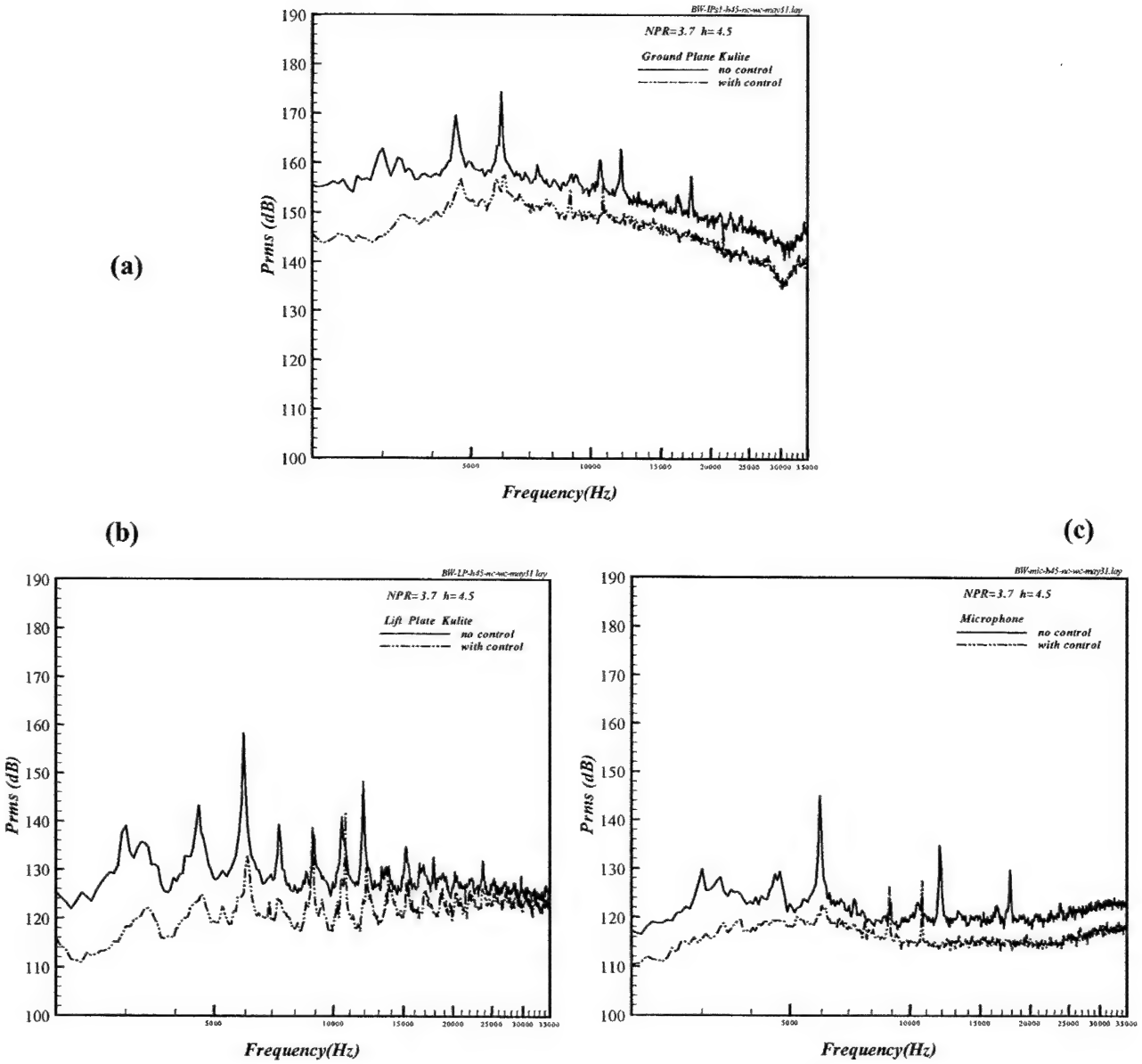

Fig. 11 - Unsteady pressure and microphone spectra with and without control, NPR=3.7, h/d=4.5. a) Ground Plane; b) Lift plate; c) Microphone.

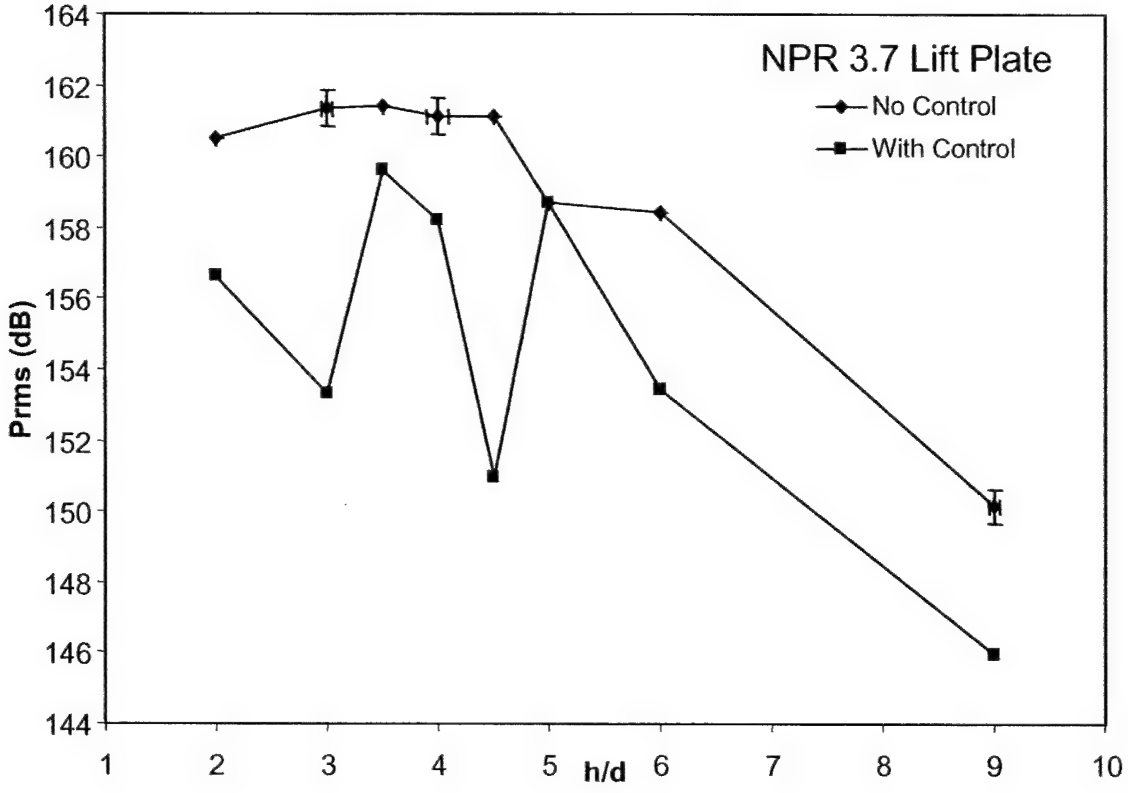

Fig. 12 - Fluctuating pressure intensities on the lift plate, with and without control. NPR = 3.7

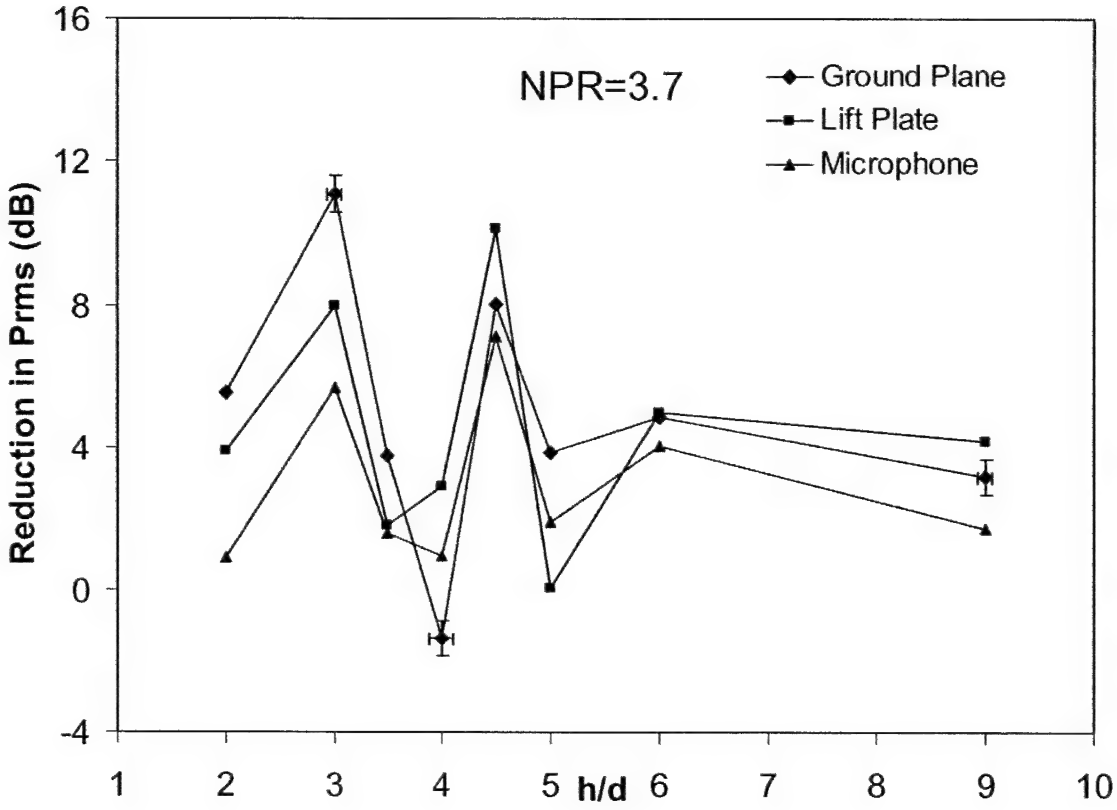

Fig. 13 – Reduction in fluctuating pressure intensities. NPR = 3.7

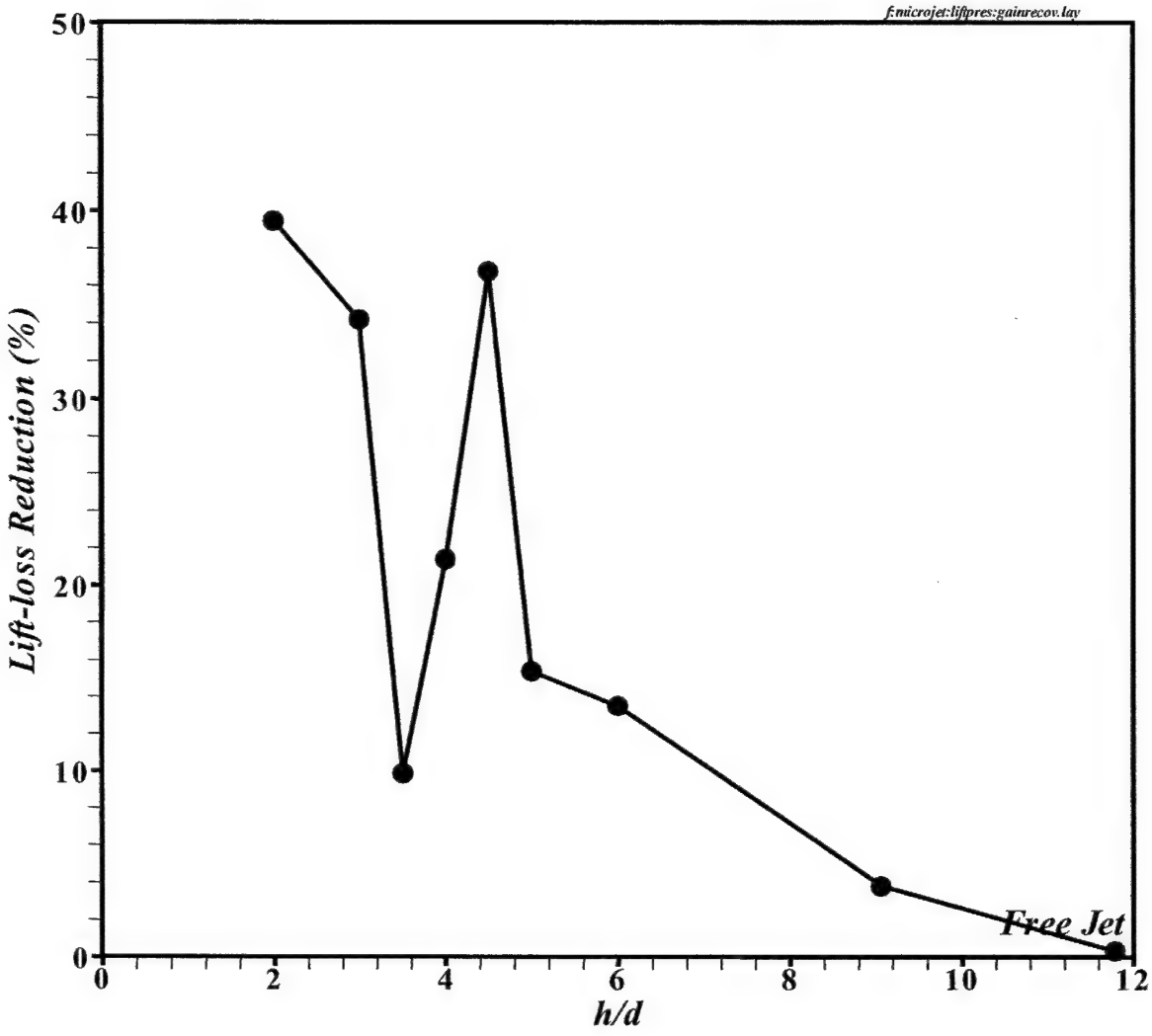

Fig. 14 - Lift loss recovery variation as a function of ground plane distance.

Appendix A2

AIAA-2001-3027

AIAA-2001-3027
Adaptive Flow Control of Supersonic Impinging Jets

C.Shih, F.S.Alvi, H.Lou, G.Garg and A. Krothapalli

Department of Mechanical Engineering
Florida A & M University and Florida State University
Tallahassee, FL

31st AIAA Fluid Dynamics Conference June 2001
Anaheim, CA

AIAA 2001-3027

ADAPTIVE FLOW CONTROL OF SUPERSONIC IMPINGING JETS

C. Shih*, F. S. Alvi†, H. Lou‡, G. Garg§ and A. Krothapalli¶

Department of Mechanical Engineering
Florida A&M University and Florida State University
2525 Pottsdamer Street
Tallahassee, FL 32310

The behavior of supersonic impinging jets is dominated by the presence of a feedback loop between the fluid and acoustic fields, which leads to many adverse effects such as strong acoustic oscillations, high unsteady loads on the nearby structures and the ground plane, and a dramatic loss in lift during hover. From previous studies[1], we have demonstrated that, using supersonic microjet control, we can successfully disrupt the feedback loop, thus leading to reductions in the lift loss, unsteady pressure loads and nearfield noise[1,2]. However, the effectiveness of the control was found to be strongly dependent on the ground plane distance. In addition, better performance improvements were achieved when the jet was operating in an under-expanded mode. This suggests that an adaptive scheme, that can track changes in the feedback loop due to the variation of ground height and jet operating modes, is necessary for optimal control. In this paper, we focus our investigation on identifying the control parameters of an adaptive flow control that can be equally effective for all operating configurations. Parameters studied include microjet pressure, microjet angle, and the use of micro-tabs instead of microjets. Based on preliminary results, it is concluded that it might be possible to devise a control strategy that can produce a more uniform control effect for all configurations. Moreover, it has been identified that the generation of streamwise vortices and the vorticity tilting and stretching mechanisms provided by the microjets might be responsible for the reduction of flow unsteadiness.

INTRODUCTION

An understanding of impinging jet flow field is important for the optimal design of STOVL aircraft which utilize downward-pointing jets to generate the lift force during hover. It is well known that when a high speed jet stream is impinging on the ground several flow-induced effects can emerge and substantially diminish the performance of the aircraft. In particular, a significant lift loss can be induced due to flow entrainment by the lifting jets from the ambient environment in the vicinity of the airframe. In addition, the impinging flow field usually generates significantly higher noise levels relative to that of a free jet operating under similar conditions. Increased OverAll Sound Pressure Levels (OASPL) associated with high speed impinging jets can pose an environment pollution problem and adversely affect the integrity of structural elements in the vicinity of the nozzle exhaust due to acoustic loading. Moreover, the noise and the highly unsteady pressure field are frequently dominated by high-amplitude discrete tones, which may match the resonant frequencies of the aircraft panels, thus further exacerbating the sonic fatigue problem. These problems become more pronounced for supersonic impinging jets, the operating regime of the STOVL version of the future Joint Strike Fighter (JSF).

In order to minimize their adverse influence on aircraft performance, it is evident that the undesirable effects of supersonic impinging jets need to be controlled. In order to devise an effective control scheme to eliminate these detrimental characteristics one must have a fundamental understanding of the physical mechanisms governing these flows. The acoustic properties of single supersonic impinging jet flow field have been investigated by a number of researchers, including Powell[3], Neuwerth[4] and Tam[5]. These studies conclusively demonstrated that the unsteady properties of impinging jet flows are dominated by the presence of discrete impingement tones. These high-amplitude tones are generated by highly coherent instability waves due to the emergence of a self-sustained feedback loop. For a detailed discussion of the feedback mechanism, the reader is referred to the above articles.

Control of the Feedback Loop

* Associate Professor, Associate Member AIAA
† Assistant Professor, Senior Member AIAA
‡ Graduate Research Assistant
§ Graduate Research Assistant
¶ Don Fuqua Eminent Professor, Associate Fellow AIAA

Based on the above discussion, it is apparent that, to effectively eliminate these unwanted effects of impinging jet flows, one must reduce the highly unsteady behavior of the impinging flow by weakening the feedback loop. There are various potential approaches for disrupting the feedback loop and achieving a measure of control on the unsteady properties of this flow. (1) Intercept the upstream propagating acoustic waves so that they can not complete the feedback loop, and/or (2) manipulate the shear layer (for examples, increase its thickness) near the nozzle lip hence reducing its receptivity to the acoustic disturbances, and/or (3) modify the nozzle shear layer using high energy streams (for example, through the generation of streamwise structures) to disrupt the azimuthally coherent interaction between the flow instabilities and the acoustic field.

Based on these concepts, a few attempts have been made in the past to suppress the feedback mechanism. For instance, Karamcheti et al.[6] successfully suppressed edge tones in low speed flows, which are governed by a similar feedback mechanism, by placing two plates normal to the centerline of the jet. Motivated by their work, Elavarasan et al.[7] employed a similar technique to attenuate the feedback loop in an impinging jet flow by introducing a control plate near the nozzle exit. This passive control approach resulted in a reduction of about 6-7 dB in the near-field OASPL. Glass[8] and Poldervaart et al.[9] used similar passive control techniques with limited success. Although passive control techniques have shown promising results, any significant performance gains were confined to a limited range of operating conditions, especially for impinging jets. This is due to the fact that a relatively small change in the nozzle-to-ground separation (h/d) can lead to a significant change in the magnitude and frequency of the tones that are responsible for the undesired flow unsteadiness (Alvi & Iyer[10]). Therefore, any efficient control technique aimed at suppressing the feedback loop must be 'active' and capable of adapting to the shift in frequencies/wavelengths of the modes that lock on to the feedback loop.

Sheplak and Spina[11] used a high-speed co-flow to shield the main jet from the near field acoustic disturbances. For a suitable ratio of the main jet and co-flow exit velocity, they measured a reduction of 10-15 dB in the near-field broadband noise level in addition to the suppression of impinging tones. Shih et al.[12] used counterflow near the nozzle exit to successfully suppress screech-tones of non-ideally expanded jets. They were also able to obtain modest reductions in OASPL, approximately 3-4 dB while enhancing the mixing of the primary jet. However, these active control schemes require additional design modifications and/or high operating power rendering them impractical for implementation in aircraft.

In the current program, we are proposing the implementation of a control-on-demand strategy using supersonic microjets to provide controlled, high-energy perturbations to the main flow to achieve flow control. The proposed control system has the advantage that, depending upon the operating flow conditions, optimal flow control can be achieved by activating the supersonic microjets with the appropriate magnitude and frequency at the desired time instants. In contrast to the traditional passive control methods, the proposed control-on-demand system can be switched on and off strategically. Therefore, it will not degrade the operational performance of the aircraft when it is not needed. The very small size of the actuator hardware and the minimal mass flow rates requires minimal power consumption and is expected to result in negligible thrust loss of the primary jet.

In the present system, a total of 16 supersonic microjets were distributed around the nozzle exit. Based on the earlier discussion of the feedback loop, it is evident that the presence of these supersonic micro-flow streams can be effective in weakening the loop in a number of ways. First, the microjet streams may play a role in the interception of the upstream propagating acoustic disturbances. Second, these high momentum jets can provide spatial/temporal distortions to the coherent shear-layer instabilities thus disrupting their interactions with the acoustic field. A more detailed description of the microjet hardware will be provided in the experimental setup section.

EXPERIMENTAL SETUP & PROCEDURES

The experiments were carried out at the STOVL supersonic jet facility of the Fluid Mechanics Research Laboratory (FMRL) located at the Florida State University. A schematic of the facility with a single impinging jet is shown in Fig. 1. This facility is used primarily to study jet-induced phenomenon on STOVL aircraft hovering in and out of ground effect.

The measurements were carried using a shock free, nearly ideally expanded jet issuing from a convergent-divergent (C-D) axisymmetric nozzle. The throat and exit diameters ($\mathbf{d}$, $\mathbf{d_e}$) of the nozzle are 2.54cm and 2.75cm. The divergent part of the nozzle is a straight-walled conic section with a 3° divergence angle from the throat to the nozzle exit. The nozzle was designed for an exit Mach number of 1.5 and operated at a Nozzle Pressure Ratio (NPR, where NPR = stagnation pressure/ambient pressure) of 3.7 to produce an ideally expanded impinging jet. The primary reason for running an ideally expanded jet was to isolate the effect of the impingement tones from screech tones, since the latter only occur in jets operating at off-design conditions. A circular plate of diameter **D** (25.4 cm~10d) was flush mounted with the nozzle exit. The

circular plate, henceforth referred to as the 'lift plate', represents a generic aircraft planform and has a central hole, equal to the nozzle exit diameter, through which the jet is issued. A 1m x 1m x 25mm aluminum plate serves as the ground plane and is mounted directly under the nozzle on a hydraulic lift.

The flow induced lift forces were estimated by measuring the mean pressure distribution on the lift plate. This was accomplished by using the 17 pressure taps arranged along a radial line on the lift plate. The pressure measurements were obtained by scanning the static pressure ports using a Scanivalve™ system connected to a Validyne™ strain gauge transducer. In addition to the mean pressure taps, a high frequency response miniature Kulite™ pressure transducer was also mounted on the lift plate at a distance of about 35 mm from the nozzle lip. This transducer was used to measure the unsteady pressure loads on the lift plate. The unsteady pressure field created by the jet impingement on ground plane was measured with two additional high frequency 100psi, Kulite™ pressure transducers (model-XCQ-062-100), one at the impinging point on the jet centerline and the other 25mm away from the centerline. The near field acoustic measurements were made using a 0.635cm diameter B&K microphone placed 25 cm away from the nozzle exit oriented 90° to the jet axis. In order to minimize sound reflections during the near-field acoustic measurements, near-by exposed metal surfaces were covered with 10 cm thick acoustic foam. The flow was visualized using a conventional single-pass shadowgraph arrangement. A stroboscopic white-light flash unit with variable pulse frequency of up to 1 kHz was used as a light source. Cross flow shear layer characteristics was examined by laser sheet illumination visualization technique. Laser sheet, generated by a Spectra Physics Nd-YAG pulsed laser, was projected normal to the primary jet axis. Light scattered by the condensed water droplets in the mixing region was recorded by a CCD camera. These condensed droplets were formed when warm, humid air from outside come into contact with the cold air in the jet. It is worth noting that the flow visualization images can also be used to measure the level of mixing inside the shear layer.

The microphone and the lift plate surface pressure signals were acquired through National Instruments digital data acquisition cards using LabView™ software. For unsteady measurements, i.e. microphone and Kulite pressures, 100k points were recorded for each signal. Standard statistical analysis techniques were used to obtain the spectral content and the OverAll Sound Pressure Level (OASPL) from these measurements. The spectral content of the unsteady signals was obtained by segmenting each data record into 100 subgroups with 1k points each and an FFT with a frequency resolution of 68.4Hz was computed for each segment. The 100 FFT's thus obtained were averaged to obtain a statistically reliable estimate of the narrow-band noise spectra. The uncertainty associated with the unsteady lift plate pressure, P_{rms}, is ± 0.02 psi while the rms intensities of the ground plane pressures was estimated to be accurate within ± 0.2 psi. The microphone signal was measured with an estimated uncertainty of ± 1 dB.

The main controlling parameter in the experiment was the ground plate height h with respect to the nozzle exit, which was varied from $2d$ to $60d$. As stated earlier, the experiments were conducted at NPR=3.7, which corresponds to a nearly ideally expanded primary jet flow. The jet stagnation temperature was maintained at 20°C ± 2°C. The nominal exit Reynolds number at exit of the nozzle was $7x10^5$ (based on exit velocity and nozzle diameter).

Active flow control was implemented using sixteen microjets, flush mounted circumferentially around the main jet as shown in the Fig. 2. The jets were produced using 400 μm diameter stainless tubes, mounted on the lift plate with an inclination of ~ 20° with respect to the primary jet axis. The supply for the micro jets was provided from a compressed air cylinder through a main and four secondary plenum chambers (Fig. 2). The high-pressure air was passed through a micron-sized filter to prevent the micronozzles from becoming clogged. The secondary plenum chambers ensured that the flow coming out of the micro jets were free of any unsteadiness. The microjets were connected to the secondary plenum chamber through four solenoid-controlled valves in such a way that any four microjets can be controlled (on/off) individually. The microjets were operated at an NPR ≈ 7. At this operating condition, the combined mass flow rate of all sixteen microjets was well below 0.5 % of the primary jet mass flux.

RESULTS AND DISCUSSION

Previous Microjet Control Studies

It has been demonstrated in earlier works[1,2] that the use of microjets is effective in reducing both the impinging tones and the overall noise level of a supersonic impinging jet. The key results from that work will be briefly summarized in the following for their relevancy to this paper. Fig. 3 shows instantaneous shadowgraph images of the impinging jet flowfield at h/d = 4.0 with and without control. The instantaneous shadowgraph for the uncontrolled case, i.e. microjets off, in Fig. 3a clearly shows the presence of multiple, strong acoustic waves. These waves signify the presence of impinging tones as they impinge and reflect from both the ground pane and the lift plate.

The emergence of large-scale structures in the jet shear layer is also evident from this picture indicating that, in addition to the acoustic field, the unsteady flow properties are also dominated by periodic, discrete frequency disturbances. On the other hand, these structures have been significantly reduced when the microjets are turned on, as shown in figure 3b, and this is accompanied by the total disappearance of the strong acoustic waves. It can be clearly seen that the microjet control can indeed significantly disrupt the feedback loop and leads to a global reduction of the flow unsteadiness.

Also visible in Fig. 3b are the 'streaks' generated by the supersonic microjets. Such streaks are very similar to those generated by tabs[13] and tape[14] elements on the nozzle surface; they have been used as indication of the presence of substantial streamwise vorticity. It is worth noting that the presence of such tabs and the concomitant generation of streamwise vorticity have been known to suppress screech tones. It is therefore speculated that the generation of streamwise vorticity might be partially responsible for the reductions of flow unsteadiness and this consideration will be discussed in more details later.

Given the striking effect of the microjet control observed in the shadowgraphs one would expect the unsteady flow properties be similarly influenced. This is indeed the case as seen in the near field narrow band frequency spectra for h/d = 4.0 in Fig. 4. Here Fig. 4a and 4b show the ground and lift plate unsteady pressures, respectively. The nearfield microphone frequency spectrum, which shows an almost identical trend, will not be presented here. Upon comparing the control data (solid lines) to the uncontrolled case (dashed lines), one observes that the distinct tones present in the uncontrolled impinging jet are either entirely eliminated or significantly diminished by the activation of microjets. In addition, and perhaps more significantly, the attenuation in the discrete tones is accompanied by a broadband reduction in the spectral amplitudes. This broadband reduction is observed for all spectra due to lower acoustic and pressure fluctuations, which indicates an overall decline of the unsteadiness in the flow under control.

Plots summarizing the overall reduction in the unsteady pressure levels (P_{rms}) on the lift plate, the ground plane, and in the nearfield noise are shown in Figs. 5 and 6 for NPR = 3.7 and 5, respectively. Although a range of microjet pressures were tested, the data shown in these plots correspond to the microjets operating at ~ 100 psia. The trends observed here are very similar to those obtained at other microjet pressures. These plots clearly show that the fluctuating loads are significantly reduced at all three measurement locations for both NPR's, at almost all heights. However, the magnitude of reduction is strongly dependent upon the ground plane distance (h/d) and to a lesser degree on the nozzle pressure (NPR). In general, the microjets are more effective for the under-expanded jet (NPR=5) where the lift and ground plate pressures are reduced by 10-14 dB and the nearfield noise by 5-6 dB.

However, as seen in Fig. 5, the reductions for NPR = 3.7 are also substantial for all three unsteady pressures except for selected h/d. The variation of the level of reduction appears to have a staging behavior. It has a low value at h/d=2 and increases to a maximum at h/d=4 before it drops drastically to a minimum at h/d=4.5. This is then followed by another increase of the reduction level at h/d=6 and a decrease at h/d=9. We believe that this trend of non-uniform reductions for the microjet control should be closely related to the well-known staging behavior of the impinging tones variation with ground plane distance[15]. A comprehensive study correlating the effectiveness of microjet control to the staging behavior is currently being undertaken. Preliminary results indicate that maximum reduction of unsteadiness can usually be achieved if the microjet control can change the frequency of the dominant tones. This seems to suggest that the optimum control can be obtained if the microjets can alter the global flow condition to force the impinging tones to transition to less favorable stages. As a result, the flow interactions between the acoustic waves and shear layer structures could be weakened leading to a global reduction of the flow unsteadiness.

This issue is further complicated by the co-existence of the asymmetric (helical), axisymmetric, and other higher order instability modes in the shear layer. It has been shown that[15] a switch from the helical to axisymmetric mode occurs when the ground distance is decreased to h/d<6. This has been attributed to the generation of strong standing waves as a result of the emergence of duct modes between the lift plate and the ground plane[15]. A further decrease in ground plate distance results in the re-establishment of the helical mode. This switch in modes could also be responsible for the ineffectiveness of the flow control at certain distances. For example, microjets might be effective in eliminating only one of the dominant modes but not all of them. More investigation is needed to clarify this consideration.

The non-uniform reductions indicate that the control technique is not equally efficient at all heights, presumably because it does not track changes in the feedback loop due to a variation in h/d. This suggests that efficient control of this flow requires an adaptive control approach where the microjets can be actively manipulated to provide optimal control at all heights.

Effects of Microjet Operating Configurations

Currently, we are conducting a comprehensive parametric study on the effect of microjet control configurations on the overall flow control. We have examined a wide range of operating parameters in order to devise an optimum control strategy. We also hope to acquire a better physical understanding of how the proposed microjet control system works through this exhaustive investigation. With this in mind, the testing matrix chosen include microjet operating pressure, microjet angle, the use of micro-tabs instead of microjets, microjet size, number/spacing of microjets, and spatial distribution of microjets relative to the main jet. The first three considerations will be discussed in this paper.

Microjet Pressure

The first parameter tested is the operating pressure of the microjets. The microjet angle is chosen to be 20 deg. with respect to the streamwise direction. It has been shown by authors[16] that a strong jet stream with long supersonic length can be generated if high pressure is applied to the nozzle. Control jet stream with high momentum is needed in order to perturb the robust primary jet shear layer. Moreover, a supersonic stream can shield the local shear layer from the upstream acoustic waves through which the spatial coherence of the interaction between the acoustic and instability waves might be disrupted. The effect of microjet pressure on the reduction of unsteady flow fluctuations for different h/d is shown in Figs. 7 and 8. The microjet pressure is gradually increased from 80 psi to 120 psi with an increment of 10 psi. For the ideally expanded case, the reductions of the averaged pressure fluctuations increase relatively faster for increasing microjet pressure up to 100 psi. Beyond this value, the gains are getting smaller. In addition, the increasing microjet pressure seems to have minimal effect at three ground plane position: h/d=2, 4.5, and 9. These are also the positions where the microjet control is found to be the least effective. However, the variation of microjet pressure seems to have a negligible effect when the primary jet is operating under an under-expanded condition. In general, the overall reductions of pressure fluctuations of the under-expanded jet are much higher for all h/d, in the order of 10 to 14 dB. The least effective ground plate distance for microjet control has shifted from h/d=4.5 to h/d=4, nevertheless, the staging behavior of the control effectiveness still exist for the under-expanded case.

Another factor contributing to the ineffectiveness of the microjet operating under ideally and over-expanded conditions might be due to the relatively short "penetration depth" of the control jet under these conditions. The penetration depth can be loosely defined as the extent of the control jet that can penetrate into the primary jet with high enough momentum to modify the shear layer instability. It is expected that the effective penetration depth is longer for the under-expanded case since the jet boundary expands outward in order to compensate the difference between the higher pressure at the nozzle exit and the ambient pressure. On the other hand, the jet boundary expansion is more moderate for the ideally-expanded case and actually experiences a contraction for the over-expanded condition. Shorter penetration depth means less influence on the jet flowfield for over- and ideally-expanded cases. The opposite is true for the under-expanded case.

Using isentropic assumption, the expansion angle is estimated to be about 6° between the ideally-expanded and the under-expanded cases and it is not a significant value. From our study[16], the supersonic length for a 400 μm jet is about 4 mm (10 jet diameters) at an operating pressure of 80 psi. This means that the microjet should be able to penetrate the shear layer with a speed exceeding the local speed of sound even at this lowest pressure used. Therefore, penetration depth factor is not enough to account the drastic difference of the control effectiveness for ideally-expanded and the under-expanded cases. Nevertheless, this issue will be examined more in the next section when we place all microjets at a 90° angle with respect to the primary jet. In this configuration the control jets are aligned flushed against the outer edge of the nozzle so that penetration depth is no longer a factor anymore. The effect of the microjet angle on the control is presented in the following.

Microjet Angle

The overall pressure fluctuations for microjet control angles of 20° and 90° are compared in Figs. 9 and 10. For the ideally-expanded case (NPR=3.7), the reductions increase for almost all h/d when the angle is changed from 20° to 90°. This increase in reductions is especially impressive for short ground plate distance cases (h/d <3.5) such that the unsteady pressure loads on both lift plate and ground plane decrease additional levels of 6 to 9 dB as compared to the 20° jet angle cases. The only exception is the h/d=4 case when the reduction is a maximum when the angle is 90°. At this ground plane distance, there is no further reduction of the flow unsteadiness by placing the microjets right next to the primary jet shear layer. This suggests that the improvement of control effectiveness might not solely due to the increase of penetration depth. The increased reduction at h/d=4.5 is a promising sign since it implies that a more uniform control for all h/d is possible if an adaptive control scheme could be identified and implemented.

Surprisingly the reductions actually either decrease slightly or remain the same for the under-expanded case. The decrease seems to be more severe for short (h/d<3.5) and long (h/d>6) ground plane distance cases. For example, an 8 dB decrease can be found in the ground pressure fluctuations for the h/d=3 and h/d=6 cases. This again indicates that an adaptive control scheme is critical since the flowfield responds in a totally different way when the control configuration changes.

It can also be concluded that the close proximity of the microjets to the primary jet shear layer provides no control advantage for an under-expanded impinging jet. This means that the physical mechanism for the effective control might be different for the ideally-expanded case as compared to the under-expanded case. This observation is supported by studying the effect of control when the microjets are replaced by micro-tabs, which will be discussed in the following.

Micro-tabs vs Microjets

As discussed in the introduction section, tabs have been used successfully in reducing supersonic jet noises and enhancing mixing in the jet shear layer[13,17]. It has been demonstrated that the generation of counter-rotating streamwise votex pairs around the tabs is responsible for the improvement of performance. Placing at a 90° angle at the nozzle lid, the supersonic microjets have a similar function compared to that of tabs. In this paper, the micro-tab is made by inserting a thin stainless wire (400 μm in dia.) into the microjet nozzle. The wire tab extends 2.5 mm (approximately 10% of the primary jet diameter) outward from the micro nozzle into the primary jet. The results of using micro-tabs verse microjets are presented in Figs. 11 and 12 for both ideally- and under-expanded cases, respectively. For the under-expanded case, the micro-tab control produces almost identical effect as compared to the microjet control. This supports the notion that the generation of counter-rotating, streamwise vortex pair is responsible for the reductions of flow unsteadiness when microjets are used in an under-expanded jet. However, relatively little effect in control can be found when the micro-tabs are used in the ideally-expanded case (Fig. 11). Most interestingly, the micro-tab control seems to have the least effect when h/d=4 while it is most effective in h/d=4.5, while the outcome is exactly the opposite when 20° microjet control is used (Fig. 5). This once again indicates that different flow physics are responsible for the flow control at different h/d and a better understanding of these mechanisms is necessary for the development of an effective adaptive scheme.

Possible Physical Mechanisms

Three possible physical mechanisms, as proposed in the introduction section, have been considered to be responsible for the effective control of a supersonic impinging jet using microjets. The first one suggests that the supersonic micro-streams might be able to intercept upstream propagating acoustic waves and interrupt the feedback loop. It appears that we can eliminate this possibility from our list since 90° microjets placed at the nozzle exit cannot intercept the acoustic waves but still manage to provide more effective control than 20° microjets.

Based on previous discussion, the microjet control is more effective at under-expanded condition than both over- and ideally-expanded cases. This observation seems to be consistent with our previous assertion that the emergence of streamwise streaks might be responsible for the attenuation of the feedback loop. Because it is well known that the streamwise vorticity streaks are enhanced by the emergence of a highly concave curvature on the jet boundary when a jet is operating at an under-expanded condition. Therefore, if the generation of streamwise vortices is the main physical mechanism responsible for the flow control, it is expected that perturbing an under-expanded jet is much easier than that of an ideally-expanded jet. This is further supported by the fact that, for an under-expanded case, the use of micro-tabs produces the same control effect as compared to the use of microjets.

Generation/Enhancement of Streamwise Vortices

To examine the streamwise flow structures, a laser sheet illumination technique was used to record the cross stream scattering images of the jet. Instantaneous images for an under-expanded jet (NPR=5) without and with control are shown in Figs. 13 and 14. These images were taken at one diameter downstream of the jet nozzle before the formation of large-scale structures in the shear layer. Without control, moderate indentations can be observed around the condensation ring and they have been related to the presence of counter-rotating vortex pair (Fig. 13a). More clearly defined indentations emerge if the microjets are turned on and one can identify a total of 16 of these modulations inside the ring (Fig. 13b). Time-averaged images (averaged over 20 instantaneous images) show a similar pattern (Fig. 14). Without control, there appears to be fewer identifiable indentations, indicating that the streamwise vortices are not stationary in an average sense. This is expected since NPR=5 is not a highly under-expanded situation. However, with microjet control, the averaged pattern displays a strongly modulated ring with a total of 16 indentations. It has also been found that these indentations align along the streamwise direction with the corresponding microjets at the primary jet nozzle. Further downstream at two

jet diameters, fewer indentations can be seen from the visualization picture indicating merging of the streamwise vortices as has also been observed by others.

What is the source of these streamwise vortices? One potential source is the vorticity containing in the microjet streams. Based on simple dimensional analysis, one can easily show that the collective circulation from all microjets is only about 0.4% of the circulation of the primary jet. It is not possible for this to be the sole source of these strong streamwise vortices. Therefore, the vorticity must have come from the primary jet vorticity. It is speculated that by redirecting the vorticity away from the main shear layer, the microjet control can effectively weaken the primary shear strength and, consequently, reduce the flow instabilities. This strategy will be most effective for the under-expanded condition since the concave curvature of the under-expanded jet boundary enhance the growth of the streamwise structures. Therefore, microjet control takes advantage of the intrinsic instability mechanism of the formation of streamwise vortices in an under-expanded jet to stabilize the primary shear layer instability. Moreover, strong modulations on the primary vortical structures due to the emergence of these streamwise vortices reduce the azimuthal coherence of the primary vortices and make them less sensitive to the upstream-propagating acoustic excitations. The end result is a significant reduction of the feedback loop coupling and an overall reduction of the flow unsteadiness. This is consistent with our observation that microjet control is most effective for an under-expanded jet and not as effective for other cases.

However, the generation of streamwise vortices cannot be used to explain why the control also works, although not as effective, for both over- and ideally-expanded jets. This is illustrated by the fact that micro-tabs produce little or no control effect in an ideally-expanded jet even when longitudinal vortices indeed have emerged downstream of the tabs. The main explanation is that these longitudinal structures are stable under over- or ideally-expanded conditions and they will neither grow downstream nor extract energy from the main shear layer. Consequently, the formation of streamwise vortices cannot provide strong enough modifications to the primary jet instability in these situations.

Vorticity Tilting and Stretching

As discussed in the previous section, redirecting vorticity away from the primary jet shear layer through the generation of secondary, streamwise instability might be responsible for the reduction of flow unsteadiness for an under-expanded jet. In this section, we present two possible flow mechanisms that might lead to similar effect for over- and ideally-expanded cases, that is the tilting and stretching of vorticity. Vorticity tilting is the reorientation of the vortex element as the result of a locally non-uniform velocity distribution, as illustrated schematically in Fig. 15. In the current situation, the microjet stream can redirect the azimuthal vorticity component into either transverse or streamwise direction and significantly reduce the primary shear layer vorticity. Once the vortex element is displaced by the microjet into the center of the primary jet, it experiences much faster streamwise convection and the vortex element is stretched along this direction. The longitudinal vorticity component intensifies to satisfy the conservation of angular momentum. It is believed that the vorticity tilting and stretching mechanisms are important elements responsible for the control for over- and ideally-expanded jets. Vortex tilting weakens the primary shear layer instability and also displaces vorticity away from the jet boundary where the growth of streamwise structures is not supported due to the non-concave curvature. As a result, vortex stretching can strengthen the displaced vortex element and generate enough perturbations to the azimuthal coherence of the shear layer so that strong coupling between the acoustic waves and flow instabilities cannot be established. This is consistent with the fact that 90° microjet is more effective than 20° microjet since the former can displace the vortex element further away from the jet boundary than the latter.

SUMMARY

Previous studies have shown that the use of supersonic microjets is effective in disrupting the feedback mechanism in supersonic impinging jet flows. This control strategy results in significant performance gains relative to the uncontrolled case. Lift loss, overall noise levels, and the fluctuating pressure loads on the lift and ground surfaces all experience substantial reductions. However, the performance enhancements due to microjet control were not uniform over the entire parametric space. This is due to the fact that the microjets are presently used in a 'passive' mode without taking into consideration of the dynamic nature of this flow and the fact that the properties of the flow-acoustic interactions change with operating conditions. In this paper, a systematic study of control parameters was carried out. Parameters studied include microjet pressure, microjet angle, and the use of micro-tabs instead of microjets. The effectiveness of microjet control depends strongly on the microjet pressure for an ideally-expanded jet but is insensitive when the jet is operating in under-expanded condition. On the other hand, considerable improvement on the reduction of

flow unsteadiness can be obtained if the microjet angle is changed from 20° to 90° for an ideally-expanded jet, while the angle change has little or no effect for the under-expanded jet. Finally, the use of micro-tabs instead of microjets produce exactly the same control effect for an under-expanded jet, yet it has negligible when the jet is operating in ideally-expanded mode.

Based on these preliminary results, it is concluded that a control strategy that produces a more uniform control effect for all configurations might be possible. Moreover, formation of streramwise vortices as well as the vorticity tilting and stretching mechanisms generated by the microjets might be responsible for the reduction of flow unsteadiness.

ACKNOWLEDGEMENTS

Our research program on STOVL aircraft jet induced effects is supported by NASA Ames Research Center (Technical monitor: Mr. Doug Wardwell), Air Force Office of Scientific Research (Technical Monitor: Dr. Steven Walker) and The Boeing Corporation (Technical Monitor: Dr. William Bower); their support is gratefully acknowledged. We also thank Mr. K. Phalnikar for characterizing the supersonic microjets and Mr. O. Egungwu for his help in conducting the tests.

REFERENCES

1. Elavarasan, R., Alvi, F.S., Shih, C. and Krothapalli, A., "Control of Supersonic Impinging Jet Flows Using Microjets, " AIAA Paper 2000-2236
2. Alvi, F.S., Shih, C. and Krothapalli, A., "Active Control Of The Feedback Loop in High-Speed Jets," AIAA Paper 2001-0373
3. Powell, A., "The Sound-Producing Oscillations of Round Underexpanded Jets Impinging on Normal Plates", *J. Acoust. Soc. Am.*, 83 (2), 1988, 515-533.
4. Neuwerth, G.," Acoustic Feedback of a subsonic and Supersonic Free Jet which Impinges on an Obstacle", NASA TT F-15719, 1974.
5. Tam, C.K.W., and Ahuja, K.K., "Theoretical model of discrete tone generation by impinging jets", *J. Fluid Mech.*, Vol. 214, 1990, pp 67-87.
6. Karamcheti, K., Bauer, A.B., Shields, W.L., Stegen, G.R., And Woolley, J.P., "Some Features of an Edge Tone Flow Field", NASA SP 207, 1969, pp275-304.
7. Elavarasan, R., Krothapalli, A., Venkatakrishnan, L. and Lourenco, L., " Suppression of self-sustained oscillations in a supersonic impinging jet". Submitted for publication in *AIAA* journal. Also see, Elavarasan R., Venkatakrishnan, L., Krothapalli, A. and Lourenco, L., "A PIV study of a supersonic impinging jet," *Journal of Visualization*, Vol. 2, No.3/4, 213-222, 2000.
8. Glass, D.R., "Effect of acoustic feedback on the spread and decay of supersonic jets," *AIAA Journal*, Vol.6, No.6, 1968, pp1890-1897.
9. Poldervaart, L.J., Wijnands, A.P.J., vanMoll, L.H.A.M., and vanVoorthuisen, E.J., "Modes of vibration", *J. Fluid Mech*, Vol. 78, 1976, pp.859-862.
10. Alvi, F S. and Iyer, K. G., "Mean and Unsteady Flowfield Properties Of Supersonic Impinging Jets With Lift Plates", AIAA Paper 99-1829, presented at the 5th AIAA/CEAS Aeroacoustics Conference, May 1999.
11. Sheplak, M. and Spina, E.F., "Control of high-speed impinging-jet resonance", *AIAA Journal*, Vol.32, No.8, 1994, pp1583-1588.
12. Shih, C., Alvi, F. S., and Washington, D., "Effects of Counterflow on the Aeroacoustic Properties of a Supersonic Jet," *AIAA Journal of Aircraft*, Vol. 36, No. 2, March/April 1999, pp. 451-457.
13. Samimy, M. Zaman, K. B. M.Q. and Reeder, M. F., "Effect of Tabs on the Flow and Noise Field of an Axisymmetric Jets," *AIAA Journal*, Vol.31, No.4, 1993, pp. 609-619.
14. Krothapalli A., Strykowski P. J. and King C. J., "Origin of Streamwise Vortices in Supersonic Jets," *AIAA Journal*, Vol. 36: No. 5, 1998, pp. 869-872.
15. Krothapalli, A., Rajakuperan, E. Alvi, F. S. and Lourenco, L., "Flow field and Noise Characteristics of a Supersonic Impinging Jet," *Journal of Fluid Mechanics,* Vol. 392, August 1999, pp. 155-181.
16. Phalnikar, K.A., Alvi, F.S., and Shih, C., "Behavior of Free and Impinging Supersonic Microjets, " AIAA Paper 2001-3047.
17. Ibrahim, M.K and Nakamura, Y., "Effects of Rotating Tabs on Flow and Acoustic Fields of Supersonic Jet," AIAA Journal, Vol. 39, No. 4, pp745-748, 2001.

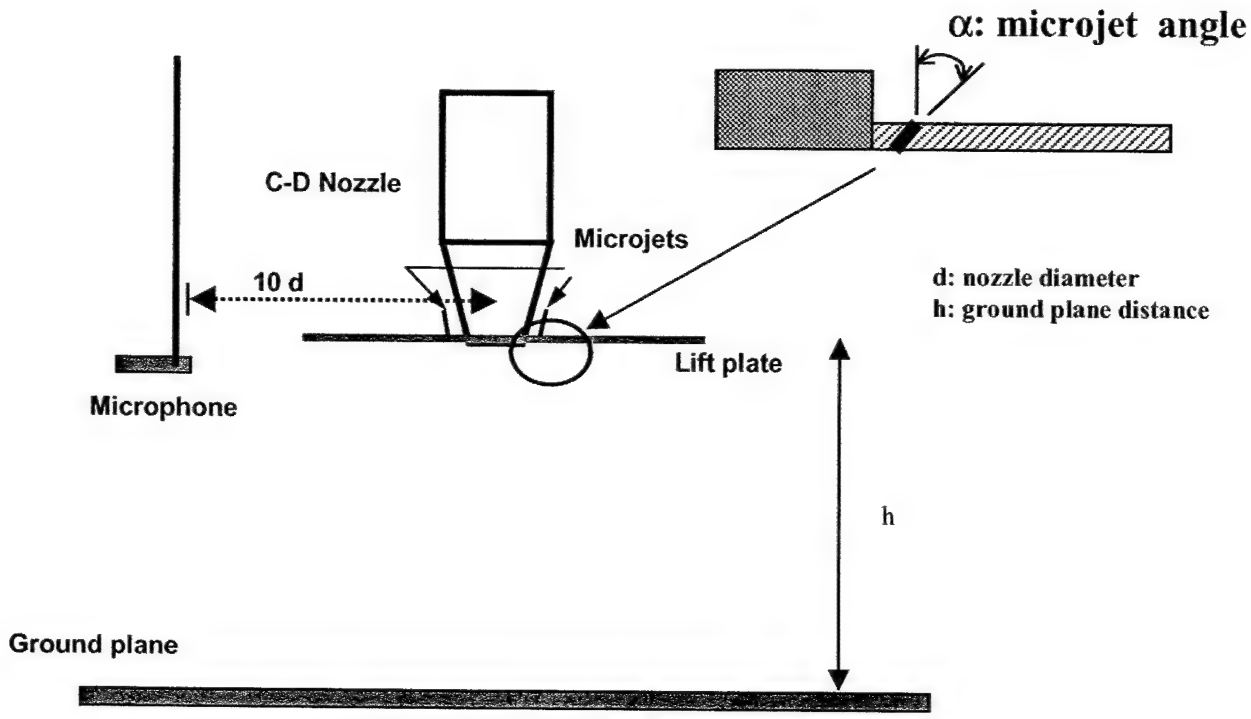

Fig. 1 - Schematic of the experimental arrangement.

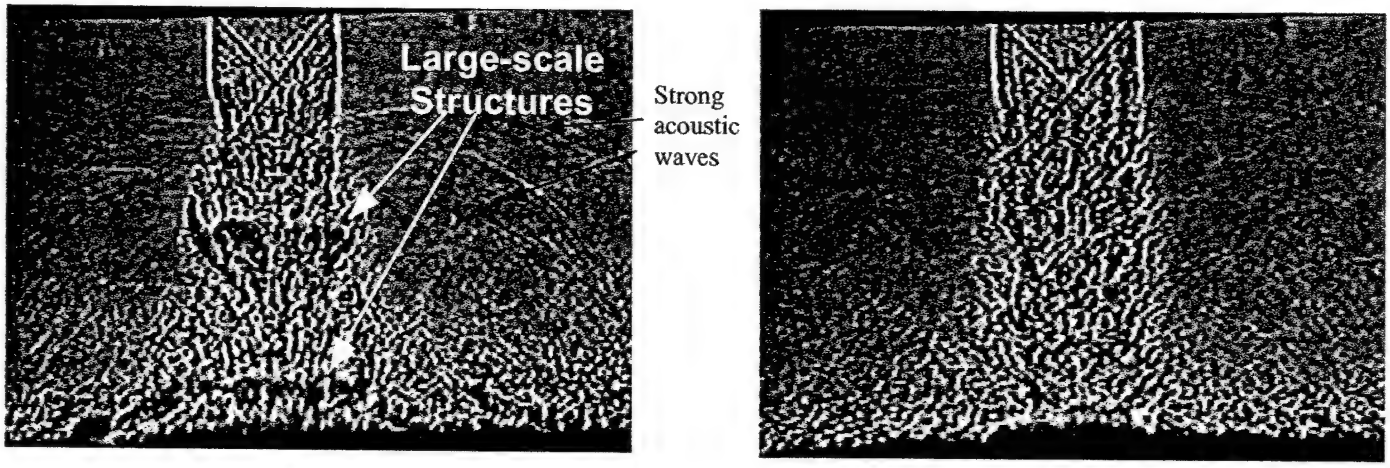

(a) No control

(b) With control

Fig. 2 - Instantaneous shadowgraph images, NPR = 3.7, h/d = 4.0.
(a) No control; (b) With microjet control.

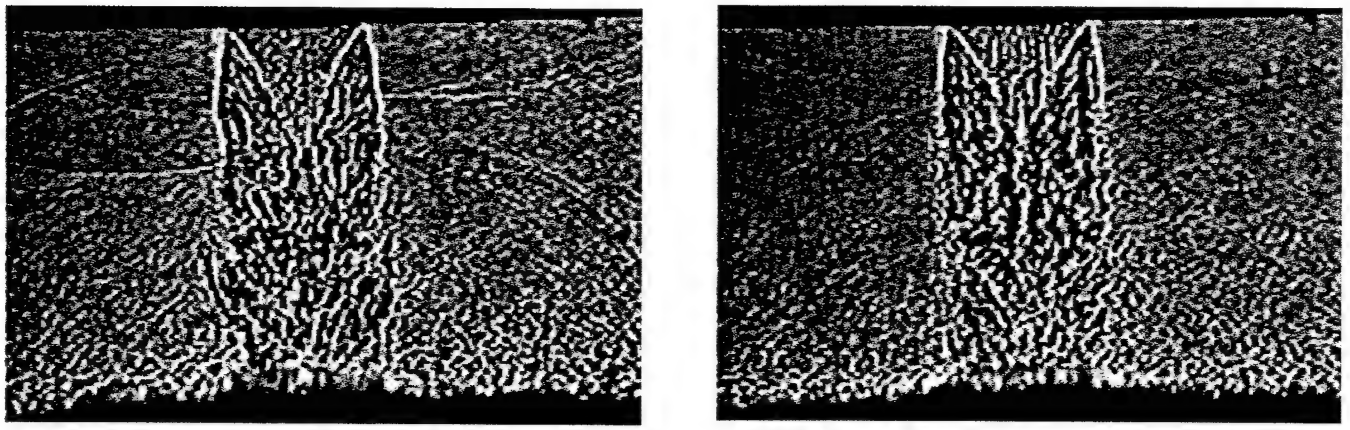

(a) No control (b) With control

Fig. 3 - Instantaneous shadowgraph images, NPR = 5.0, h/d = 3.5.
(a) No control; (b) With microjet control.

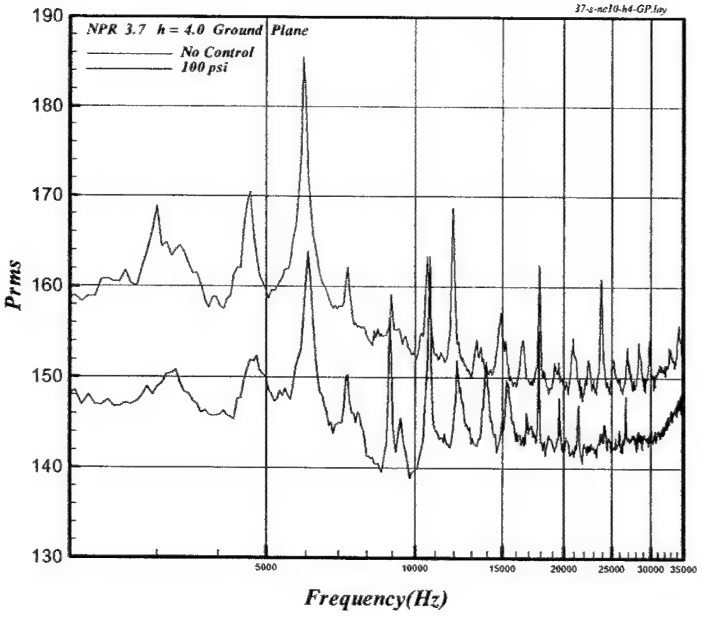

(b) Ground plane

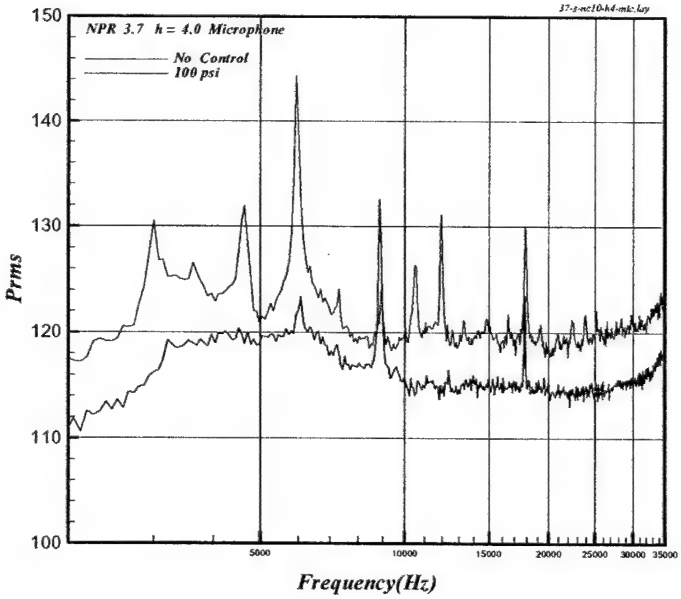

(b) Microphone

Fig. 4 - Unsteady surface pressure and microphone spectra for NPR = 3.7, h/d = 4.0;
(a) Ground plane, (b) Microphone.

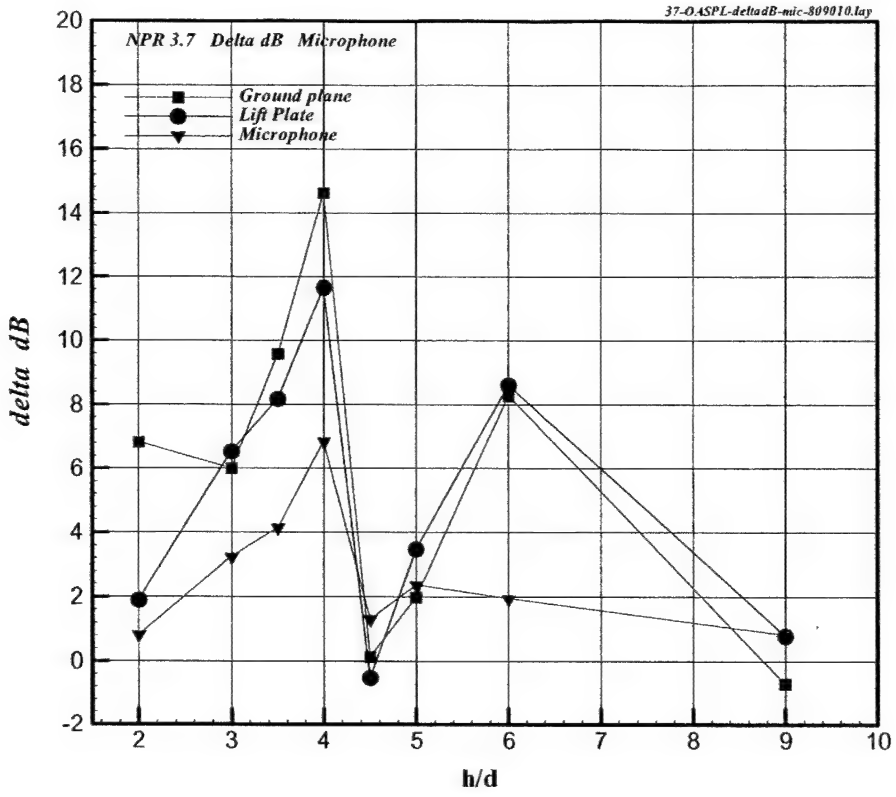

Fig. 5 Reductions in fluctuating pressure intensities as a function of h/d, NPR=3.7 (microjet angle 20°, pressure 100 psi).

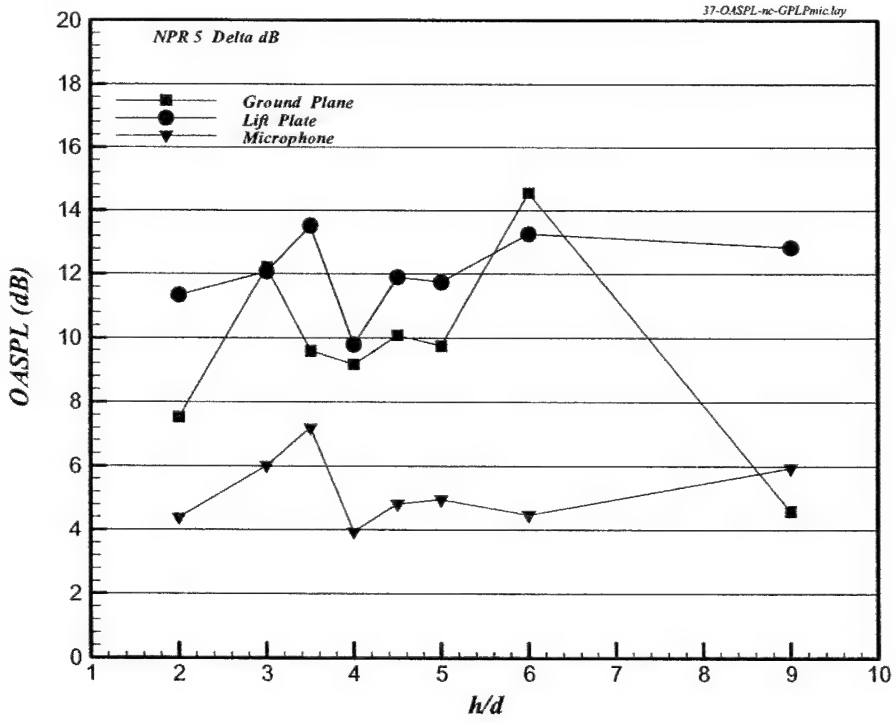

Fig. 6 Reductions in fluctuating pressure intensities as a function of h/d, NPR=5.0 (microjet angle 20°, pressure 100 psi).

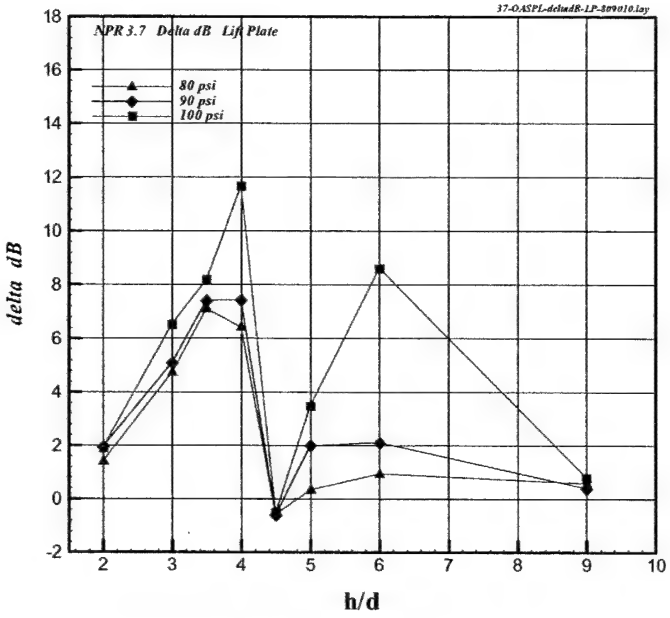

(a) microjet pressure 80-100 psi

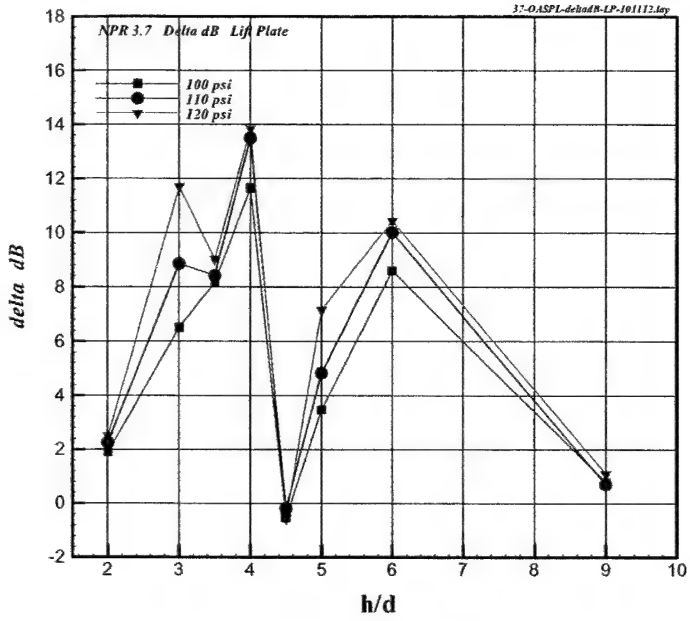

(a) microjet pressure 100-120 psi

Fig. 7 Reductions of fluctuating ground plane pressure intensities for different microjet operating pressure; (a) 80 to 100 Psi, (b) 100 to 120 psi. NPR=3.7.

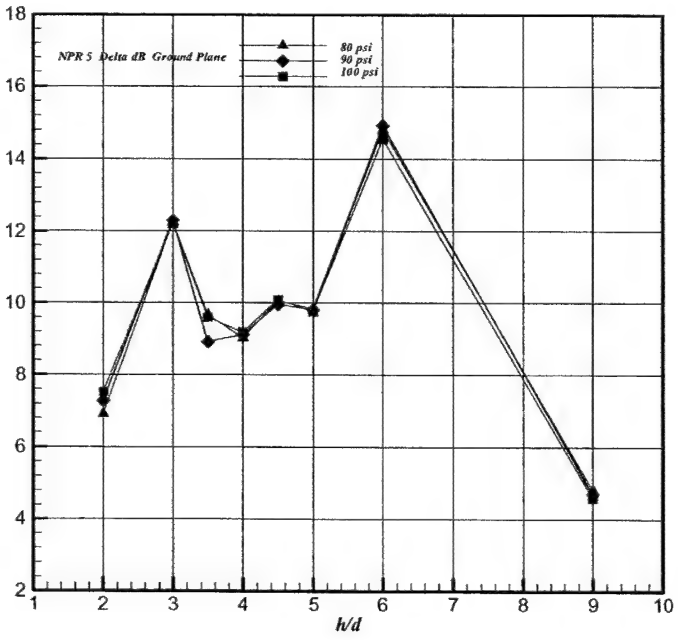

(a) microjet pressure 80-100 psi

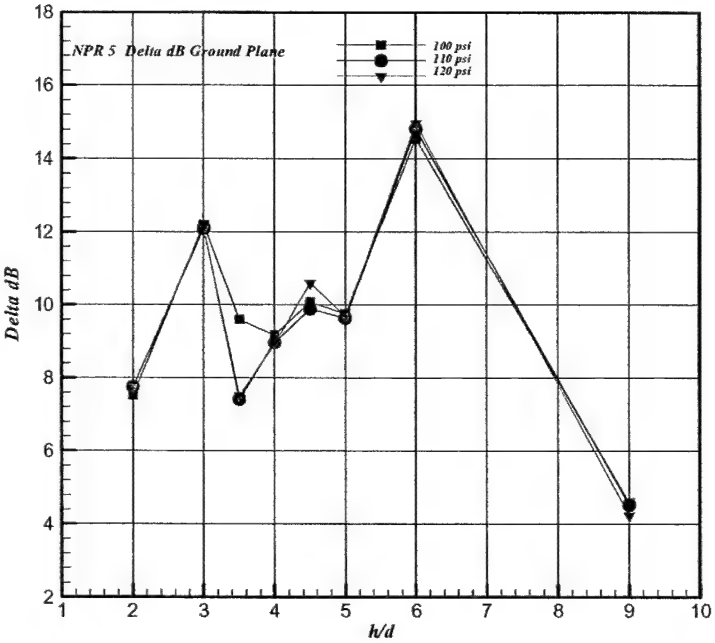

(a) microjet pressure 100-120 psi

Fig. 8 Reductions of fluctuating ground plane pressure intensities for different microjet operating pressure; (a) 80 to 100 Psi, (b) 100 to 120 psi. NPR=5.0.

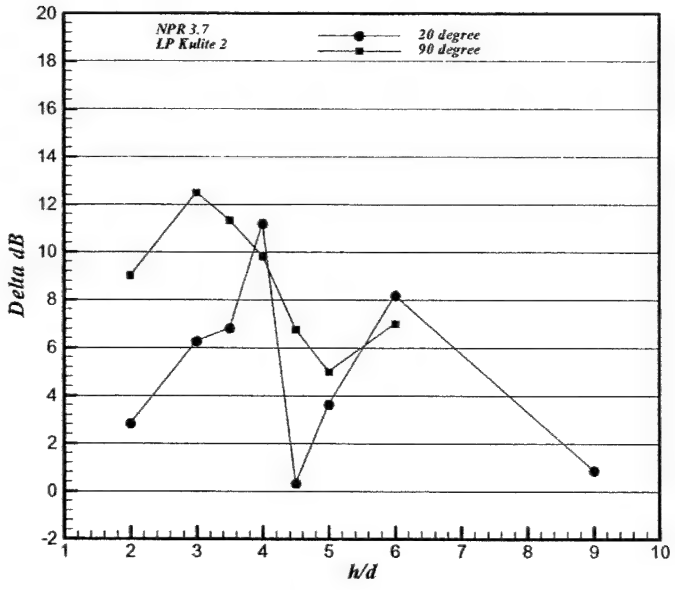

(a) Lift plate

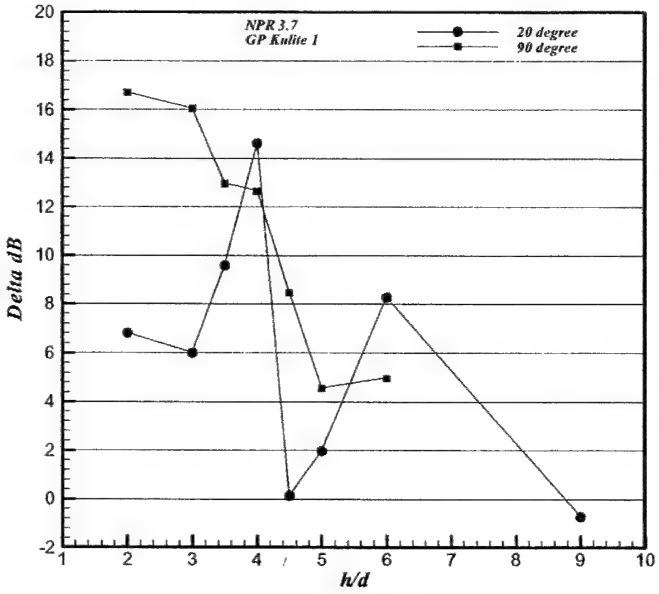

(a) Ground plane

Fig. 9 Reductions of fluctuating pressure intensities, 20° verse 90° microjet control; (a) lift plate, (b) ground plane, NPR=3.7.

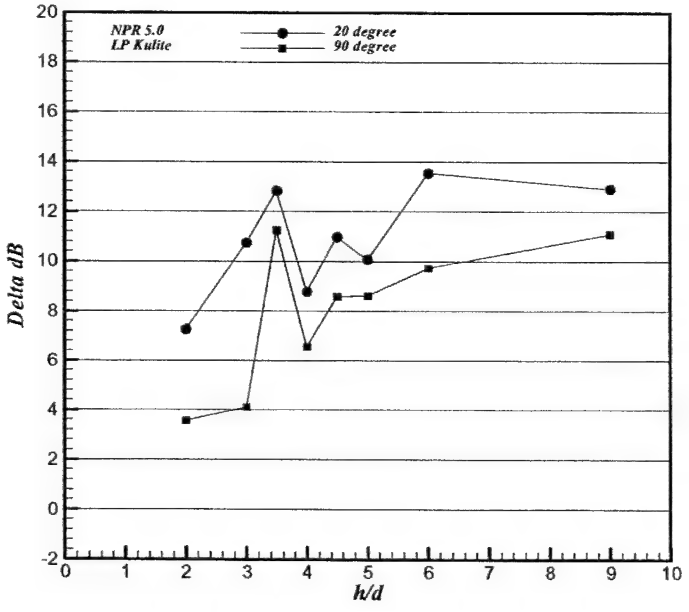

(a) Lift plate

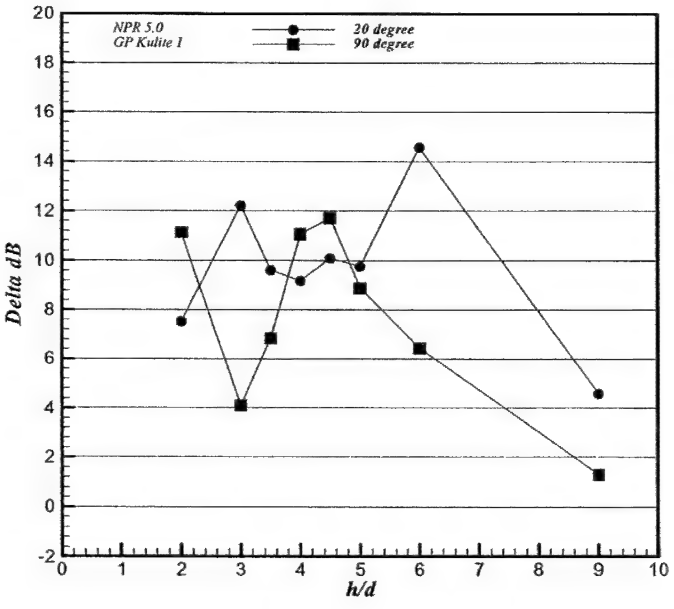

(a) Ground plane

Fig. 10 Reductions of fluctuating pressure intensities, 20° verse 90° microjet control; (a) lift plate, (b) ground plane, NPR=5.0.

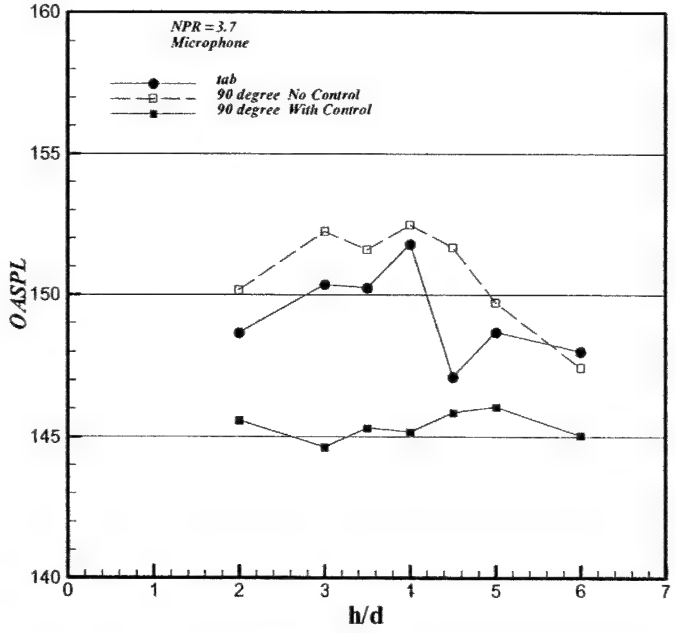

(a) Microphone

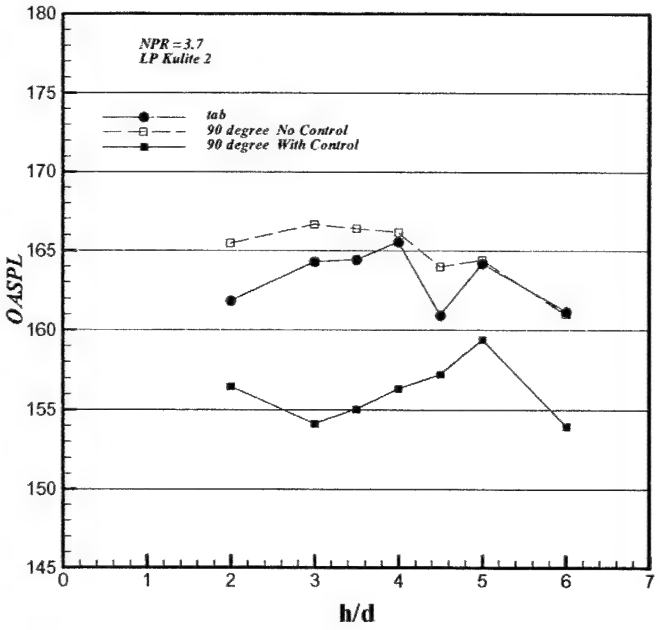

(a) Lift plate

Fig. 11 Reductions of fluctuating pressure intensities for microtabs verse 90° microjets and no control; (a) microphone, (b) lift plate, NPR=3.7.

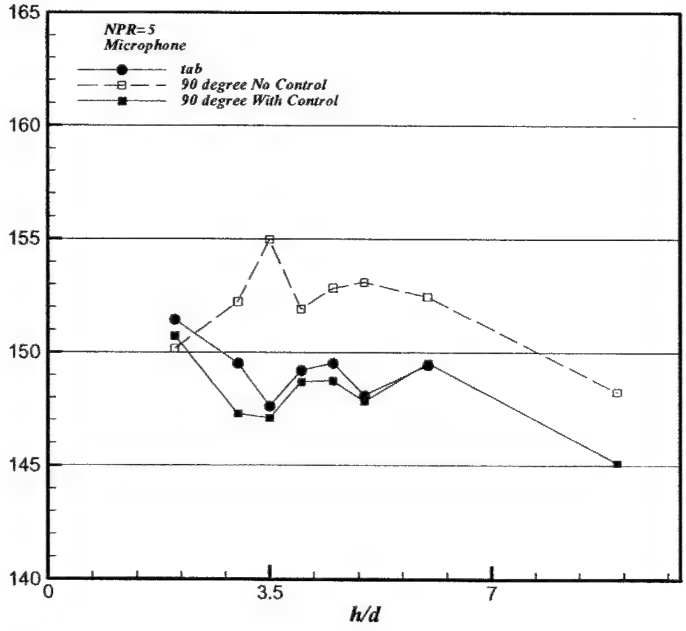

(a) Microphone

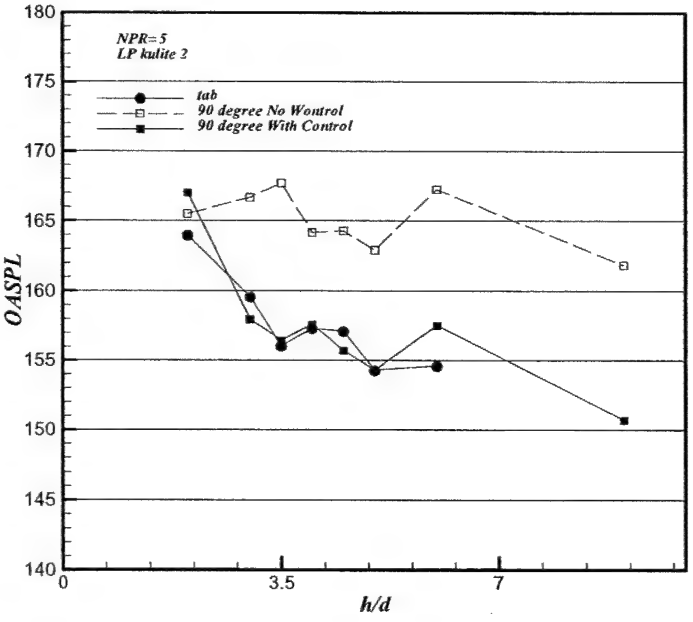

(a) Lift plate

Fig. 12 Reductions of fluctuating pressure intensities for microtabs verse 90° microjets and no control; (a) microphone, (b) lift plate, NPR=5.0.

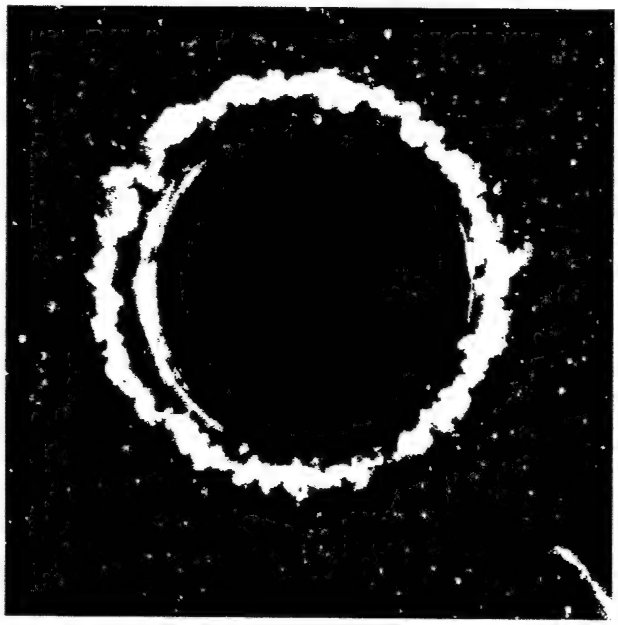

(a) No control

(a) With control

Fig. 13 Instantaneous PLS images taken at one diameter downstream of the nozzle, NPR=5, h/d=4; (a) No control, (b) With control.

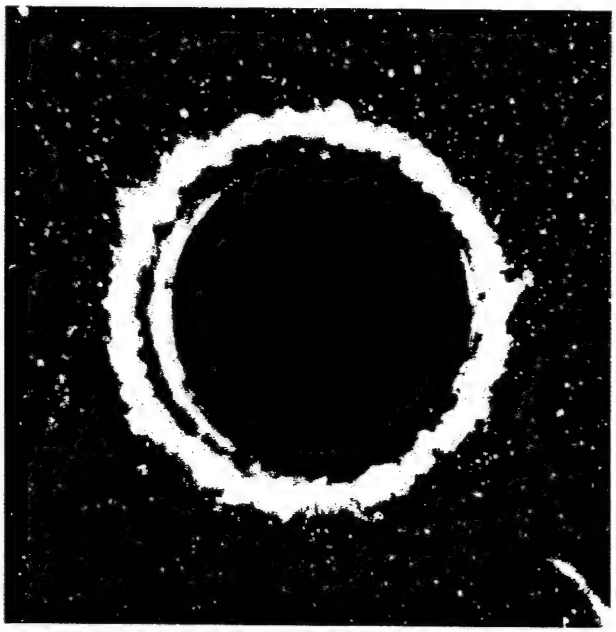

(a) No control

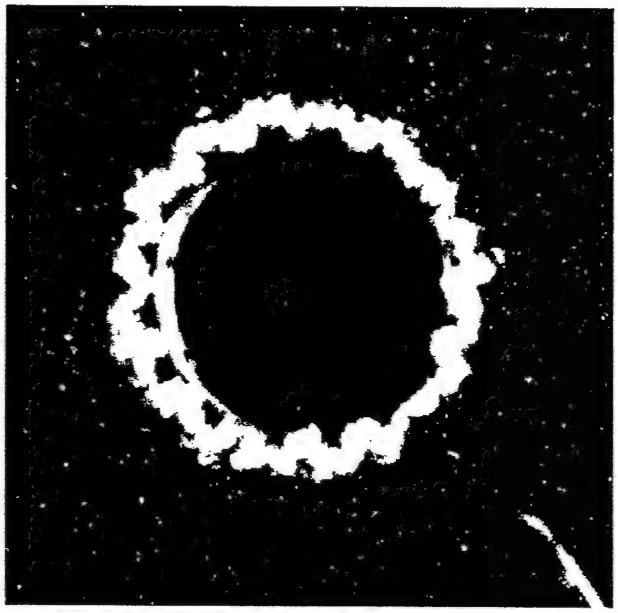

(b) With control

Fig. 14 Time-averaged PLS images taken at one diameter downstream of the nozzle, NPR=5, h/d=4; (a) No control, (b) With control.

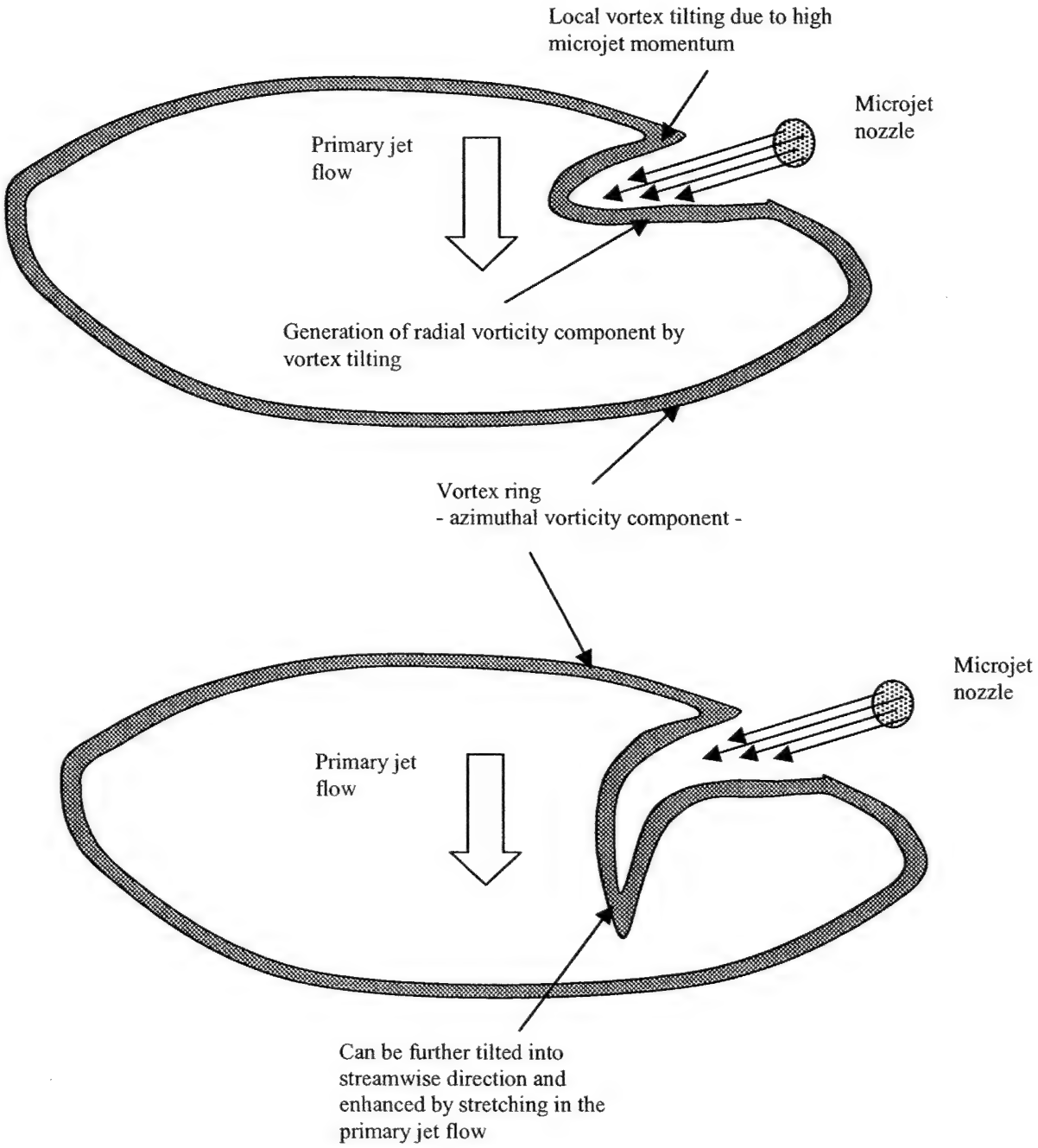

Fig. 15 Proposed vortex tilting and stretching mechanisms due to the microjet control

Appendix A3

AIAA-2001-3047

AIAA 2001-3047

Behavior of Free and Impinging Supersonic Microjets

K. A. Phalnikar‡, F. S. Alvi§ and C. Shih†

Department of Mechanical Engineering
2525 Pottsdamer Street
Florida A & M University and Florida State University
Tallahassee, FL 32310

The fluid dynamics of microflows has recently commanded considerable attention because of their potential applications. To date, most of this work has been limited to low velocity flows. The present study examines supersonic microjets in the range of 100 - 400 microns with exit velocities in the range of 400-500 m/s. Such microjets are presently being used to actively control larger supersonic impinging jets, which occur in STOVL (Short Takeoff and Vertical Landing) aircraft. The flow field is visualized using a Micro-schlieren system with effective magnifications greater than 100x. Schlieren images, which to the best of our knowledge have never before been obtained at this scale, clearly show the characteristic shock cell structure observed in large-scale jets. Based on these images, the jet is clearly supersonic as far as 10-12 diameters downstream. Quantitative measurements providing jet decay and spreading rates as well as shock cell spacing are also obtained via pressure surveys using micro-pitot probes. Overall, the microjet properties are similar to larger supersonic jets, especially those operating at similar Reynolds number. However, pronounced viscous effects in the present microjets do lead to some differences. The impingement of these supersonic microjets on flat surfaces is also examined in this study. A comparison reveals that the flow structure of impinging microjets strongly resembles that of larger, macro supersonic impinging jets.

1. INTRODUCTION

Recent years have seen considerable research in the fluid dynamics of high-speed microjets due to their potential use in applications such as micro-propulsion, cooling of MEMS (Micro-Electro Mechanical Systems) components, fine particle deposition and removal as well as in inkjet printer heads. Supersonic microjets present several advantages over subsonic jets. For example, in cooling applications by jet impingement, supersonic microjets offer a concentrated source of cooling fluid because of lower jet spreading rates, as well as rapid heat removal due to high heat transfer rates in the jet impingement region and inherently high velocities. Microjets are also presently being used as actuators to control the ground effects created by large-scale supersonic impinging jets which typically occur in STOVL (Short Take-Off and Vertical Landing) aircraft.[1]

To-date studies have mainly focused on internal flows in micro-channels and nozzles. Meinhart et al [2] describe a MicroPIV investigation of flow through an inkjet printer. Breuer and Bayt [3] carried out a detailed computational and experimental study examining the flowfield inside silicon-etched converging–diverging (c-d) micronozzles with throat heights ranging from 10-50 μm. Their study emphasized the behavior and influence of the nozzle boundary layer on the thrust performance of these micronozzles. No measurements of the external flow were made in their work, the presence of supersonic flow was estimated via mass flow and thrust measurements. A comprehensive analysis of MEMS based Microthruster system has been conducted by Bayt [4]. Scroggs and Settles [5] obtained schlieren images as well as pitot pressure surveys for supersonic jets issuing from c-d nozzles ranging in size from 1200

‡ Graduate Research Assistant.

§Assistant Professor, Senior Member AIAA.

†Associate Professor, Senior Member AIAA.

μm to 600 μm. Smedley et al [6] discuss an application of supersonic microjets for surface entrainment of particles for shock induced cleaning.

The present study examines the external flow properties of supersonic microjets smaller than those investigated to-date. The flowfield is characterized both visually and through quantitative measurements for a number of microjets operating over a range of pressure ratios. These measurements are expected to yield useful insight into the behavior of supersonic microjets at relatively low Reynolds numbers compared to conventional, larger 'macrojets'. They are also expected to shed some light on the viscous effects in microjets due to relatively larger boundary layers.

2. THE EXPERIMENTAL PROGRAM

2.1 Micronozzles

The nozzles used to obtain supersonic microjets were manufactured using stainless steel hypodermic tubing. Such tubing is commercially available in a range of sizes with internal diameters as small as 50 μm. The nozzles were fabricated by starting out with larger diameter tubing which was large enough to connect to the high pressure source via flexible plastic tubing; in the present case the largest tube was 1.6 mm in outer diameter. Small straight sections of successively smaller hypodermic tubing were cut, ground and concentrically inserted (press-fit) inside the larger tubing. This process was continued until the final section was of the desired size. A final coat of epoxy was applied on the outer surface at the junctions of different size tubes in order to prevent leakage.

Care was taken to keep the length of the final smallest-diameter section of tubing as small as possible in order to minimize the viscous losses by reducing the size of the nozzle boundary layer. Using the above method, micronozzles of internal diameters 400 μm and 200 μm were fabricated along with a pitot probe of 50 μm diameter. In order to examine the impingement of microjets on a flat surface, a circular aluminum impingement plate was also fabricated. Using the same technique of press-fitting successively smaller straight tubes as described earlier, a 50 μm circular surface pressure port was fabricated at the center of the plate, to provide surface pressure measurements during impingement. Figure 1 shows the micronozzles and the pitot probe. Also shown is a human hair, included to provide some perspective of the physical length scales. Details of the optical setup are provided next.

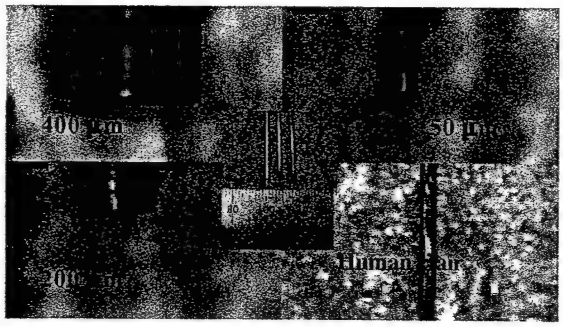

Figure 1 : Nozzles and pitot probe used in the experiments.

2.2 Micro-schlieren system

Mirror based schlieren systems have been traditionally used for the study of fluid flows. Conventionally, a mirror-based system is used for flowfields involving larger length scales, since larger front-surface mirrors are relatively inexpensive with fewer optical aberrations. However, the scales being dealt with in the present study are of the order of tens of microns (~10μm), which is too small to be resolved by conventional schlieren optics. Hence a specialized schlieren system, which is capable of visualizing flows at the present microscales, must be designed. The main factors, which have to be controlled for optimal visualization, are *magnification, resolution, field of view* and *sensitivity*. In the present case, diffraction effects, not generally an issue in conventional 'macro-scale' schlieren systems, also become important.

In selecting the optics, the linear magnification of the final image was used as the primary design criteria. The parameters which affect the magnification are the focal length of primary mirrors (or lenses, for lens based system), the focal length of camera or imaging lens, and the distances between the mirror/lens and jet as well as that

between the mirror/lens and the camera. A higher magnification can be achieved by using primary mirrors/lenses with short focal lengths and camera lenses with longer focal lengths. We used the thin lens equation given by :

$$1/f = 1/u + 1/v \qquad (1)$$

to select the focal lengths to be used on all optics. Here f represents the focal length, u is the object distance from the mirror/lens and v is the image distance. Although the above formula is approximate, it is an efficient way to choose an appropriate combination of lenses and yields acceptable results for our application.

In designing a Micro-schlieren system with very high magnifications, several aspects have to be taken into consideration. First, there is a limitation on using long focal length imaging lenses for the camera, since the working distance for commercially available imaging lenses increases with focal length, whereas these larger working distances lead to lower magnifications. Therefore, there is a need to optimize the two parameters, i.e high magnifications and lower working distances, which display opposing trends. Secondly, the image of the source formed by the optics must be a real image in order for a knife-edge, a critical part of any schlieren system, to be used. This also places a limitation on the magnification that can be obtained. Furthermore, due to the small scales involved in the present flow, the optics have to be aligned very precisely which requires considerable fine-tuning during optical alignment

After experimenting with and evaluating a number of combinations of schlieren mirrors/lenses and imaging lenses, a pair of 2 inch, *f*/6 mirrors was selected for the 400 μm jet. Similarly, a pair of 1 inch, *f*/2.6 achromatic lenses was chosen for the 200 μm jet flow visualization. Resultant magnifications obtained from the mirror-based system for 400 μm jets is 41x and that obtained by the lens-based system for the 200 μm jets is 113x. A graded filter, instead of a sharp knife-edge, was used as a cut-off where a graded cutoff minimized diffraction effects while providing good sensitivity. A white light stroboscopic lamp with adjustable frequency (up to 1 KHz) and intensity served as the light source. The camera used for imaging was Kodak Megaplus 1.4 with a CCD array resolution of 1024 x 1024 pixels. A 200 mm Nikon imaging lens in conjunction with a 2X converter was used with this camera providing an effective focal length of 400 mm. Using the calculated magnification and the camera pixel resolution, image resolutions as high as 1.5 μm/pixel were achieved for the 200 μm jet flow visualization system. Due to the approximation inherent in the thin lens equation along with other optical aberrations, the actual spatial resolution is expected to be lower than the calculated value.

2.3 Facility

The nozzles, impinging plate, schlieren optics and the probes were mounted on an optical table. The gas used was bottled, compressed Nitrogen which was filtered through a 50 μm filter before delivery to the plenum chamber. We note that Nitrogen was used instead of air because it was much easier to obtain high purity bottled nitrogen. However, given the similarity in the gas dynamic properties between air and nitrogen, the behavior observed in the present experiments should also be valid for air. A plenum chamber was connected to the nozzles through a large-diameter vinyl tubing. Both the nozzles and the pitot probe were mounted on precision machined v – blocks, which were aligned with each other in the axial direction by using precision ground and polished stainless steel shafts.

2.4 Pressure Measurements

Both free jets and impinging jets were characterized in this study; for all cases discussed in this paper the jets were issuing into a quiescent ambient environment at atmospheric pressure. Free jet pressure surveys were performed by mounting the 50 μm probe on a v-block, which in turn was traversed using a precision 3 - axis micrometer stage. The stage allowed precise increments as small as 25 μm in the horizontal plane and 10 μm in the vertical plane. In the impinging jet studies, the impingement plate replaced the probe on the micrometer stage. Pressure measurements were carried out with a Validyne pressure transducer connected to a Validyne CD 19A module. Tests were carried out for the microjets operating under subsonic conditions as well as underexpanded

supersonic conditions. The results of the flow visualization and pitot pressure studies are presented in the following sections.

3. RESULTS AND DISCUSSION

3.1 Supersonic Free Jet Structure Using Flow Visualization

This section presents the results obtained from the flow visualization of the free jets using the micro-schlieren arrangement described earlier. The impinging jets are discussed in a later section of this paper. Flow visualization was mainly carried out to provide a global view of the overall flowfield and to allow for a comparison of the microjet flowfield to that of macroscale supersonic underexpanded jets. The nozzles used for the above study were the 200 μm and 400 μm nozzles fabricated with straight hypodermic tubing using the process described earlier. In addition, visualizations were also obtained for a 100 μm c-d nozzle, which was fabricated using a Deep Reactive Ion Etching (DRIE) process commonly used for MEMS fabrication [7]. The wall contour for the c-d nozzle was designed using Method of Characteristics. The plenum pressure was varied from 60 psia to 120 psia thus providing flowfield images for a wide range of operating conditions representing different degrees of underexpansion. To the authors' knowledge, this is the first clear visualization of external supersonic flow at these microscales. Earlier documented studies were mainly concerned with internal flow in silicon etched microchannels [2,3], while Settles and Scroggs[5] examined external flow from comparatively larger – 600 μm and 1200 μm – microjets.

Figures 2 (a), (b) and (c) show a series of schleiren images of the underexpanded flow from the 100 μm nozzle at plenum pressures of 60, 80 and 100 psia, respectively. It should be noted that the nozzle exit of the 100 μm nozzle is blocked from view due to the nature of construction. Hence the flow structure is captured only from about 3 diameters downstream, missing the strongest shock cells formed near the nozzle exit.

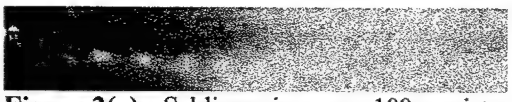

Figure 2(a) : Schlieren images - 100 μm jet at 60 psia.

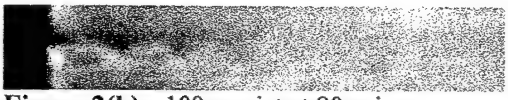

Figure 2(b) : 100 μm jet at 80 psia.

Figure 2c) : 100 μm jet at 100 psia.

Figure 3 shows schlieren images of 200 μm jet flowfield are shown in 3 (a), (b), (c) at plenum pressures of 80, 100 and 120 psia, respectively. Similarly, figures 4 (a), (b), (c), (d) show the flowfield for 400 μm jets at plenum pressures of 60, 80, 100 and 120 psia, respectively.

Figure 3(a) : Schlieren images - 200 μm jet at 80 psia.

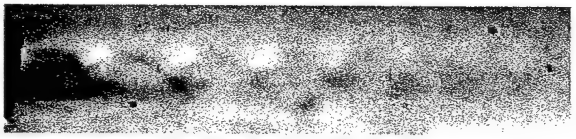

Figure 3(b) : 200 μm jet at 100 psia.

Figure 3(c) : 200 μm jet at 120 psia.

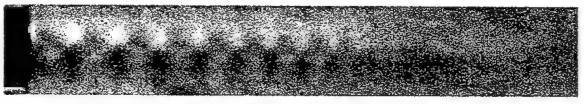

Figure 4(a) : Schlieren images - 400 μm jet at 60 psia.

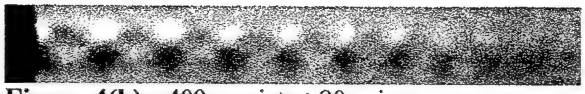

Figure 4(b) : 400 μm jet at 80 psia.

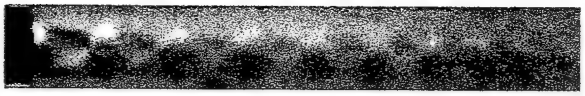

Figure 4(c) : 400 μm jet at 100 psia.

Figure 4(d) : 400 μm jet at 120 psia.

A summary of the flow visualization test cases is provided in Table 1 for the 200 and 400 μm nozzles. Due to viscous losses between the plenum and the nozzle exit, the total pressures at the nozzle exit are necessarily lower than the plenum pressures. The total pressures at the nozzle exit corresponding to each plenum pressure are shown in the table. Also listed in this table is the corresponding Nozzle Pressure Ratio, NPR, where NPR is the ratio of total pressure at the nozzle exit to ambient pressure: $P_o/P_{ambient}$, M_j, the fully-expanded jet Mach number and the Reynolds number based on the nozzle exit diameter.

Nozzle Size (μm)	P_{plenum} (psia)	$P_{0,exit}$ (psia)	NPR	M_j	Re_d
200	60	56.4	3.83	1.53	11750
200	80	76.9	5.23	1.74	15700
200	100	92.2	6.27	1.86	19600
200	120	107.4	7.3	1.96	23500
400	60	50.4	3.42	1.45	23500
400	80	67.2	4.57	1.65	31000
400	100	83.8	5.7	1.8	40000
400	120	97.5	6.63	1.89	47000

Table 1: Test cases for microjet characterization

Several common features of the three different microjets can be observed in these images. Overall, increasing the stagnation pressure makes the jet plume more visible for all three nozzles, primarily due to stronger density gradients, which persist over longer axial distances. In addition, the length of the supersonic core, roughly indicated by the streamwise extent of the shock cells also increases with increasing NPR as expected. This trend has also been well-documented for larger, high Reynolds number jets [8] as well as for supersonic microjets [5]. The pitot surveys also confirm this observation.

The quasi-periodic shock cell structure clearly seen in all the images is characteristic of supersonic flow of underexpanded jets, this structure is qualitatively very similar to that observed in larger jets. The effect of increasing the NPR, i.e. the degree of underexpansion, on the shock cell spacing can be clearly seen in all three series of images. The shock-cell spacing increases with increasing NPR, resulting in a corresponding increase in the supersonic length for all three jets. The increase in shock cell spacing with increasing fully developed jet Mach number (or NPR) is expected and has been well-documented for a wide range of supersonic jets. Pitot measurements carried out on the 200 μm and the 400 μm jets confirm this observation, as discussed later.

Closer examination of the 200 μm and 400 μm jet images shows that at lower plenum pressures, when the jet is moderately underexpanded, the oblique shocks originating at the jet exit form a normal crossing. However, as the jet underexpansion ratio increases an irregular crossing occurs, resulting in a central Mach disk. The presence of such Mach disks can be seen in figures 3(b) and (c) and 4(c) and (d). Settles and Scroggs [5] observed similar features in underexpanded flows in supersonic microjets of 600 μm and 1.2 mm diameter. These features are also similar to larger jets operating at much higher Reynolds numbers.

The shock cell spacing can also be determined from such schlieren images which can then be compared to the spacing measured using micro-pitot probe surveys. Such a comparison was made for the 400 μm jets and the agreement between experimental and visual data was found to be very good, as seen in figure 5. A more detailed discussion of this behavior is delayed until later, after the results of the pressure surveys have been presented.

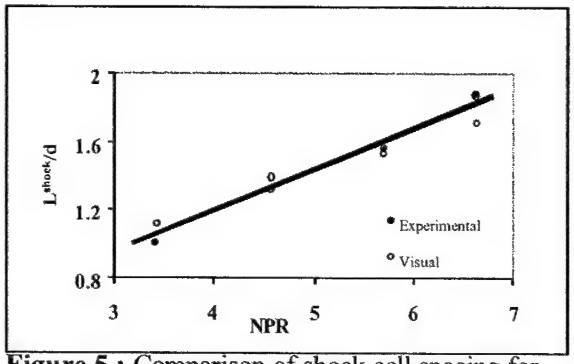

Figure 5 : Comparison of shock cell spacing for 400 μm measured experimentally and visually.

Before proceeding to the pitot results, we note a few more features observed in the free jet visualization. The micro length-scales involved in the present flow coupled with the very high fluid velocities, leads to time scales associated with the large-scale turbulent structures, which are in the sub-microsecond range. As a result, the microsecond flash duration of the schlieren light source – in the range of 5 to10 μs – would effectively 'smear' the turbulent structures. Consequently, the microschlieren images obtained are in essence time-averaged. A "flapping" of the jets was visible towards the end of the supersonic core length and it is believed to be a result of the acoustic feedback instability due to screech, which is a widely observed phenomenon in larger scale jets [9]. In the following, we first present the results of pitot pressure measurements of a high subsonic (almost sonic) jet followed by measurements in supersonic underexpanded jets.

3.2 Properties of High Subsonic (M = 0.9) Free Jets

3.2.1 Pressure Surveys

Centerline and radial surveys were carried out on the 200 μm and the 400 μm jets operating at subsonic conditions. The initial aim of these tests was to produce and examine shock-free, perfectly expanded, sonic jets, which would make the characterization of the potential core region unambiguous. Theoretically, a perfectly expanded sonic jet would issue from the converging micronozzle into the ambient environment for a plenum pressure of 28.5 psia as this corresponds to an exit static pressure of 14.7 psia. However, due to viscous losses, which are especially significant in the present micronozzles, this plenum pressure resulted in an exit Mach number lower than 1 thus producing a subsonic jet. Exit Mach numbers of 0.9 and 0.88 were obtained for the 200 μm jet and 400 μm jet respectively. Accounting for the experimental uncertainty in the Mach number calculation of +/- 0.03, the exit Mach numbers of both these nozzles is essentially the same. The Reynolds number obtained in the present work approximately matches that of the large-scale jets examined in detail by Morrison and Mclaughlin [10] allowing for a direct comparison to their results. Such a comparison is made in the next section where details of Mach 0.9 pressure surveys, shown in figs. 6 through 11, are discussed.

3.2.2 Jet Centerline Surveys

Figure 6 shows the variation of centerline Mach number for the 200 μm and 400 μm jets as a function of the non-dimensional axial distance from nozzle exit.

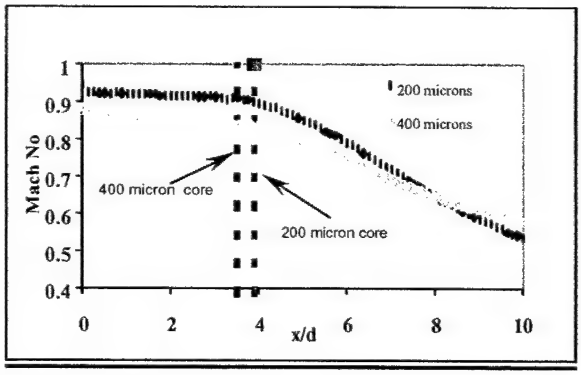

Figure 6 : Variation of centerline Mach no for 200 μm and 400 μm jets operating at $M_j = 0.9$

The Mach number was calculated by assuming that the static pressure is equal to ambient pressure. The pitot probe was traversed in increments of 25 μm along the jet centerline. The presence of a potential core, as indicated by the region of constant pitot pressure can be clearly seen in the plot indicating the presence of a significant inviscid region even at very low Reynolds numbers. This result is significant because, at such small scales, one would expect increased viscous effects due to the low Reynolds number. The

resultant thicker nozzle boundary layer would cause a rapid merging of jet shear layers very close to nozzle exit, resulting in the absence of a potential core. In fact, experimental investigations by Jindra [11] led him to conclude that nozzles with throat dimensions less than 350 μm produced fully viscous flows. The 200 μm nozzle used in the present study is well below this threshold and clearly produces a jet with a significant inviscid region. Although the present flow is subsonic, it is reasonable to assume that increasing the Mach number slightly above 1 should not produce any significant changes in the flow physics and the resulting supersonic jet will also contain an inviscid core.

Even though a supersonic core is present and at first glance the centerline surveys in Fig. 6 appear very similar to those of larger jets, a closer look reveals significant differences. The end of the potential cores for both jets is indicated by dashed lines in Fig 6; it is determined by defining the end as the point at which the centerline Mach number drops below 95 % of the jet exit Mach number. Using this definition, the 200 μm jet is seen to have a potential core length of 3.9 diameters, and similarly the core length for 400 μm jet is found to be 3.5 diameters. The Reynolds numbers of the jets based on jet exit diameter, are estimated to be 6000 for the 200 μm jet and 11000 for the 400 μm jet. These non-dimensional potential core lengths are substantially lower than the corresponding larger jets at higher Re numbers.

Witze[12] derived empirical correlations which provide the variation of the potential core length with Mach number. One such relation between x_c (the potential core length) and M_j (fully-expanded jet exit Mach number) is given by:

$$x_c/D = 4.2 + 1.1\ M_j^2 \qquad (2)$$

where D is the jet diameter. Using the above equation, it is found that the experimentally measured potential core lengths for both microjets are shorter by about 25 % to 30 % when compared to the above correlation.

A possible reason for the shorter inviscid cores may be as follows. By definition, the potential core region where the jet shear layers merge. The point at which this occurs is a function of the *initial* shear layer *thickness* at jet exit and the *rate* of shear layer growth. Since the present study involves very low Reynolds numbers where the viscous losses in the nozzle are expected to be substantial, a larger nozzle wall boundary layer will result in a larger initial shear layer at jet exit leading to shorter potential cores. This is supported in the study by Scroggs and Settles [5]; who obtained measurements of the boundary layer displacement thickness of a Mach 2 microjet. Their measured displacement thickness for the case of a 600 μm exit diameter Mach 2.0 nozzle was 0.038 mm which was 24 % of nozzle exit area in their study. Therefore, by similar reasoning, the relative boundary layer thickness in the present microjets is expected to be significant relative to the nozzle exit dimension. This is especially true since the Reynolds numbers in the present flows are much lower that the microjets used by Scroggs and Settles. Consequently, the larger initial boundary layer would lead to a correspondingly shorter potential core length, as observed in the present study.

A final comment regarding the relative potential core lengths of the 200 and 400 μm before closing this section. Intuitively, one would expect the potential core of the 400 μm jet to be longer whereas the centerline surveys show the reverse. Although the exact reason for this behavior is not known, following are a few possible explanations. Probe interference effects may partly be responsible for this behavior particularly for the case of 200 μm jet. It is well known that a relatively larger sized pitot probe biases the measurements to higher values of pitot pressure because of a velocity gradient effect [13]. In our case, the ratio of probe internal diameter to the jet diameter is four for the 200 μm jet , hence the error due to the velocity gradients may be significant. This may explain the higher values obtained in the measurements on the 200 μm jet as compared to those on the 400 μm jet, although one would expect more losses in the former due to a thicker boundary layer. However, we note that, due to the difficulty of fabricating and using very small probes, previous microjet studies have used probes that are much larger relative to the jet dimensions[5]. An additional contributor to the lower values of

pitot pressure for the 400 μm may be the surface roughness, which was not controlled in the fabrication process for the micronozzles and may be significant due to the small length scales.

3.2.3 Jet Shear Layer Properties

Figures 7 and 8 show the Mach number variation with radial position, for both 200 μm and 400 μm jets. Radial surveys were obtained at 6 locations, namely at x/d = 1,2,3,4,5, and 8. However, for the sake of clarity surveys at only three representative axial locations are shown.

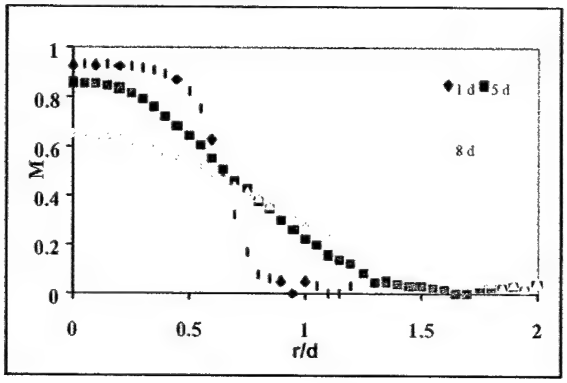

Figure 7 : Variation of local Mach number with radial position for 200 μm jet

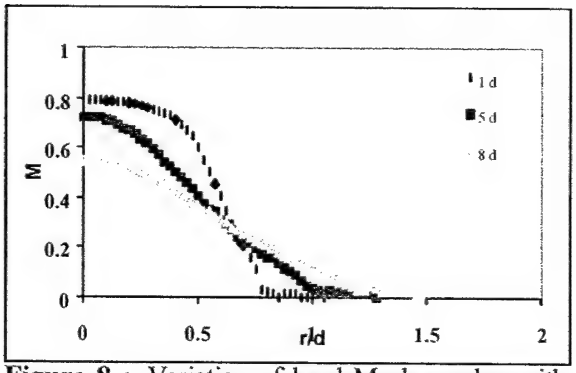

Figure 8 : Variation of local Mach number with radial position for 400 μm jet

A top hat velocity profile is present at the axial location x/d = 1 for both jets. This corresponds to the presence of a potential or inviscid core region which is evident from the near flat velocity profile near the center of the jet. As we go further downstream to x/d = 2 and 3, the size of the inviscid region in the cross-stream profiles reduces progressively due to the growth of jet shear layers. At subsequent downstream stations (x/d = 4,5, and 8), the profile changes to a central peak with a near-Gaussian shape indicating the merging of the shear layers and the development of fully viscous jet flow.

Figures 9 and 10 show the non-dimensional radial profiles for the 200 μm jet and the 400 μm jet, respectively. These correspond to the dimensional plots shown in Figs. 7 & 8, however data for all 6 axial locations obtained in the present study is included in these non-dimensional plots.

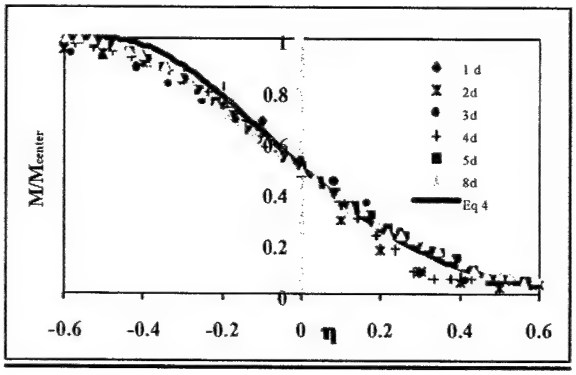

Figure 9 : Non-dimensionalized radial profiles for 200 μm jet at $M_j = 0.9$

In both these figures, the Mach number is normalized by the local centerline Mach number and the abscissa is the non-dimensional parameter η which is defined as:

$$\eta = (r - r_{0.5}) / \delta \qquad (3)$$

where r is the radial location, $r_{0.5}$ is the local jet half width and δ is the shear layer thickness. The shear layer thickness is estimated using the standard 95%-5% criteria [14]. The solid line in the plots represents the patched half – Gaussian profile as described by Morrison and McLaughlin [10] and given by the following:

$$M/M_j = \exp\{-2.773 * (\eta + 0.5)^2\} \text{ for } \eta > -0.5$$
$$= 1 \text{ for } \eta \le -0.5 \qquad (4)$$

It is seen that the profiles collapse well on a common curve, with some scatter near the outer edge of the jet shear layers, generally for η >0.4.

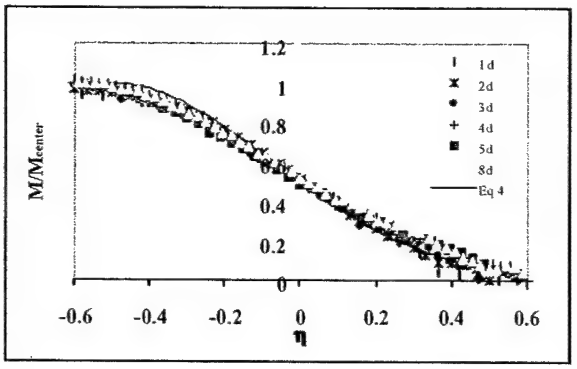

Figure 10 : Non-dimensionalized radial profiles for 400 μm jet at $M_j = 0.9$

The collapse of the cross-stream profiles in the free shear layer region - the first three axial stations – as well as in the fully viscous region is significant. It indicates that the microjet flows have achieved reasonable self-similarity in the free shear layer as well as in the downstream fully viscous region. And that the same similarity parameters can be used to describe the free shear layer and fully viscous jet behavior, at least up to two potential core lengths.

A similar collapse of radial velocity profiles in the free-shear layer and fully viscous regions was also obtained out by Morrison and McLaughlin [10] for much larger supersonic jets operating at a Mach number of 2.5. Such a representation has also been used by Morris and Tam [15] to fit a substantial amount of conventional high Reynolds number supersonic jet data. The Reynolds number used in the experiments by Morrison and McLaughlin is around 8000, which is in the range of our current experiments. However, the nozzles used in their study are larger in diameter (6.9 to 10 mm). Hence, even though we are operating at diameters which in some cases are almost two orders of magnitude (as much as 50 times or more) smaller, the very good collapse of profiles is noteworthy. This indicates that flow properties of microjets as small as 200 μm in diameter can be reliably predicted by analogy with larger jets, as long as Reynolds numbers are close. It also suggests that the substantially larger boundary layer (relative to nozzle size) does not substantially affect the Reynolds number similarity.

Having seen the effect of operating at microscales on high subsonic (or transonic) jets, it is of interest to study the behavior of supersonic microjets. This was achieved by obtaining similar pitot measurements for moderately and highly underexpanded jets; these results are presented in the following sections.

3.3 Underexpanded Jets

3.3.1 Centerline Surveys

Centerline pitot pressure surveys were conducted for both the 200 μm and 400 μm jets operating at a range of underexpanded conditions. The results of these surveys are presented in Figs 11(a) and 11(b). The surveys were carried out for four different plenum pressures for each jet which resulted in NPR values ranging from approximately 3.5 to 7.5 corresponding to moderately to highly underexpanded jets The difference in behavior of the flow field with NPR is easily evident both in the schlieren visualizations (figures 3 and 4) presented earlier as well as in the centerline surveys discussed next.

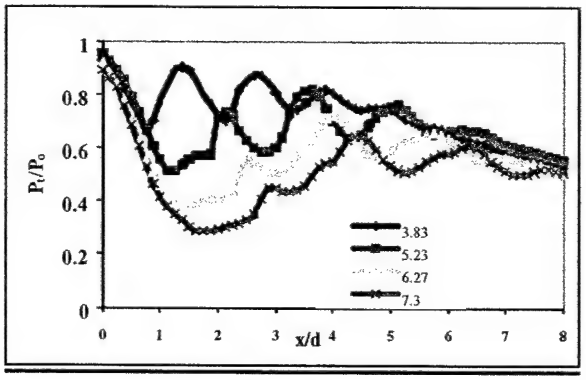

Figure 11 (a) : Centerline pitot pressure variation for 200 μm jet at various NPR

Figure 11(a) shows the centerline surveys for the 200 μm jet. The plenum pressure is varied from 60 psia to 120 psia, the data is non- dimensionalized on the abscissa by the jet exit diameter and on the ordinate by the ambient pressure. Several observations can be made regarding these surveys. The variation in pitot pressure shows the characteristic quasi- periodic structure, which is due to the presence of shock cells in the flow field. Visual observations (see figures 3 and 4) indicate that these shock cells are present as far as 10 jet diameters downstream, however in the surveys,

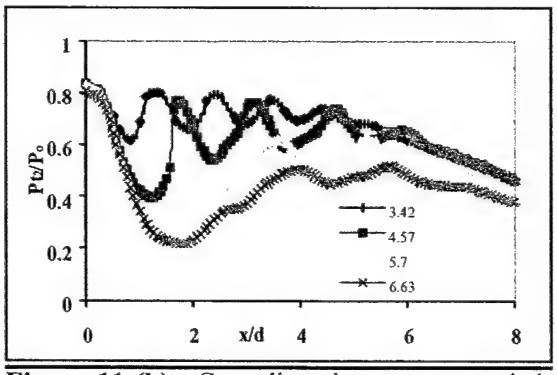

Figure 11 (b) : Centerline pitot pressure variation for 400 μm jet at various NPR

they are detected only up to ~ 7 diameters. This discrepancy may in part be attributed to probe mis-alignment. The v-blocks that hold the nozzle and pitot probe are initially aligned with each other using precision-ground, polished, stainless steel guiding shafts. As the probe is traversed downstream, any angular misalignment present initially will translate into large linear misalignments, thus affecting the measurements. Another reason for this discrepancy may be that as we travel downstream, the shock strength progressively decreases and the pitot probe may no longer be able to resolve the change in pressure as it traverses a weak oblique shock. Nevertheless, the average shock cell spacing measured visually and by pitot measurements show good agreement, as discussed previously (see figure 5). A representative comparison between a flow visualization and centerline survey is shown in figure 12.

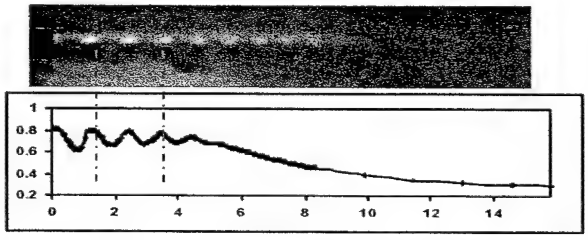

Figure 12 : Comparison of visual and measured flowfield.

The effect of increasing NPR on the overall flowfield, visually observed in Fig. 2 through 4, is confirmed by the centerline surveys. As the NPR is increased, the flow field is seen to stretch, where the shock cell spacing increases, leading to an increase in the length over which the shocks are present. At low NPR, the oblique shocks cross in a normal fashion, which changes to irregular crossing as the total pressure is increased. At a plenum pressure of 100 psia corresponding to NPR = 6.3; a Mach disk is first visually observed at the end of the first shock cell. In the pitot surveys, the Mach disk is manifested as a sudden drop in the pitot pressure because flow downstream of it is subsonic. In the schlieren visualizations too, the formation of Mach disk can be clearly seen. Figure 11(b) shows the centerline surveys for the 400 μm jet, which in general displays characteristics very similar to the 200 μm jet. Similar to the 200 μm jet, the Mach disk appears when the plenum pressure is raised to 100 psia. The periodic shock cell structure is evident from the plots and the variation in spacing with NPR also displays similar trends.

3.3.2 Shock Cell Properties

The centerline surveys, coupled with the schlieren visualization, provide an insight in to the shock cell spacing and other parameters of these jets. These can then be compared to larger scale jets, to understand the effect of Reynolds number on flow properties. We again note that conventional larger scale supersonic jets that exhaust into ambient conditions operate at Reynolds numbers that are orders of magnitude larger than the present case. Therefore an understanding of shock cell parameters, which are commonly used to characterize most supersonic jets [9] is important from a fundamental perspective.

Tam and Tanna [16] carried out computations on shock cell spacing of supersonic jets and proposed an approximate formula for round jets:

$$L_s = 2\pi R\,(M_j^2 - 1)^{1/2} / 2.405 \qquad (5)$$

where L_s is the shock cell spacing, R is the radius of the jet and M_j is the fully expanded jet Mach number.

Extensive comparisons between experimental results and those predicted by the above correlation were carried out by Tam et al [17] who found good agreement between the two. For the present case,

the shock cell spacing was determined from centerline measurements and compared to Tam's prediction. Studies carried out at a Mach number of 1.4 for both 200 μm jet and 400 μm jets showed the shock cell spacing to be 12 % and 18 % lower, respectively, than Tam's predictions. Similar comparisons were also made by Hu and McLaughlin [18] for low Reynolds number (8000) underexpanded supersonic jets exhausting from convergent nozzles. They found the shock cell spacing to be 10 % smaller than estimated values. This was attributed to thicker boundary layer thickness due to low Reynolds number of the jets. In the present case, the nozzles are much smaller and are fabricated using short straight tubes without a well-designed nozzle wall profile. Consequently, viscous effects in the present nozzles are expected to be higher, compared to the contoured nozzles used by Hu and McLaughlin. This would also account for the larger discrepancy in the shock cell spacing with Tam's predictions, which was validated for jets with thin nozzle boundary layers.

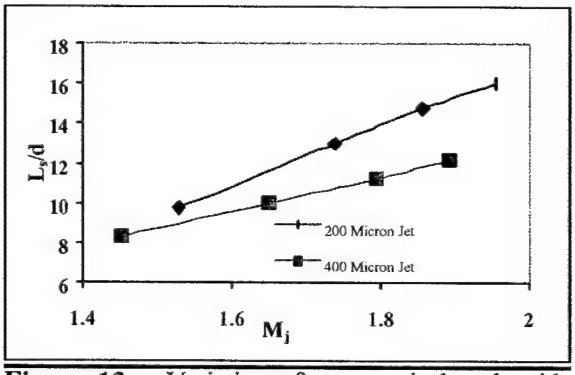

Figure 13 : Variation of supersonic length with Mach number for 200 and 400 μm jets.

Figure 13 shows the variation of the supersonic core length as a function of fully expanded jet Mach number M_j. As expected, the supersonic core length non-dimensionalized by the jet exit diameter is a linear function of the fully expanded jet Mach number. Such a linear dependence on NPR has been reported in previous studies carried out on larger supersonic jets [8]. However, the present authors have not found a universal linear fit published for this parameter. This is in part, due to the significant differences in the results obtained by various researchers. As an example, supersonic core lengths measured by Snedker and Donaldson [19] differ from those obtained by Nagamatsu & Sheer [20] for jets operating under similar conditions. When the experimentally observed supersonic core length in our study is compared with their results, the values for microjets are 25 % to 45 % lower, with the difference increasing with increasing NPR. The shorter supersonic core lengths are expected for the same reasons responsible for the shorter potential cores and shorter shock cell spacing of microjets. In short, viscous effects appear have a noticeable effect on the behavior of microjets with respect to these parameters.

3.3.3 Cross Stream Surveys

Radial pitot pressure variation was examined for both jets operating at under-expanded conditions. Pressure profiles for the 400 μm jet, which are representative of profiles at other conditions, are presented in Figs 14 through 16. The radial profiles were obtained at 6 axial stations ranging from x/d = 0.5 to x/d = 4 .The plenum pressure was maintained at 120 psia corresponding to an NPR of 6.6, the highest degree of underexpansion in the present study.

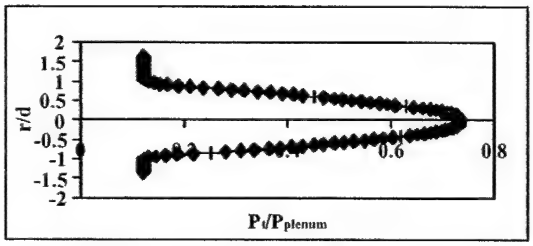

Figure 14 : Radial pitot pressure profile for 400 μm underexpanded jet at x/d = 0.5, NPR = 6.6.

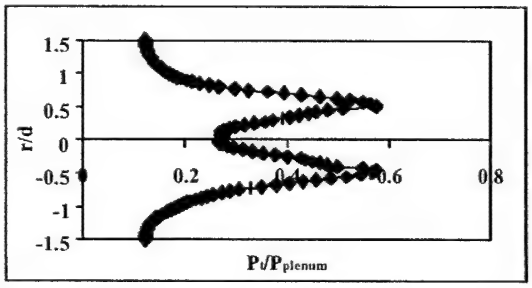

Figure 15 : Radial pitot pressure profile for 400 μm underexpanded jet at x/d = 2, NPR = 6.6.

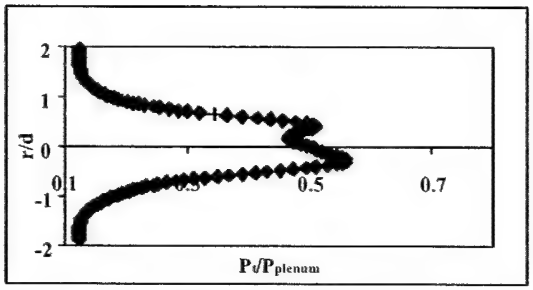

Figure 16 : Radial pitot pressure profile for 400 μm underexpanded jet at x/d = 4, NPR = 6.6.

The aim of these measurements was mainly to study the jet spreading under under-expanded conditions. Figure 14 shows the radial profile at x/d = 0.5, figure 15 shows the profile at x/d = 2 and figure 16 shows the profile obtained at x/d = 4. It is seen that the profile initially has a central peak, which is mainly due to the expansion fan located right at the exit. Figure 15 represents profiles at the axial location just after the Mach disk and hence the depression in the center is pronounced due to the flow becoming subsonic for some distance downstream. As we move further away from the jet exit, the shape relaxes back to the central peak profile; at large distances it will return to the Gaussian-type distribution as the shock cells become weaker in strength and shear layers merge.

A qualitative comparison of this radial pitot pressure distribution to that obtained by Hu & McLaughlin [18] for low Reynolds number underexpanded jets at M_j = 2, (M_j for the present case is 1.89), reveals some similarities. Both cases show a lower velocity core and a higher velocity annulus, that eventually changes to a Gaussian shape at large distances downstream. One of the fundamental characteristics of supersonic mixing layers is the linear spreading of the shear layer with downstream distance. However, when the jets are operating at off design conditions, the exact determination of the shear layer thickness is not trivial because of the presence of expansion and compression waves. Hence, the use of the local centerline velocity as a reference velocity will not provide meaningful and consistent results. This problem is overcome by considering the slope of the velocity profile [21]. Defining the shear layer thickness using the 95% - 5% criteria applied to the pitot pressure profile, we can determine the variation of shear layer thickness as a function of the axial distance from the jet exit. This is shown in figure 17 where the y-axis displays the shear layer pitot thickness δ, non-dimensionalized by the jet diameter and the abscissa represents the axial location. The plot suggests that the shear layer displays fairly linear growth, similar to large-scale high Reynolds number jets.

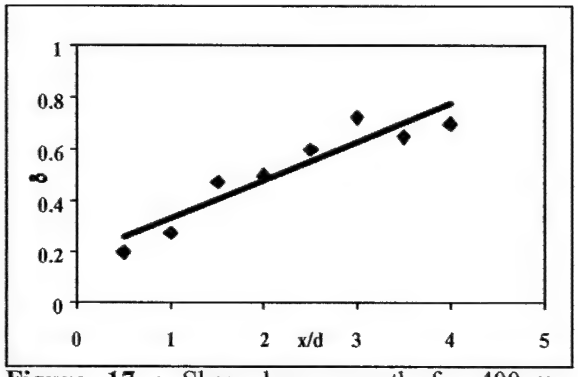

Figure 17 : Shear layer growth for 400 μm underexpanded jet

3.4 Supersonic Impinging Jets

Another aspect of the present research is the study of microjet impingement on a flat surface. Both the 200 μm and 400 μm converging nozzles operating at NPR 5 were used as sources of supersonic impinging jets. The impact plate described earlier in the paper was used for measuring the pressure distribution on the surface. The plate was traversed in steps of 10 μm to obtain pressure readings all over the flow field.

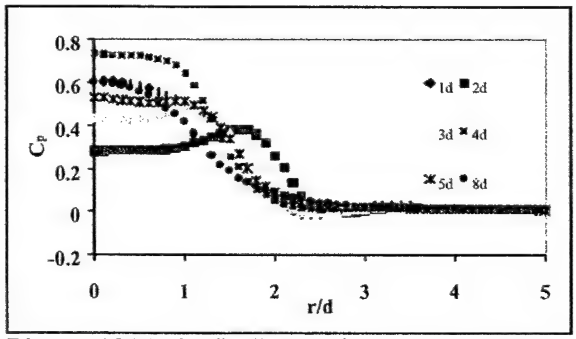

Figure 18(a) C_p distribution for 200 μm impinging jet at NPR 5.

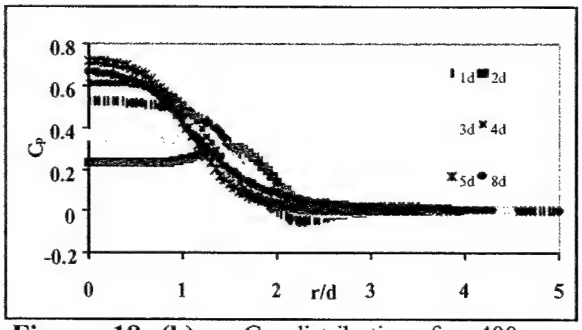

Figure 18 (b) : C_p distribution for 400 μm impinging jet at NPR 5.

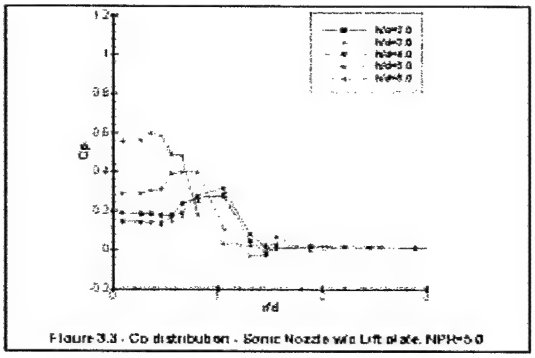

Figure 18(c) : C_p distribution for 1 inch impinging jet at NPR 5 (reference 23).

Figures 18 (a) and (b) show the radial distribution of the non-dimensional pressure coefficient, Cp, which is defined as $Cp = (P - P_{ambient})/(P_{plenum} - P_{ambient})$ for both the jets. Cp is plotted on the Y axis while the abscissa represents the radial location on the plate, non-dimensionalized by the jet diameter. The tests were carried out at different nozzle-to-plate distances, denoted in the plots by the values of h/d, while the nozzle pressure was maintained for NPR ~ 5. Preliminary examination of the plots shows an annular region of maximum pressure for both jets at h/d = 2 and h/d = 3. This corresponds to the formation of a recirculation region near the stagnation point, which is also referred to as 'stagnation bubble'. Such a stagnation bubble forms only for a certain range of impingement distances, being absent for very low and very high values of h/d. Flow visualization of the normal impingement also confirms the appearance and disappearance of stagnation bubble at various heights. The presence of a stagnation bubble is a function of several parameters, most important amongst them being NPR and h/d. Stagnation bubbles are generally observed for higher NPRs and over a limited range of h/d values for a given NPR. The formation of such stagnation bubbles and their appearance and disappearance at various heights has also been observed in previous investigations of large-scale supersonic impinging jets by various investigators (Kalghatgi & Hunt [22]; Alvi & Iyer [23]).

For the purpose of comparison to large-scale impinging jets, data obtained by Iyer [24] for a one inch diameter supersonic impinging jet is presented in figure 18(c). This plot represents the pressure distribution for a jet issuing from a converging nozzle at NPR 5. As can be clearly seen from the plot, the stagnation bubble is present for all h/d values, which is in contrast to the microjet impingement behavior. This difference may be attributed to several factors. The presence of a Mach disk at the end of the first shock cell for the large-scale jet at all h/d values, influences the formation of the recirculating region. The effect of Mach disk location on the stagnation bubble formation has been studied in detail by Iyer[24]. For the microjets, the Mach disk is not observed at NPR 5 due to higher viscous losses, discussed earlier, which accounts for the difference in surface pressure profiles. In addition, the lower average velocities and weaker shocks in the microjet flowfield can also contribute to the difference. However, as can be seen in Fig 19(a) and (b), at least visually, the flowfield of impinging microjets compares very well with that of the larger impinging jets at the same h/d and NPR value.

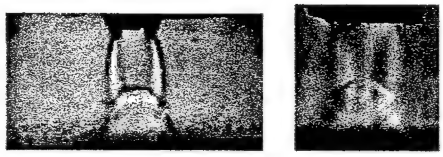

(a) d = 25000 μm (b) d = 400 μm

Figure 19 : Visual Comparison of jet impingement flowfield at NPR 5 and h/d = 2.

Figures 20(a), (b) and (c) show the impingement of 200 μm jet at different h/d values. A similar flowfield development is observed in the visualizations of the 400 μm impinging jet.

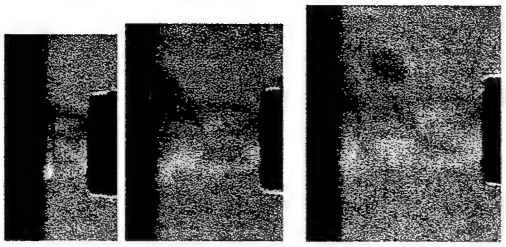

(a) h/d = 1 (b) h/d = 2 (c)h/d = 3

Figure 20 : 200 μm impinging jet at NPR ~ 7

Furthermore, the evolution of the supersonic microjet impinging flowfield is qualitatively very similar to that of large scale impinging jets operating under similar conditions [23, 24]. The impinging jet results are important from a practical point of view, since they are the first step in developing new applications for impinging microjets including cooling/heating, particle removal and others mentioned in the introductory section of this paper.

4. CONCLUSIONS

The present study was an effort to characterize supersonic jets issuing from converging micronozzles, in order to study the effect of microscales and low Reynolds number on their flow properties. Supersonic flow was produced from relatively inexpensive micronozzles fabricated without using specialized manufacturing techniques. The flowfield was successfully visualized using a Micro-schlieren system and the images obtained showed the characteristic shock cell structure similar to that observed for larger scale supersonic jets. To our knowledge, these are the smallest supersonic jets to be visualized to date. Studies on near-sonic jets showed the existence of a potential core over a measurable streamwise extent even at such low Reynolds numbers and small length scales. The collapse of radial profiles on a similarity curve was particularly interesting from a fundamental point of view. This indicates that flow properties of microjets as small as 200 μm in diameter can be reliably predicted by analogy with larger jets, as long as Reynolds numbers are close. It also suggests that the substantially larger boundary layer (relative to nozzle size) does not substantially affect the Reynolds number similarity.

Pitot surveys revealed that the variation in flow properties of microjets such as the supersonic core length and shock cell spacing show trends which match those observed in their larger counterparts. However, there are some differences in the actual values of these parameters between micro and macrojets; differences which can be reasonably attributed to the pronounced viscous effects at microscales.

Underexpanded jet impingement on flat plate was studied and the results showed good agreement with larger scale jet impingement. The presence of a stagnation bubble, normally observed in large-scale impinging jets, was also confirmed from surface pressure measurements. We believe that this work provides a better understanding of compressible microjets and serves as a good starting point for developing future applications involving both free and impinging supersonic microjets.

5. ACKNOWLEDGEMENTS

The authors would like to thank Prof. A. Krothapalli for his support and advice. This research program is supported by grants from NASA Headquarters and AFOSR (monitored by Dr. Steve Walker); their support is gratefully acknowledged.

6. REFERENCES

1) Alvi, F. S., Elavarasan, R., Shih, C. and Garg. G., "Active Control of Supersonic Impinging Jets Using Microjets", AIAA Paper 2000-2236, AIAA, Fluids 2000 Conference, June," 2000, Denver, CO.

2) Meinhart, C. D. and Zhang, H., "The Flow Structure Inside a Microfabricated Inkjet Printhead", *Journal of Microelectromechanical Systems*, Vol. 9, No. 1, March 2000.

3) Bayt, R. and Breuer, K. "Viscous Effects in Supersonic MEMS-Fabricated Micronozzles", Proceedings of the 3rd ASME Microfluids Symposium, Nov 1998.

4) Bayt, R., "Analysis, Fabrication and Testing of a MEMS – Based Micropropulsion System", Ph. D. Dissertation, MIT, June 1999

5) Scroggs, S. D. and Settles, G. S., "An Experimental Study Of Supersonic Microjets" in Experiments in Fluids 21 (1996) .

6) Smedley, G. T., Phares, D. J. and Flagan, R. C. "Entrainment of fine particles from surfaces by impinging shock waves" *Experiments in Fluids*, Vol. 26, 1999.

7) Heschel,M., Mullendorn, M., Bouwstra, S., "Fabrication and Characterization of Truly 3D Diffuser/Nozzle Microstructures in Silicon" in Journal of Microelectromechanical Systems, 1997 March ,Vol 6, No 1, 41-46.

8) Wishart, D.P., "The Structure of a Heated Supersonic Jet Operating at Design and Off-Design Conditions", PhD. Dissertation, Florida State University, 1995.

9) Tam, C.K.W., "Supersonic Jet Noise", in Annual Review of Fluid Mechanics, 1995, 27, pp 17-43

10) Morrison, G.L., and McLaughlin, D.K., "Instability Process in Low Reynolds Number Supersonic Jets" , *AIAA Journal,* Vol 18, No 7, July 1980, page 793.

11) Jindra, K.J., Geometric Effects on the Performance Characteristics of Very Small Nozzles", 1970, Masters Thesis, Air Force Inst. Of Tech., Wright-Patterson AFB, Ohio School of Engineering, Dec.

12) Witze, P.O , AIAA Journal, 1974, 12, 417-418

13) "Measurement Techniques in Fluid Dynamics", von Karman Institute for Fluid Dynamics, October 1994.

14) Shih, C., Alvi, F. S., Washington, D.M., "Effects of Counterflow on the Aeroacoustic Properties of a Supersonic jet", in Journal of Aircraft, Volume 36, No 2, Pages 451-457.

15) Morris, P.J., and Tam, C.K.W., "Near and Far Field Noise from Large-Scale Instabilities of Axisymmetric Jets", AIAA paper 77-1351, 1977.

16) Tam, C.K.W., and Tanna, H.K., "Shock Associated Noise of Supersonic Jets from Convergent – Divergent Nozzles", Journal of Sound and Vibration, 1982,81(3), 337-358

17) Tam, C.K.W., Jackson, J. , and Seiner, J.M., "A Multiple-Scales Model of the Shock Cell Structure of Imperfectly Expanded Supersonic Jets", Journal of Fluid Mechanics, Vol 153, 1985, pp. 123-149

18) Hu , T. and McLaughlin, D.K., "Flow and Acoustic Properties of Low Reynolds Number Underexpanded Supersonic Jets , Journal of Sound and Vibration, 1990, 141(3), 485-505.

19)Snedeker,R.S., and Donaldson,C., "Experiments on Free and Impinging Underexpanded Jets from a Convergent Nozzle",1964, Aeronautical Research Associates of Princeton, Inc, ARAP Rept. 63, DDC 461,622

20) Nagamatsu ,H.,T. and Sheer, R.E., "Supersonic Jet Noise Theory and Experiments" , 1969, NASA SP- 207.

21) Alvi, F.S., Krothapalli, A., Washington, D., "Experimental Study of a Compressible Countercurrent Turbulent Shear Layer", in AIAA Journal, Volume 34, No. 4, Pages 728 – 735.

22) Kalghatgi, G.T. , and Hunt, B.L., "The Occurrence of Stagnation Bubbles in Supersonic Jet Impingement Flows", Aeronautical Quarterly, 27,1976, 169-185.

23) Alvi, F. S. and Iyer, K., "Mean and Unsteady Properties of Supersonic Impinging Jets with Lift Plates," AIAA Paper 99-1829, 5th AIAA/CEAS Aeroacoustics Conference, Bellevue, WA, May 10-12, 1999.

24) Iyer, K., "Experimental Investigation of Supersonic Impinging Jets in STOVL Configuration", Masters Degree Dissertation, 1999, Florida State University.

Appendix A4

AIAA-2002-2728

AIAA-2002-2728
Active Control of Supersonic Impinging Jets: Flowfield Properties and Closed-loop Strategies

H. Lou, F. S. Alvi and C. Shih
Department of Mechanical Engineering
Florida A & M University and Florida State University
Tallahassee, FL

J. Choi, A. Annaswamy
Department of Mechanical Engineering
Massachusetts Institute of Technology
Cambridge, MA

1st AIAA Flow Control Conference and Exhibit
24 - 27 June 2002
St. Louis, Missouri

AIAA 2002-2728

Active Control of Supersonic Impinging Jets: Flowfield Properties and Closed-loop Strategies

H.Lou * F.S.Alvi † and C.Shih ‡

Fluid Mechanics Research Laboratory, Department of Mechanical Engineering
Florida A & M University and Florida State University
Tallahassee, FL

J.Choi§, A.Annaswamy¶
Department of Mechanical Engineering
Massachusetts Institute of Technology
Cambridge, MA

Supersonic impinging jets produce a highly unsteady flowfield leading to a very noisy environment with very high dynamic pressure loads on nearby surfaces. In prior work, we demonstrated that supersonic microjets can be used to disrupt the feedback loop inherent in high-speed impinging jet flows, thereby significantly reducing the adverse effects produced by this flow. In this paper, we explore two aspects of the microjet control scheme. First, detailed PIV measurements are used to examine the role of streamwise vorticity in the feedback interruption using microjets. Second, a novel closed-loop control strategy which uses on-line pressure measurements near the nozzle exit to achieve optimal flow control irrespective of flow conditions, is explored. The PIV measurements revealed that the activation of microjets produces substantial streamwise vorticity in the form of well organized, counter-rotating pairs of streamwise vortices. The production of significantly higher streamwise vorticity due to microjets comes at the expense of the azimuthal vorticity in the shear layer. This weakens the large-scale axisymmetric structures in the jet shear layer while also introducing more three-dimensionality into the flow. Both these factors, lead to a weakening of the feedback loop, which may account for the success of this control scheme. The closed-loop control strategy consisted of determining the dominant POD mode using pressure measurements at the nozzle exit and using a 'mode matched strategy' to determine the microjet pressure distribution along the nozzle. The results demonstrated a significant reduction in the unsteady pressure loads along with a consistent improvement compared to an open-loop control strategy where the microjet pressures were kept constant. It is proposed that this improved reduction may be due to the fact that the mode-matched strategy results in the intensity of the microjets to be proportional to the corresponding acoustic wave intensity near the nozzle. The stronger microjets then provide a stronger local disruption and perhaps generate more streamwise vorticity, both of which lead to more efficient local disruption of the feedback loop resulting in larger reductions in the flow unsteadiness.

1. Introduction

The impingement of high-speed jets, on a surface, generally results in an extremely unsteady flowfield accompanied by a host of undesirable aeroacoustic properties. These include, but are not limited to, very high ambient noise levels dominated by discrete frequency tones – referred to as impingement tones – and highly unsteady pressure loads on the ground plane and on nearby surfaces.

Unfortunately, high-speed impinging jets are ubiquitously present in Short Take-Off and Vertical Landing (STOVL) aircraft during hover. In this context, the flow induced effects such as the high noise levels and impingement tones can lead to structural fatigue of the aircraft surfaces in the vicinity of the nozzles, while the high dynamic loads on the impingement surface results in increased erosion of the landing surface. For STOVL aircraft these problems are collectively referred to as ground effect.

A host of studies on the aeroacoustics of impinging jets by Neuwarth (1974), Powell (1988), Tam and Ahuja (1990), and more

---

*, § Graduate Research Assistant
† Associate Professor, Senior Member AIAA
‡ Professor, Associate Fellow AIAA
¶ Principal Research Scientist, Member AIAA

recently Krothapalli *et al.* (1999) have clearly established that the self-sustained, highly unsteady behavior of the jet and the resulting impinging tones is governed by a feedback mechanism, between the instability waves in the jet that originate at the nozzle and grow as they propagate downstream towards the impingement surface, and the acoustic waves that are produced upon impingement which then travel upstream and excite the nascent shear layer near the nozzle exit. For further details of the feedback loop, the reader is directed to the above articles.

A few years ago, a study was initiated at the Fluid Mechanics Research Laboratory (FMRL), FSU, in Tallahassee, Florida, with the aim of understanding, and more importantly controlling, supersonic impinging jet flows in order to eliminate or at least substantially reduce the ground effect.

The logical approach to controlling the adverse ground effect is to disrupt the feedback mechanism responsible for this behavior. A number of researchers have attempted varied passive and active methods in order to accomplish this goal. A brief summary of some the past attempts can be found in Alvi *et al.* (2000) (also Shih *et al.*, 2001) who describe a unique approach for controlling supersonic impinging jets. The results discussed in this paper are part of this ongoing study discussed by Alvi *et al.* (2000) and Shih *et al* (2001) where arrays of supersonic microjets are used to control much larger supersonic impinging jets.

The geometry used is very simple and consists of a single jet as shown in Fig. 1. The microjets are arranged around the primary nozzle as shown in Fig. 2. Further details of the hardware will be discussed in the Experimental section.

The reasoning behind this control approach was based on the fact that the array of supersonic microjets may disrupt the feedback loop in number of ways. The microjet streams may partially intercept the upstream propagating acoustic disturbances and this attenuates their influence on the shear layer. Second, these high momentum jets can provide spatial/temporal distortions to the coherent shear-layer instabilities thus disrupting their interactions with the acoustic field. Third, the microjet streams may generate streamwise vorticity, which could weaken the downstream traveling large-scale structures thus further weakening the feedback loop. A brief summary of earlier results of this control approach is provided in § 3. As this subsequent discussion will show, this control technique proved to be very effective overall. However, some questions remained, requiring further investigation.

First, the efficacy of this control was not uniform at all the operating conditions. Furthermore, the underlying physical mechanisms behind its effectiveness were not well-understood. However, the earlier work provided strong circumstantial evidence that the generation of streamwise vorticity might perhaps be one of the primary mechanisms responsible for the success of this approach.

In this paper, we focus on two aspects of the impinging jet control problem. The first concerns direct measurements of the velocity and vorticity field using Particle Image Velocimetry (PIV), which provide further insights into the role of vorticity in this control scheme. The second concerns the use of closed-loop control to obtain a uniform reduction of the ground effect over the entire operating range. This is achieved through the use of a novel POD-based, on-line parametric control strategy. The motivation, design, development, and implementation of this control method are also presented in this paper.

2. Experimental Details

2.1 Test Configuration and Facility

The experiments were carried out at the STOVL supersonic jet facility of the Fluid Mechanics Research Laboratory (FMRL) located at the Florida State University. A schematic of the test geometry with a single impinging jet is shown in Fig.1. This facility is used primarily to study jet-induced phenomenon on STOVL aircraft hovering in and out of ground effect. Further facility details can be found in Krothapalli *et al.* (1999).

The measurements were conducted using an axisymmetric, convergent-divergent (**C-D**) nozzle with a design Mach number of 1.5. The throat and exit diameters ($\mathbf{d}$, $\mathbf{d_e}$) of the nozzle are 2.54cm and 2.75cm (see Figs. 1 & 2). The divergent part of the nozzle is a straight-walled conic section with a 3° divergence angle from the throat to the nozzle exit. Although tests were conducted over a range of Nozzle Pressure Ratios (NPR, where NPR = stagnation pressure/ambient pressure), the results discussed in the present paper are limited to NPR = 3.7 and 5. NPR = 3.7 corresponds to an ideally expanded Mach 1.5 jet, while NPR = 5 produces a moderately under-expanded jet. A circular plate of diameter D (25.4 cm ~10d) was flush mounted with the nozzle exit. The circular plate,

henceforth referred to as the 'lift plate', represents a generic aircraft planform and has a central hole, equal to the nozzle exit diameter, through which the jet is issued. A 1m x 1m x 25 mm aluminum plate serves as the ground plane and is mounted directly under the nozzle on a hydraulic lift.

Active flow control was implemented using sixteen microjets, flush mounted circumferentially around the main jet as shown in Fig. 2a. The jets were fabricated using 400 μm diameter stainless tubes and are oriented at approximately 20° with respect to the main jet axis. The supply for the microjets was provided from compressed Nitrogen cylinders through a main and four secondary plenum chambers. In this manner, the supply pressures to each bank of microjets could be independently controlled. The discussion in the controls portion of this paper (§ 5) will illustrate why independent control of the microjet banks is an important requirement. The microjets were operated over a range of NPR = 5 to 7 where the combined mass flow rate from all the microjets was less than 0.5% of the primary jet mass flux.

2.2 Pressure Measurements

The unsteady loads generated by the impinging jet flow were measured using Kulite™ transducers on the lift plate and the ground plate. In addition, near-field noise was measured using B&K ™ microphones placed approximately 25 cm away from the jet. As discussed in § 5, in order to implement closed loop control, the azimuthal distribution of the unsteady loads on the lift plate was needed. Six high frequency response miniature Kulite ™ pressure transducers, placed symmetrically around the nozzle periphery plate, at r/d =1.3 from the nozzle centerline, were used to obtain this distribution (Fig. 2). The transducer outputs were conditioned and simultaneously sampled using National Instruments digital data acquisition cards and LabView ™ software. Standard statistical analysis techniques were used to obtain the spectral content and the Overall Sound Pressure Level (OASPL) from these measurements.

2.3 Particle Image Velocimetry

Particle Image Velocimetry was used to obtain whole-field velocity data at various jet cross-sectional planes. The primary jet was seeded with small (~0.3μm) oil droplets generated using a modified Wright Nebulizer. The ambient air was seeded with smoke particles (~1-5μm) produced by a Rosco 1600 fog generator. A schematic of the experimental arrangement of the PIV system is shown in Fig. 3.

For PIV measurements, a double-pulsed Nd:YAG laser (Spectra-Physics, 400 mJ) was used for flow field illumination. A light sheet, about 1.5 mm thick, was created using a combination of spherical and cylindrical lenses. The images were recorded by a cross-correlation CCD camera (Kodak ES 1.0) with a 1k x 1k resolution. The PIV images were acquired at a rate of 15 image pairs per second. Although it was possible to cover a larger area, the present measurements were limited to approximately 60 x 60 mm square cross section. The time between pulses was optimized at 1.2 μs. The double-pulsed images were acquired through an Imaging Technologies ICPCI board, which resides on a single slot of the PCI bus of a personal computer.

An image matching approach was used for the digital processing of the image pairs to produce the displacement field. To achieve velocity data with high spatial resolution, a novel processing scheme was used. Details of this technique are described in Lourenco *et al.* (1998). We simply note that a principal advantage of this approach is that velocity field is obtained with second-order accuracy, hence the spatial derivatives are computed with a higher precision.

The main controlling parameter in the experiment was the ground plane height h with respect to the nozzle exit, which was varied from 2d to 5d. For the PIV tests, the laser sheet position, z (see coordinate frame in Figs. 1 & 3) with respect to the nozzle exit, was varied from 1d to 3d. Experiments were conducted at NPR=2.5, 3.7 and 5, which corresponds to an over-expanded, ideally expanded and under-expanded primary jet flow, respectively. However, PIV results presented here will be limited to NPR = 5 and 3.7. The jet stagnation temperature was nominally maintained at 320 ±5 K. The slight heating of jet was used to avoid condensation during PIV measurements.

The rest of the paper is arranged as follows. In the next section we briefly summarize the results of our microjet control experiments (§ 3). This is followed by a discussion of the PIV results with an emphasis on the role of vorticity on this control scheme (§ 4). Finally, the development and implementation of the closed-loop control algorithm is presented in § 5.

3. Previous Microjet Control Studies

This section summarizes the results of prior experiments using supersonic microjets for flow control. Details of these prior studies can be found in Alvi *et al.* (2000) and Shih *et al.* (2001)

As mentioned in the introduction, supersonic impinging jets produce a very unsteady flowfield, with high noise levels and discrete frequency acoustic tones. The instantaneous shadowgraph in Fig. 4a shows a representative image for an uncontrolled – microjets off – impinging jet. The presence of multiple, strong acoustic waves, marked in the figure, clearly signify the presence of acoustic tones (Alvi *et al.*, 2000). Also visible are large-scale structures in the shear layer, which are responsible for the generation of acoustic tones upon impingement on the ground plane. Furthermore, the enhanced entrainment associated with such structures is also thought to be responsible for the 'lift loss' suffered by STOVL aircraft during hover (Krothapalli, 1999). The instantaneous shadowgraph in Fig. 4b shows the visual effect of microjet control on this flow. The effect is visually dramatic: the ambient environment becomes 'quiet' since the strong acoustic waves have disappeared. Furthermore, the large-scale structures are no longer visible in the jet shear layer. Also visible in Fig. 4b are the 'streaks' generated by the supersonic microjets. It is worth noting that such streaks have been taken as an indicator of the presence of streamwise vorticity. Whether these streaks truly represent streamwise vorticity is discussed in the next section.

Fig. 5 shows the narrowband spectra of the unsteady pressure signal on the lift plate for NPR = 3.7, h/d = 4.0. The presence of multiple tone is apparent by the discrete peaks in the spectra. The effect of microjet control on the spectral content can be surmised through a comparison of the uncontrolled case (dashed line) to the control data (solid lines). The distinct tones present in the uncontrolled impinging jet are either significantly diminished or entirely eliminated by the activation of microjets. In addition, and perhaps more significantly, the attenuation in the discrete tones is accompanied by a broadband reduction in the spectral amplitudes. This broadband reduction indicates an overall decline of the unsteadiness in the flow under control. Although only data from the lift plate is shown here, the ground plane dynamic pressures and the near-field acoustic measurements show similar trends (Alvi *et al.*, 2000).

The overall reduction in the unsteady pressure and acoustic levels (P_{rms}) on the lift plate, ground plane and the nearfield noise for NPR=3.7 and 5 are summarized in Figs. 6 and 7, respectively. First of all, the fluctuating loads are significantly reduced at all three measurement locations for almost all heights. Second, the reductions due to microjet control are generally larger for the under-expanded impinging jet, operating at NPR = 5 (Fig.7). Finally, for a given NPR, the magnitude of reduction is strongly dependent upon the ground plane distance (h/d). For example, as seen in Fig. 6, the maximum attenuations occur at h/d = 4, followed by a minimum at h/d = 4.5, where the microjets have almost no effect.

It is well-known that the unsteady properties of feedback loop of the uncontrolled jet, such as the amplitude and frequency of the impingement tones and the dominant instability modes in the flow, are highly sensitive to operating conditions. It is also worth noting that, due to the sensitivity of the feedback loop on the *exact* operating conditions, the effect of microjet control can vary even if all parameters are unchanged. As an example, as discussed in § 5, although the height at which the microjets are minimally effective is h/d = 4.5 for the conditions in Fig. 6, it can on occasion shift to h/d = 4 or 5 during a particular test. Hence, an efficient control scheme should be able to *adapt* to the changes in the local flow conditions, in real time, to provide optimal control over the entire operating range. Such a control strategy is explored in § 5 of this paper.

4. PIV Results

In a previous paper (Shih *et al* 2001) it was hypothesized that the streamwise vorticity generated by the microjets weakens the primary instability structures in shear layer. This suggestion was partially based on the presence of streamwise streaks observed in the shadowgraphs (Fig. 7) and their marked similarity to the streaks observed in other studies (Samimy *et al.*, 1993 & Krothapalli, *et al.*, 1999).

The role of vorticity was also suggested by Planar Laser Scattering (PLS) visualizations of this flowfield. Figs. 8 and 9 show representative PLS images where the laser sheet cuts diametrically (Cross-stream) across the jet. The shear layer is made visible due to the scattering of the laser light by the water droplets or ice crystals which condense as the cold jet flow entrains the relatively moist ambient air.

Fig. 8 is an instantaneous image while Fig. 9 is time averaged; the laser sheet is placed one diameter downstream of the nozzle exit for both cases. For flow without control, Fig. 8a, weak-to-moderate indentations are observed around the shear layer periphery. More clearly defined indentations emerge when the microjets are turned on and one can identify a total of 16 of these modulations inside the ring in Fig. 8b. The corresponding time-averaged images support these observations. Without control, there appears to be few identifiable indentations, indicating that the streamwise vortices are not stationary in an average sense. However, with microjet control, the shear layer displays a strongly modulated ring with a total of 16 indentations where the azimuthal locations of these indentations correspond to the microjet position around the nozzle periphery.

Prompted by the visual evidence, we quantitatively examined the role of microjets on the impinging jet flow by obtaining whole flowfield measurements using PIV. The measurements presented here are limited to NPR=3.7 and 5, with and without microjets control. For the PIV results discussed here all the microjets were operated at 100 psi for the control cases. All the measurements shown here were made in cross-sectional planes normal to the jet axis. The instantaneous and mean vorticity contours extracted from the velocity-field data are shown in Figs 10-13 for NPR= 5, h/d=4, with and without control. The plotted vorticity corresponds to the out-of-plane component and has been normalized by (Uj/d) where Uj is the jet velocity at the nozzle exit. Furthermore, the color of the vorticity contours in the middle of the vorticity range for each plot has been represented by white to allow one to visually emphasize the vorticity in the jet periphery, on the 'gray-scale' contour plots.

In Fig. 10a and 10b we show instantaneous vorticity distributions at the z/d=1 cross plane without and with microjet control, respectively. Only scattered, weak vortical structures are seen in the no control case (Fig. 10a.) In contrast, much stronger, and more organized pairs of counter-rotating vortical structures are seen in Fig. 10b, when the microjets are turned on. The difference in streamwise vorticity due to microjets is much more dramatically revealed in the corresponding *ensemble-averaged* vorticity contour plots shown in Fig. 11. These contour plots were obtained by averaging data from 100 instantaneous PIV samples. (Although it is difficult to appreciate the sign of vorticity on a gray-scale image, however, the counter-rotating vortex pairs can be clearly seen in color vorticity plots.) A comparison of the no-control case, Fig. 11a, to the microjet control data, Fig. 11b, leaves no doubt that the activation of microjets introduces significant streamwise vorticity at the jet shear layer.

In order to study the evolution of the streamwise vortices due to microjets, velocity (or vorticity) measurements were made at multiple z locations. Fig. 12 and 13 show vorticity plots corresponding to those in Figs. 10 and 11 but at a further downstream location of z/d =2. At least visually, the effect of microjets on the instantaneous vorticity field in Fig. 12b, does not appear to be significant relative to the no control case in Fig. 12a. However, a comparison of the mean vorticity plots in Fig. 13 shows that although somewhat diffused, the flowfield with control, Fig. 13b, still contains significantly more vorticity than the corresponding no control case.

Fig. 14, 15 show plots of the streamwise vorticity distribution as a function of the azimuthal angle at z/d = 1 and 2, respectively. The vorticity values, shown on the ordinate in these plots, were extracted from the corresponding mean vorticity contours (Figs. 11 and 13) along a radial position roughly in the middle of the shear layer at each z/d location. Taking advantage of the flow symmetry, data for only half of the jet periphery is shown. In each plot, the solid line corresponds to the microjet control case, while the dashed line corresponds to no control. The organized, counter-rotating vorticity pairs due to microjets observed in Fig. 11b are revealed as adjacent pairs of large-amplitude, vorticity peaks and valleys in Fig. 14. In contrast, the no control data, depicted in dashed lines, shows a much weaker and more disorganized streamwise vorticity distribution. At the next downstream location as shown in Fig. 15, the difference between the control and no control case is still significant, although the maximum vorticity values are somewhat lower.

In order to further quantify the effect of microjets on the streamwise vorticity, the overall circulation, Γ, was calculated at various z/d locations. A plot summarizing the non-dimensionalized circulation, Γ/U_j*d as a function of z/d is shown in Fig. 16. Note that the circulation shown here is calculated by integrating the absolute values of the ensemble-averaged vorticity over a specified area in the cross-flow plane. In order to provide a reliable,

consistent estimate, normalized vorticity levels below 0.3 were assigned a zero value. The magnitude of the circulation can be interpreted as a measure of the overall strength of the streamwise vorticity at the specific z/d location.

A comparison between the no control circulation values (open symbols) to the control data (filled symbols) reveals that the overall circulation is significantly higher when the microjets are turned on. Also, there is a substantial difference in the circulation with microjets between the underexpanded (NPR = 5) and the ideally expanded case (NPR=3.7). The significantly higher vorticity for the underexpanded case is not altogether unexpected. It is well known that the concave curvature and the presence of a strongly accelerated flow at the nozzle exit of an underexpanded jet makes it more susceptible to a Talyor-Goërtler type instability, which enhances the growth of streamwise vorticity (Samimy et al., 1992 and Krothapalli, 1998). Whether this is truly in the present situation is difficult to state conclusively.

Regardless of the reason for the emergence of higher streamwise vorticity for the under-expanded jet, it seems reasonable to suggest that there is a direct correlation between the presence of streamwise vorticity and the efficacy of microjet control. A review of Figs. 6 and 7 demonstrates that microjets are much more effective for the under-expanded jet, that is also the jet with much stronger streamwise vorticity.

Having shown that the microjets introduce measurable and substantial vorticity, we come back to the physical mechanism responsible behind microjet control. Using an order of magnitude analysis, it is easily shown that total streamwise vorticity due to all sixteen microjets is less than 10% of the streamwise vorticity measured in the main jet when microjets are turned on. This suggests that a significant portion of the streamwise vorticity has to come from the primary shear layer. As suggested by an earlier study (Shih *et al.* 2001), vorticity tilting and stretching mechanisms for the spanwise or azimuthal vorticity in the primary jet shear layer are the most plausible candidates responsible for this vorticity redirection. This drainage of azimuthal vorticity into streamwise direction can also be thought of as a weakening of the large-scale axisymmetric structures in the jet shear layer, a result clearly revealed in the shadowgraph images. Consequently, the weakening vortical structure produce weaker acoustic waves when they impinge on the ground plane, thus further attenuate the feedback loop. In addition, the introduction of strong counter-rotating pairs of vortices in the shear layer near the nozzle exit due to microjets further weakens the spatial coherence of the coupling between the acoustic waves and shear layer instability, an important characteristic for efficient feedback loop lock-in.

5. Active Closed-loop Control of Impingement Tones

The motivation for considering active control comes from the behavior of the flow-field in the presence of the supersonic microjets. As can be seen in Fig. 6 and 18, the microjets disrupt the feedback loop thereby reducing the OASPL. This reduction, however, is non-uniform with respect to the height (see Fig. 6) and is unpredictable (as seen in Fig. 6 and 18). In order to obtain a uniform and guaranteed reduction over a range of operating conditions in a reliable manner, closed-loop control that uses on-line measurements and active-adaptive algorithms is an appropriate methodology that can be employed.

Much of feedback control consists of designing suitable external actuators that introduce a control input so as to alter, typically, the dynamic characteristics of the process being controlled. In many of these problems, the control method begins with a description of the process in the form of a differential equation

$$\dot{x} = f(x,u)$$

where x denotes the process state, and u denotes the control input-source. The control strategy then consists of determining a feedback signal according to the rule

$$u = g(x)$$

where $g(.)$ is to be determined so as to realize the desired objective in the process. When f and g are linear, which corresponds to the most ubiquitous case in dynamic systems, the control design and implementation is considerably simplified.

In the above scenario, it is clear that the control input is typically required to be modulated at the natural frequencies of the system. It is therefore necessary that the external actuator have the necessary bandwidth for operating at the natural frequencies (see for example, Cattafesta *et al.,* 1999, Williams *et al.,* 2000). In the problem under consideration, the edge tones associated with the flow-field are typically a few kilohertz. Given the current valve technology, the above control

methodology of modulating the control input at the system frequencies is a near impossibility.

The approach adopted in this paper is distinctly different from the standard control framework, and consists of modulating a control input at a slow time-scale, so that it behaves like a parameter. If this control input is chosen judiciously, then even small and slow changes in this "parameter" can lead to large changes in the process dynamics, as will be shown below.

5.1 Active Closed-loop Control of Impingement Tones

With the goal of identifying a control input that has a maximum impact on the impingement tones even with a small and slow change, we take a closer look at the feedback mechanism that produces the self-sustained oscillations of the impinging shear layer. Instability waves are generated by the acoustic excitation of the shear layer near the nozzle exit, which then convect down and evolve into spatially coherent structures. These waves in turn excite the shear layer at the nozzle exit, thereby providing the feedback (see Fig. 17 for a schematic). As indicated by the active control results in Fig. 5, the introduction of the microjets at the nozzle has a large impact on the flowfield even for a mass-flux addition of 0.5% of the main flow. Given the strong sensitivity of the flow-field as well as the tendencies of specific shear-layer modes to be driven into resonance to the boundary conditions at the nozzle, we chose the microjet pressure distribution at the nozzle exit as the control input. Based on the pressure data both without and with microjets at the nozzle, a reduced-order model of the impingement tones can be derived as

$$\begin{aligned} \dot{x} &= A(u)x \\ p &= Cx \end{aligned} \qquad (1)$$

where x corresponds to the amplitudes of the impingement tones, p corresponds to the pressure measurements at the nozzle and u corresponds to the microjet pressure distribution along the nozzle.

5.2 The POD-based Closed-loop Control Strategy

The aim here is to choose u, the microjet pressure distribution such that x is reduced in magnitude by making use of the measurements p. In order to extract as much information possible about the state of the system, x, we adopt the Principal Decomposition Method (POD), which is briefly described below.

The Proper Orthogonal Decomposition (POD) is used to systematically extract the most energetic modes from a set of realizations from the underlying system. These modes can be used as basis functions for Galerkin projections of the model in order to reduce the solution space being considered to the smallest linear subspace that is sufficient to describe the system. The decomposition is 'optimal' in that the energy contained in an N-ordered POD base is greater than any other N-ordered base in a mean-squared sense. Over the years, it has been applied in several disciplines including turbulence in fluid mechanics, stochastic processes, image processing, signal analysis, data compression, process identification and control in chemical engineering, and oceanography, and has been referred to by various names including Karhunen-Loeve decomposition, principal component analysis, and singular value decomposition.

In fluid mechanical systems, the POD technique has been applied in the analysis of coherent structures in turbulent flows and in obtaining reduced order models to describe the dominant characteristics of the phenomena. One of the earliest works was on a fully developed pipe flow, studied by Bakewell and Lumley (1967). Since then, POD models have been used to model the one-dimensional Ginzburg-Landau equation (Sirovich and Rodriguez 1987), the laminar-turbulent transitional flow in a flat plate boundary layer (Rempfer 1994), pressure fluctuations surrounding a turbulent jet (Arndt *et al.* 1997), turbulent plane mixing layer (Delville *et al.* 1999), velocity field for an axisymmetric jet (Citriniti and George 2000), low-dimensionality of a turbulent flow near wake (Ma *et al.* 2000), low-dimensional leading-edge vortices in the unsteady flow past a delta wing (Cipolla *et al.* 1998), and flow over a rectangular cavity (Rowley *et al.* 2000). The eigenfunctions were developed using both experimental and numerical database.

Although POD has been used extensively in determining reduced order models of flow systems, relatively few attempts have been made to design active control strategies based on these models (Ravindran, 2000; Graham *et al.*, 1999a,b; Atwell and King, 2001; Arian *et al.*, 2000). In this paper, our goal is to use the POD method to extract information about the mode shapes using the pressure measurements p in order to determine the control

input u. For easy reference, the POD method is briefly described below.

Using the Karhunen-Loeve expansion (Loève 1945; Karhunen, 1946), the pressure variable at the nozzle exit can be expressed as

$$p(\theta,t)=\sum_{n=1}^{N}\sqrt{\lambda_n}\psi_n(t)\phi_n(\theta)=\sum_{n=1}^{N}a_n(t)\phi_n(\theta) \quad (2)$$

where

$E[\psi_n(t)\psi_m(t)]=\delta_n^m$, $\int_D\phi_n(\theta)\phi_m(\theta)d\theta=\delta_n^m$, ? is the angular position along the nozzle circumference, $\phi_n(\theta)$ is the nth mode-shape, $a_n(t)$ is the amplitude of the nth mode, and N is the number of dominant modes. The spatial pressure distribution $\phi_n(\theta)$ can be calculated using the "method of snapshots" as follows (Tang *et al.* 2001). Let the $p^n(j)$ be the pressure variable at a spatial point n at some time j where $n = 1,....,N$ and $j = 1,....,J$, with n much smaller than J. Now the matrix Q can be expressed from singular value decomposition as

$$Q=\begin{bmatrix} p^1(1) & p^1(2) & \cdots & p^1(J) \\ p^2(1) & p^2(2) & \cdots & p^2(J) \\ \vdots & \vdots & \cdots & \vdots \\ p^N(1) & p^N(2) & \cdots & p^N(J) \end{bmatrix}=U\Sigma V^T$$

where U $(\mathrm{N}\times\mathrm{n})$ and V $(\mathrm{J}\times\mathrm{n})$ are unitary matrices, and

$$\Sigma=\begin{bmatrix} \sigma_1 & & & \\ & \sigma_2 & & \\ & & \ddots & \\ & & & \sigma_n \end{bmatrix},$$

$$\sigma_1\geq\sigma_2\geq\cdots\geq\sigma_n$$

The matrices V and S are the eigenvector and the square-root of the eigenvalue of the correlation matrix Q^TQ. The mode-shapes can then be computed as

$$\Phi\equiv QV=[\phi_1 \quad \phi_2 \quad \cdots \quad \phi_n].$$

Once the mode shape is determined, we simply choose the control strategy as

$$u=k\phi_1(\theta) \quad (3)$$

where ϕ_1 is the most energetic mode and k is a calibration gain. The complete closed-loop procedure therefore consists of collecting pressure measurements $p(?)$, expanding them using POD modes as in (2), determining the dominant mode ϕ_1, and matching the control input, which is the microjet pressure distribution along the nozzle to this dominant mode as in (3). The results obtained using such a mode-matched control strategy are discussed in the next section.

5.3 The application of closed-loop control to impinging jets

The mode-matched control strategy described above was implemented in the experimental apparatus described earlier, for a range of heights. At each height, in addition to the mode-matched control, the active control strategy as in Shih *et al.* (2001) was also implemented. Since in the latter case, the spatial distribution of microjet pressure around the nozzle exit was kept uniform, it is referred to as "symmetric control." Since the latter does not use any system measurements and is determined *a priori,* the symmetric control can also be viewed as an open-loop control procedure. In order to ensure a fair comparison between the two control methods, the main nozzle was forced to operate under the constant condition throughout whole process. The calibration constant k in (3) was chosen such that the minimum and maximum values of the POD mode over ? corresponds to 70psi and 120psi, respectively. These values were chosen since they ensured maximum effectiveness. Since the actuator configuration was such that it consisted of four microjet-banks that can be controlled independently and each bank in turn controlled four microjets, the bank input pressure was chosen as the average pressure values of the position where the four microjets are located. Fig. 19 shows the shape of the first mode and the suggested microjet bank pressure distribution for several heights.

As can be seen in Fig. 20, the mode-matched control strategy showed better performance at the experiment throughout all operational conditions, with a large improvement at heights h/D = 4, 4.5 and 5. The reason for this increased pressure reduction can be attributed to the percentage of energy contained in the dominant mode, which is used in the control strategy. As shown in Table 1, at heights 4 to 5, the energy content of ϕ_1 is above 86% where as at heights 2 and 3, the energy level drops to 55% and below. As a result, the corresponding improvement in the mode-matched strategy also drops to about half the db-value at heights 2 and 3 compared to at heights 4.0, 4.5, and 5.

6. Concluding Remarks

In this paper, two aspects of impinging jets were presented, (i) detailed PIV measurements that led to further insights concerning streamwise vorticity being a dominant mechanism in the feedback interruption using microjets, and (ii) a new closed-loop control strategy that uses on-line pressure measurements near the nozzle exit to result in an improved and uniform reduction, irrespective of the operating and flow conditions.

The PIV measurements revealed that substantially more well organized and paired streamwise vortices were present in the jet shear layer when microjets were turned on compared to when they were turned off. The ensemble-averaged vorticity field data revealed that the streamwise vortices, present as counter-rotating pairs, were highly organized within one diameter downstream of the nozzle exit. Further downstream, the vortices became more diffused but are still more organized relative to the no control case. The strength of the streamwise vorticity was found to be much higher with control than without control. This relatively stronger streamwise vorticity may be responsible for breaking up the large-scale structures, making them weaker and more three-dimensional. Thus, the feedback loop is attenuated due to two factors. First, by a weakening of the source of the acoustic waves which are generated by the impingement of the large scale structures and second, by reducing the spatial coherence of the coupling between the acoustic waves and shear layer instability due to three-dimensionality introduced by the microjets. The disruption of the feedback loop leads to a marked reduction in the unsteadiness of the supersonic impinging jet flow.

The closed-loop control strategy consisted of determining the dominant POD mode using pressure measurements at the nozzle exit and using a 'mode matched strategy' to determine the microjet pressure distribution along the nozzle. The results demonstrated a significant reduction in the unsteady pressure loads along with a consistent improvement compared to an open-loop control strategy where the microjet pressure was kept at a constant. This improved reduction may be attributed to the following: The mode-matched strategy results in the microjet pressure intensity to be proportional to the corresponding acoustic wave intensity near the nozzle. High microjet pressure in turn provides a stronger local disruption and perhaps generates more streamwise vorticity, both of which lead to more efficient local disruption of the feedback loop resulting in more efficient reduction in the flow unsteadiness. Experiments are underway to obtain more direct evidence of this hypothesis.

7. Acknowledgements

This work was supported by a grant from AFOSR, monitored by Dr. J. Schmisseur; we are grateful for their support. We would like to thank the staff of FMRL, for their invaluable help in conducting these tests. We are grateful for the assistance provided by Dr. Alkislar in making the PIV measurements and the Mr. Choutapalli for his help in conducting the tests.

8. References

1. Alvi, F.S., Elavarsan R., Shih, C., Garg G., and Krothapalli, A., 2000 " Control of supersonic impinging jet flows using Microjets," *AIAA Paper* 2000-2236.
2. Alvi, F.S., Shih, C. and Krothapalli, A., 2001 "Active control of the feedback loop in high-speed Jet," *AIAA Paper* 2001-0373.
3. Arian, E., Fahl, M. and Sachs, E.W., 2000 "Trust-region proper orthogonal decomposition for flow control," *NASA/CR-2000-210124, ICASE Report*, No. 2000-25.
4. Arndt, R.E.A., Long D.F. and Glauser, M.N., 1997 "The proper orthogonal decomposition of pressure fluctuations surrounding a turbulent jet," *J. Fluid Mech.*, Vol. 340, pp. 1-33.
5. Arnette, S.A., Samimy, M. and Elliott.G.S., 1993 " On streamwise vortices in high Reynolds number supersonic axisymmetric jets," *Phys. Fluids A* 5(1), January .
6. Atwell, J.A. and King, B.B., 2001 "Proper orthogonal decomposition for reduced basis feedback controllers for parabolic equations," *Mathematical and Computer Modeling*, Vol 33, pp.1-19.
7. Bakewell, P. and Lumley, J.L., 1967 "Viscous sublayer and adjacent wall region in turbulent channel pipe flow," *Physics of Fluids*, Vol.10, pp. 1880-1889.
8. Cattafesta III, L.N., Shukla, D., Garg, S. and Ross, J.A., May 1999 "Development of an adaptive weapons-bay suppression system," *AIAA Paper* 99-1901.
9. Citriniti, J.H. and George, W.K., 2000 "Reconstruction of the global velocity field in the axisymmetric mixing layer utilizing the proper orthogonal decomposition," *J. Fluid Mech.*, Vol. 418, pp.137-166.

10. Cipolla, K.M., Liakopoulos, A. and Rockwell, D.O., 1998 "Quantitative imaging in proper orthogonal decomposition of flow past a delta wing," *AIAA Journal*, Vol. 36, pp.1247-1255.
11. Delville, J., Ukeiley, L., Cordier, L., Bonnet, J.P. and Glauser, M., 1999 "Examination of large-scale structures in a turbulent plane mixing layer. part. 1. proper orthogonal decomposition," *J. Fluid Mech.*, Vol. 391, pp. 91-122.
12. Graham, W.R., Peraire,J.P. and Tang, K.Y., 1999a "Optimal control of shedding using low-order models, Part I-Open-loop model development," *International Journal for Numerical Methods in Engineering*, Vol.44, pp.945-972.
13. Graham, W.R., Peraire,J.P. and Tang, K.Y., 1999b "Optimal control of shedding using low-order models, Part II-Model-based control," International Journal for Numerical Methods in Engineering, Vol. 44, pp.973-990.
14. Ibrahim, M.K. and Nakamura, Y., 2001 "Effect of Rotating Tabs on Flow and Acoustic Fields of Supersonic Jet." *AIAA Journal*, Vol. 39, No. 4, pp. 745-748.
15. Karhunen, K., 1946 "Zur spektraltheorie stochastischer prozesse," *Ann. Acad. Sci.*, 34.
16. Krothapalli, A., Strykowski P.J. and King, C. J., 1998 "Origin of Streamwise Vortices in Supersonic Jets," *AIAA Journal,* Vol. 36, No. 5, pp. 869-872.
17. Krothapalli, A., Rajakuperan, E., Alvi, F.S. and Lourenco, L., 1999 "Flow field and Noise Characteristics of a Supersonic Impinging Jet," *J. Fluid. Mech.,* Vol. 392, pp. 155-181.
18. Liepmann, D. and Gharib, M., 1992 "The Role of Streamwise Vorticity in the Near-Field Entrainment of Round Jets," *J. Fluid Mech.* Vol. 245, pp. 643-668.
19. Loève, M., 1945 "Functions aléatoire de second ordre," *Comptes Rendus Acad. Sci.*, 220.
20. Lourenco., L., and Krothapalli, A., 1998 "Mesh-free, Second Order Accurate Algorithm for PIV processing," *Proceedings of the International Conference on Optical Technology and Image Processing in Fluid, Thermal and Combustion Flow.* Yokohama, Japan.
21. Ma, M., Karamanos, G.S. and Karniadakis, G.E., 2000 "Dynamics and low-dimensionality of a turbulent near wake," *J. Fluid Mech.,* Vol. 410, pp.29-65.
22. Neuwerth, G., 1974 "Acoustic Feedback of a Subsonic and Supersonic Free Jet Which Impinges on an Obstacle," *NASA TTF-15719.*
23. Paterson, R.W., 1984 "Turbofan Forced Mixer Nozzle Flowfield-A Benchmark Experimental Study," *ASME J. Eng. Gas Turbines Power* Vol. 106, 692.
24. Plesniak, M. W., Mehta, R.D. and Johnston, J. P., 1974 "Curved Two-stream Turbulent Mixing Layers: Three-dimensional Structure and Streamwise evolution," *J. Fluid Mech.* Vol. 270, pp.1-50.
25. Powell, A., 1988 "The sound –producing oscillations of round underexpanded jets impinging on normal plates," *J. Acoust. Soc.* Am 83(2), pp. 515-533.
26. Ravindran, S., 2000 "A reduced order approach to optimal control of fluids using proper orthogonal decomposition," *International Journal for Numerical Methods in Fluids,* Vol. 34, pp.425-448.
27. Rempfe, D., 1994 "On the structure of dynamical systems describing the evolution of coherent structures in a convective boundary layer," *Physics of Fluids,* Vol. 6, pp. 1402-1404.
28. Rowley, C.W., Colonius, T. and Murray, R.M., 2000 "POD based models of self-sustained oscillations in the flow past an open cavity," *AIAA Paper* 2000-1969.
29. Samimy, M., Zaman, K.B.M.Q. and Reeder, M.F., 1993 " Effect of Tabs on the Flow and Noise Field of an Axisymmetric Jets," *AIAA Journal,* Vol. 31, No. 4, pp.609-619.
30. Shih, C. Alvi, F.S., Lou. H, Garg. G and Krothapalli, A., 2001 "Adaptive Flow Control of Supersonic impinging jets," *AIAA Paper* 2001-3027.
31. Sirovich, L. and Rodriguez, J.D., 1987 "Coherent structures and chaos: A model problem," *Phys. Lett. A,* Vol. 120, pp. 211-214.
32. Tam, C.K.W and Ahuja K.K., 1990 " Theoretical model of discrete tone generation by impinging jet," *J. Fluid Mech.,* Vol. 214 1990 pp. 67-87.
33. Tang, D., Kholodar, D., Juang, J.N. and Dowell, E.H., 2001 "System identification and proper orthogonal decomposition method applied to unsteady aerodynamics," *AIAA Journal,* Vol. 39.
34. Williams, D.R., Fabris, D. and Morrow, J., June 2000 "Experiments on controlling

multiple acoustic modes in cavities," *AIAA Paper* 2000-1903.

35. Zaman, K.B.M.Q., Reeder. M.F. and Samimy, M., 1994 " Control of an axisymmetric jet using vortex generators," *Phys. Fluids. 6 (2) Feb.*

36. Zaman, K.B.M.Q., 1996 "Axis switching and spreading of an asymmetric jet: The role of coherent structure dynamics," *J. Fluid Mech.* Vol. 316. pp.1-27.

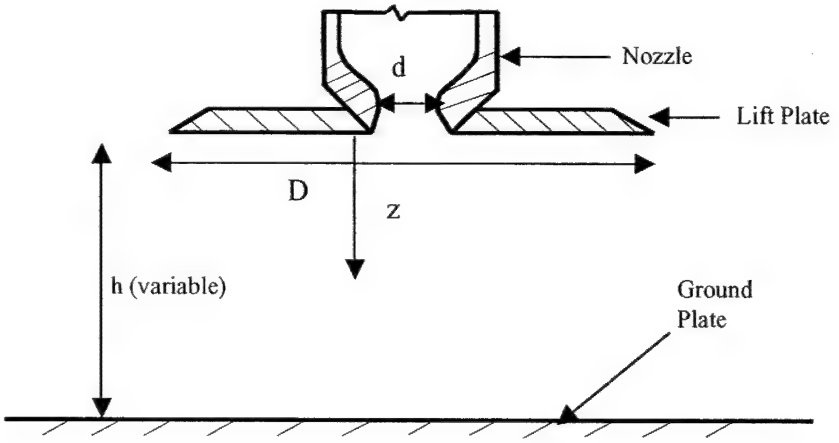

Fig. 1. - Schematic of the test configuration

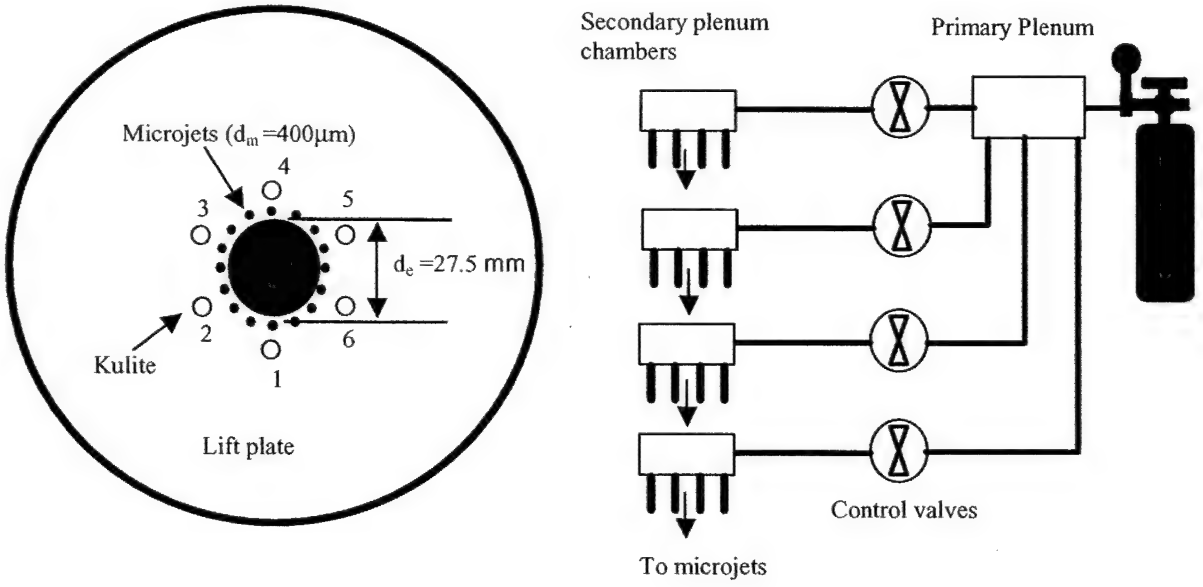

a) Geometry of the lift plate and Microjets

b) Microjets feed assembly

Fig. 2- Schematic of the flow control arrangement using microjets

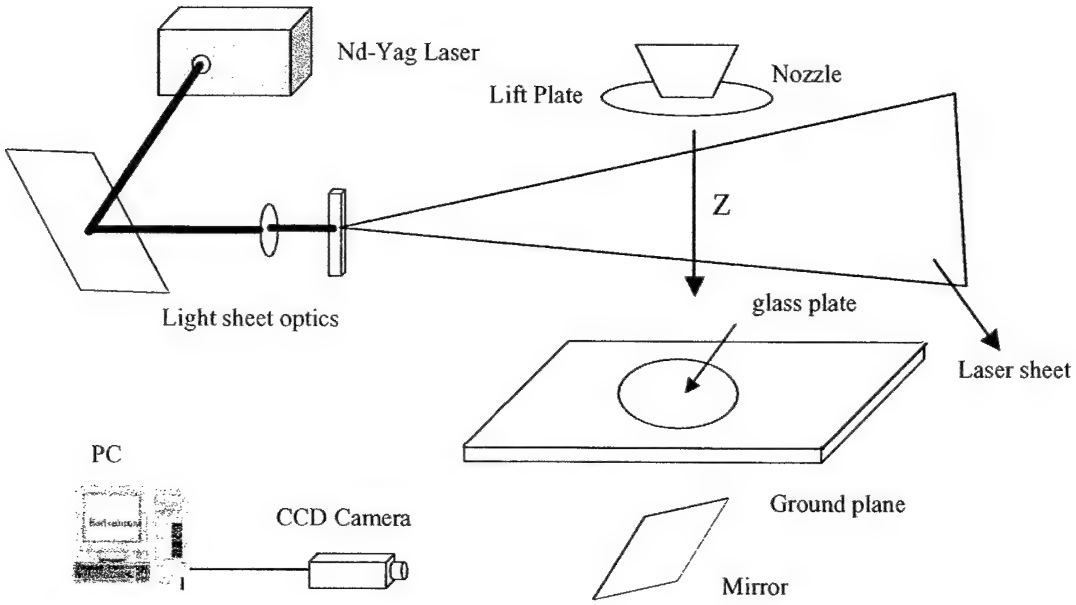

Fig 3-Schematic of the experimental arrangement of the PIV system

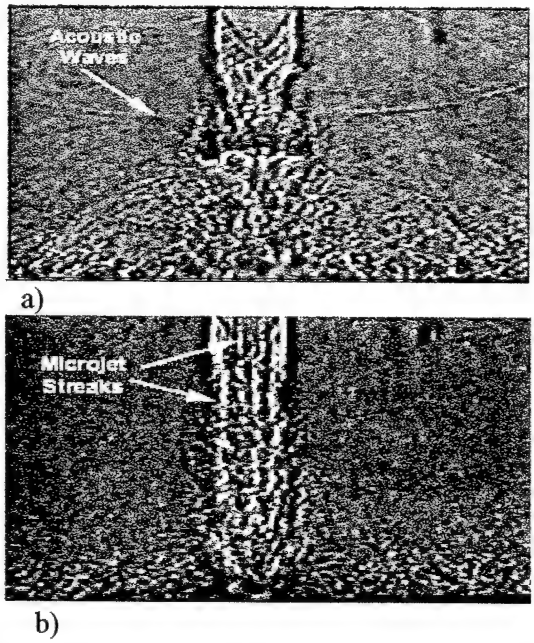

Fig. 4 - Instantaneous shadowgraph images of supersonic impinging jets without (a, top) and with control (b, bottom) NPR = 3.7 and h/d = 4

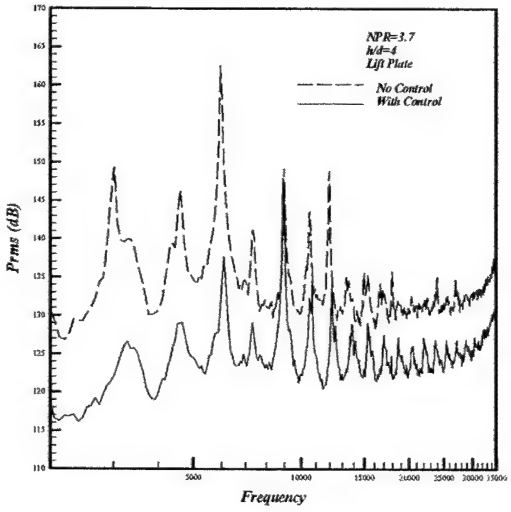

Fig. 5 Narrowband frequency spectra for unsteady pressure on thelift plate, NPR=3.7, h/d=4

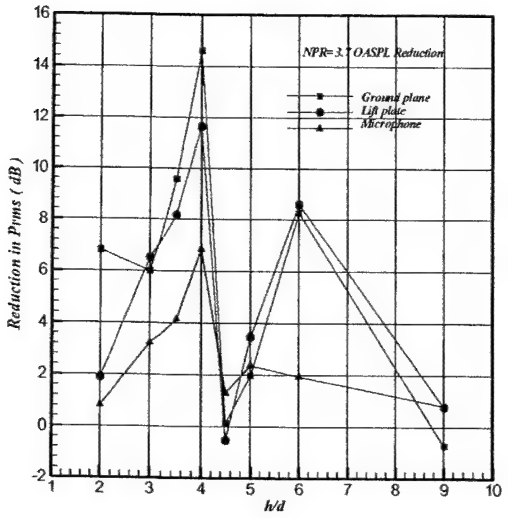

Fig.6 Reductions in fluctuating pressure intensities as a function of h/d, NPR=3.7

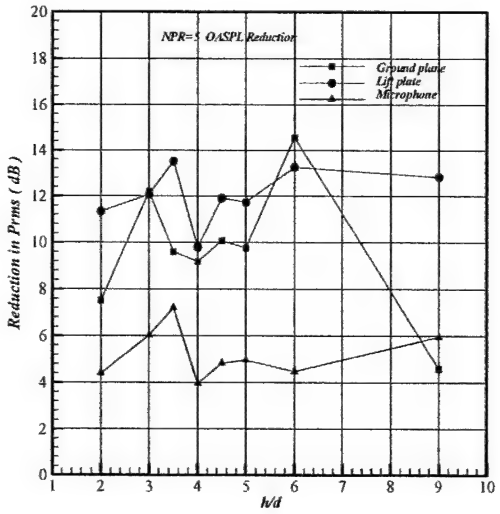

Fig.7 Reductions in fluctuating pressure intensities as a function of h/d, NPR=5

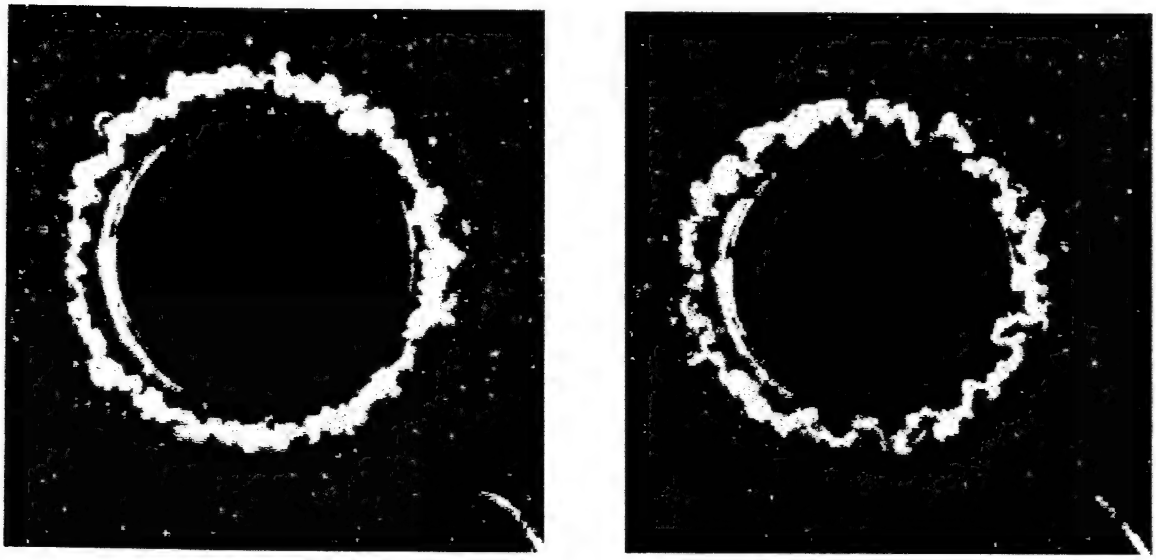

a) No control

b) With control

Fig.8 Instantaneous PLS images taken at one diameter downstream (z/d=1) of the nozzle, NPR=5, h/d=4; (a) No control, (b) With control

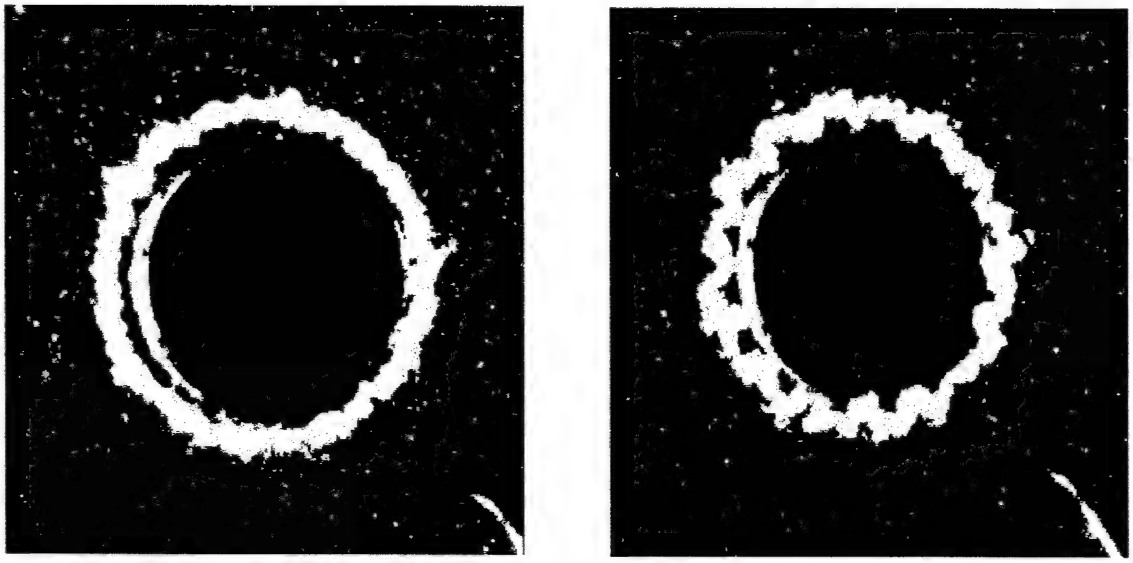

a) No Control b) With Control

Fig.9 Time-averaged PLS images taken at one diameter downstream (z/d=1) of the nozzle, NPR=5, h/d=4; (a) No Control, (b) With control

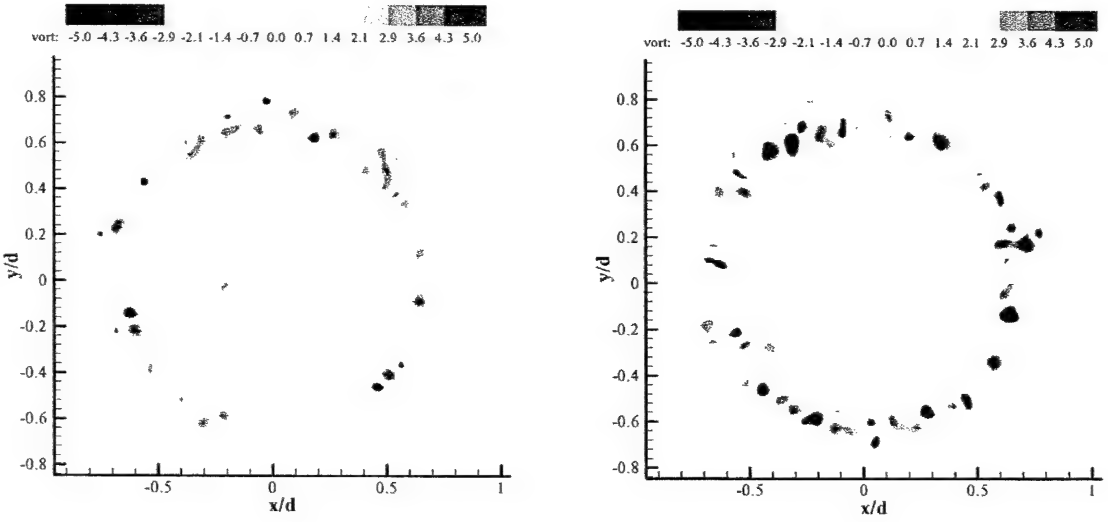

a) No control b) with control

Fig.10 Instantaneous streamwise vorticity distribution at the z/d=1 cross plane of the jet flow NPR=5, h/d=4

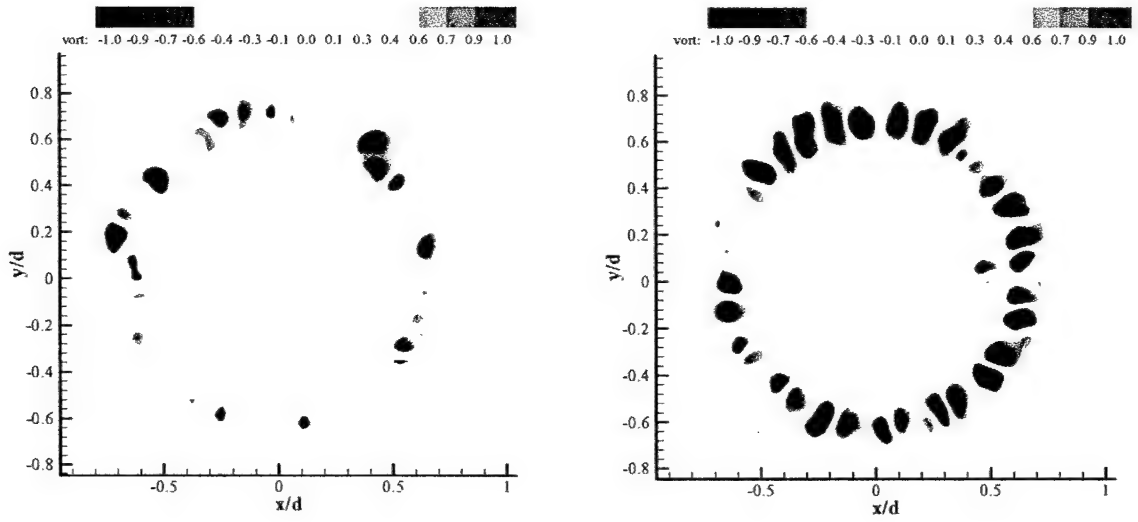

a) No control b) with control

Fig.11 Ensemble-averaged streamwise vorticity distribution at the z/d=1 cross plane of the jet flow, NPR=5, h/d=4

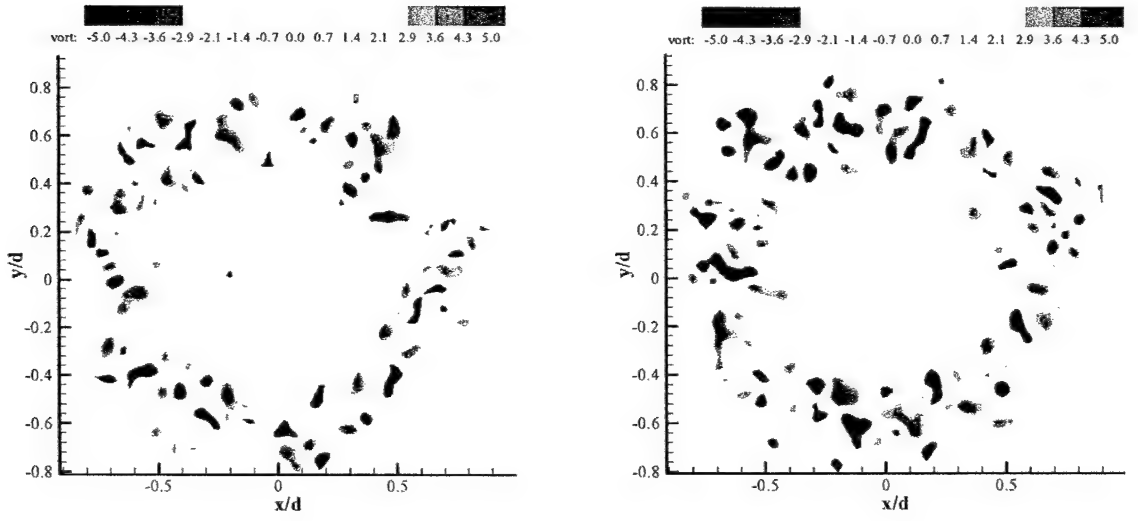

a) No control b) with control

Fig.12 Instantaneous streamwise vorticity distribution at the z/d=2 cross plane of the jet flow NPR=5, h/d=4

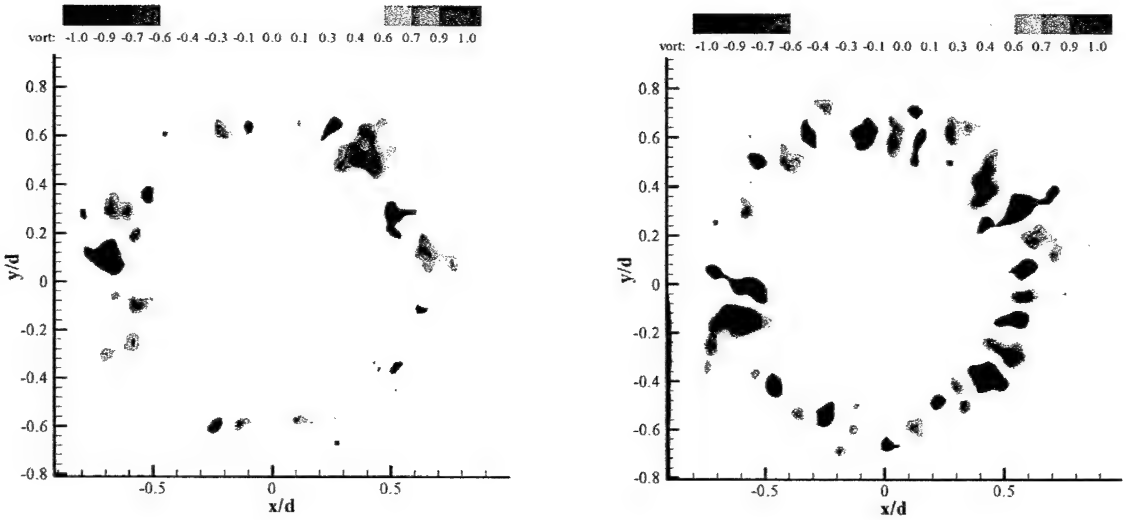

a) No control

b) With Control

Fig.13 Ensemble-averaged streamwise vorticity distribution at the z/d=2 cross plane of the jet flow, NPR=5, h/d=4

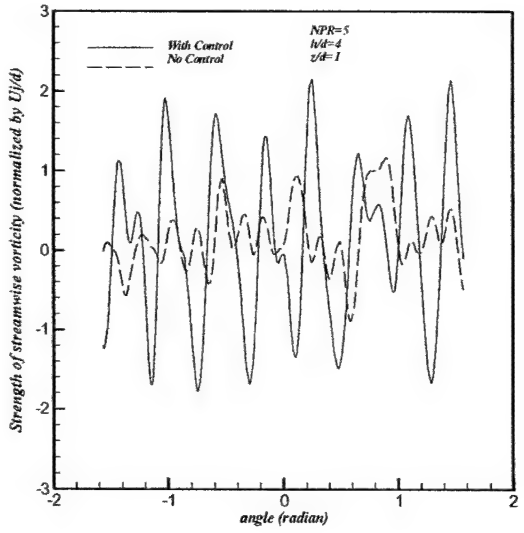

Fig.14 Ensemble-averaged streamwise vorticity distribution along theazimuthal direction in the cross plane(z/d=1) of jet flow. NPR=5, h/d=4

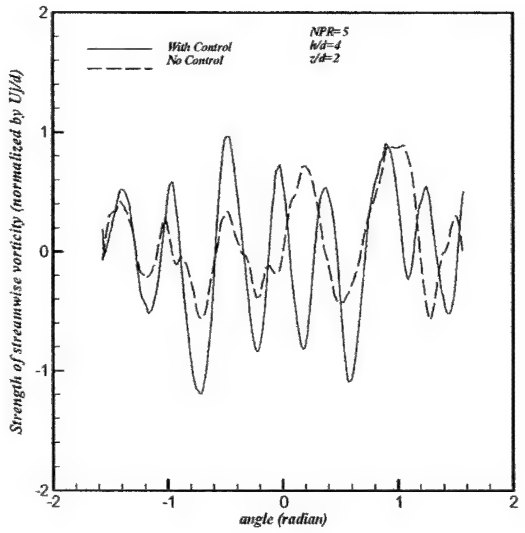

Fig.15 Ensemble-averaged streamwise vorticity distribution along azimuthal direction in the cross plane(z/d=2) of jet flow. NPR=5, h/d=4

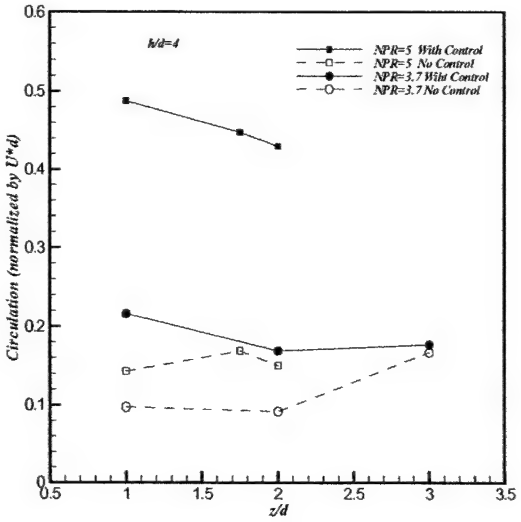

Fig.16 Streamwise development of average streamwise circulation . NPR=3.7,5, h/d=4

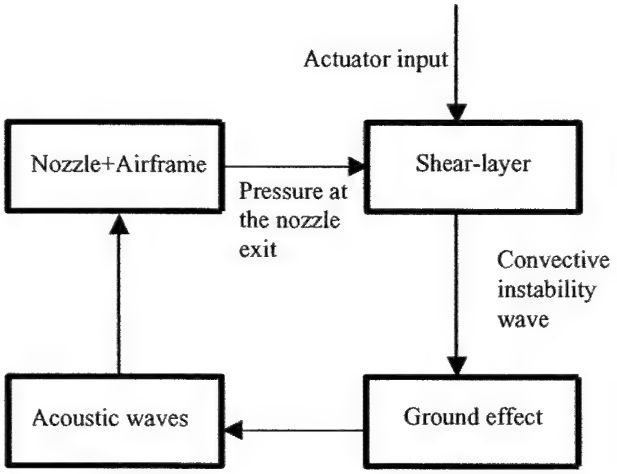

Fig.17 Schematic of closed-loop control of impinging jets

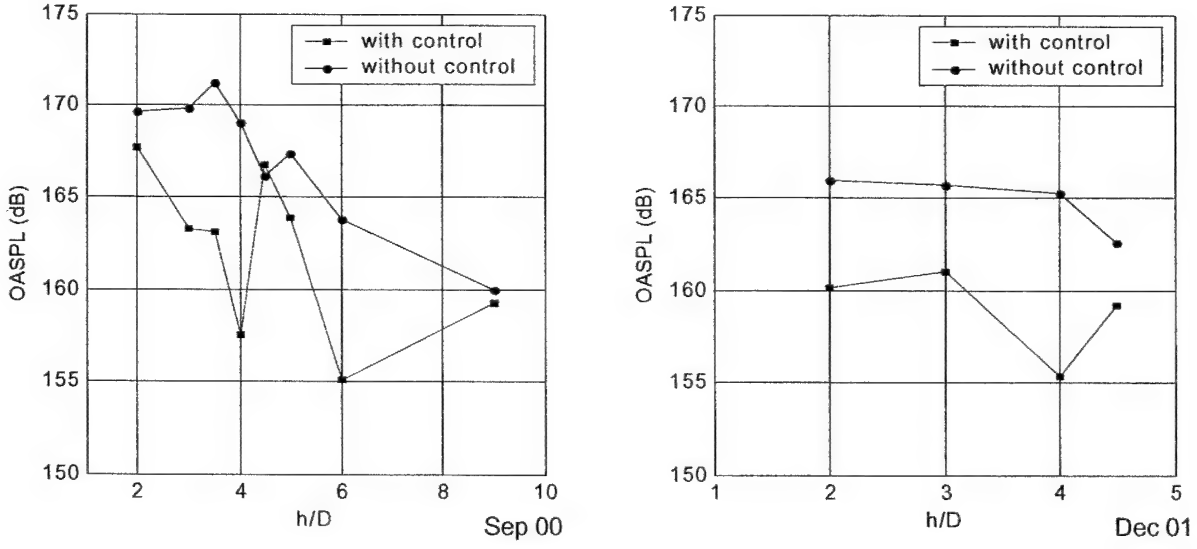

Fig. 18 Microjet effectiveness on different trials (NPR = 3.7)

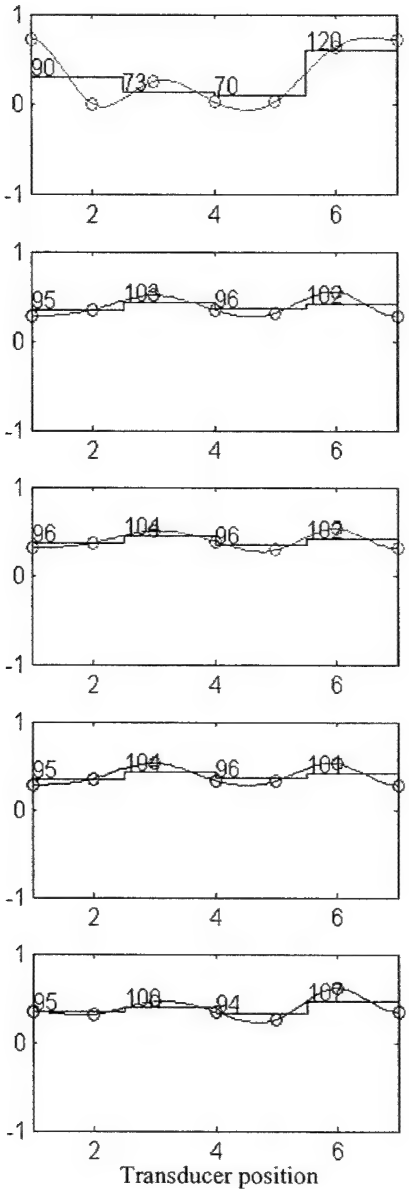

Fig.19 The first mode shape and suggested pressure for each height

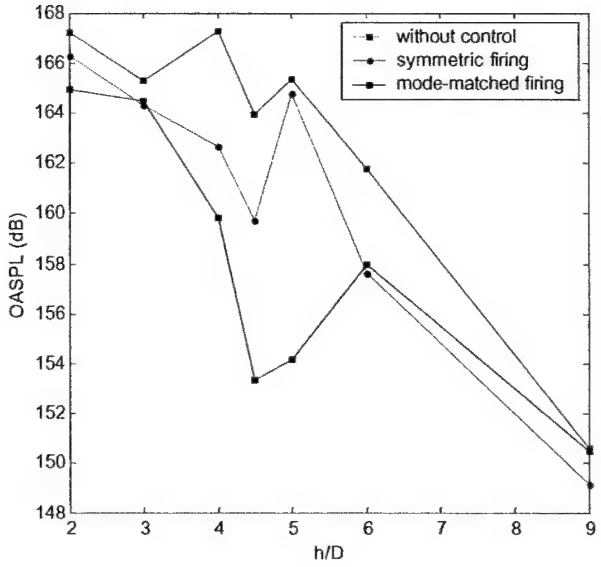

Fig.20 Overall sound pressure levels (OASPL) for different control (NPR=3.7)

h/D	Mode1	Mode2	Mode3	Mode4
2.0	0.4615	0.2488	0.1785	0.1111
3.0	0.5515	0.2745	0.1144	0.0597
4.0	0.8609	0.0691	0.0443	0.0257
4.5	0.8836	0.0517	0.0389	0.0258
5.0	0.8736	0.0757	0.0314	0.0194

Table.1 The energy content of the first four modes at each height (NPR=3.7)

Appendix A5

AIAA Journal

Volume 40, Number 4, Pages 599-609

Experimental and Computational Investigation of Supersonic Impinging Jets

F. S. Alvi, J. A. Ladd, W. W. Bower

Reprinted from

AIAA Journal

Volume 40, Number 4, Pages 599–609

A publication of the
American Institute of Aeronautics and Astronautics, Inc.
1801 Alexander Bell Drive, Suite 500
Reston, VA 20191–4344

AIAA JOURNAL
Vol. 40, No. 4, April 2002

Experimental and Computational Investigation of Supersonic Impinging Jets

F. S. Alvi*
Florida A&M University and Florida State University, Tallahassee, Florida 32310
and
J. A. Ladd† and W. W. Bower‡
The Boeing Company, St. Louis, Missouri 63166

The results of an experimental and computational study of a moderately underexpanded axisymmetric supersonic jet issuing from a converging nozzle and impinging on a ground plane are presented. The goal of this work is to develop a better understanding of the impinging jet flowfield, which is of significant practical interest because of its presence in short takeoff and vertical landing (STOVL) aircraft during hover as well as in other aerospace-related and industrial applications. The experimental measurements include flow visualization, surface-pressure distributions, and velocity field data obtained using particle image velocimetry (PIV). The experimental data, especially the velocity field measurements, were used to verify the accuracy of computational predictions. Computational results obtained using two different turbulence models produced almost identical results. Comparisons with experimental results reveal that both models capture the significant features of this complex flow and were in remarkably good agreement with the experimental data for the primary test case. The experiments and computations both revealed the presence of the impingement zone stagnation bubble, which contains low velocity recirculating flow. Other features, including the complex shock structure and the high-speed radial wall jet, were also found to be very similar. The ability to measure and predict accurately the impinging jet behavior, especially near the ground plane, is critical because these are regions with very high mean shear, thermal loads, and unsteady pressure forces, which contribute directly to the problem of ground erosion in STOVL applications.

Introduction

HIGH-SPEED impinging jets can occur in a variety of aerospace-related applications. These jet flows are particularly troublesome to short takeoff and vertical landing (STOVL) aircraft, such the Harrier/AV-8 family, during hover mode. In these instances the flowfield produced by the impingement of the high-speed lift jets produces adverse local flow conditions, which can potentially lead to the degradation of aircraft performance in a number of areas during hover. These adverse effects, collectively referred to as ground effects, are the result of the highly unsteady nature of the flow generated by the impingement of the high-speed jet(s) on the ground plane and the pressure field caused by the natural entrainment by these jets. They include lift loss caused by flow entrainment associated with the lifting jets, which induces low surface pressures on the airframe resulting in a "suckdown" force opposite to lift. The lift loss typically increases in magnitude as the aircraft approaches the ground and can be greater than 60% of the total lift jet thrust when the jets are very close to the ground plane.[1] Increased noise or overall sound-pressure levels associated with high-speed impinging jets and the sonic fatigue of structural elements in the vicinity of the nozzle exhaust caused by unsteady loading is also an area of concern. In addition to higher levels, the noise spectrum is dominated by discrete tones, which, if close to the aircraft panel frequencies, can further aggravate the sonic fatigue problem. Furthermore, the impingement of hot, high-speed lift jets on the landing surface can lead to significant erosion caused by the extremely high shear st and wall heat-transfer rates created in this flow. Finally, the ou from the hot impinging jets can be drawn into the engine a phenomenon known as hot gas ingestion, thus degrading performance and potentially risking engine failure.

Some of the problems just outlined are known to occur f subsonic Harrier family of aircraft. They are expected to b more acute for the future generation of the supersonic STO craft, where the environment is expected to be more severe b of the impingement of supersonic jets operating at higher te atures. Consequently, the study of supersonic impinging jet is of great interest from a practical perspective. Furthermo complex nature of the impinging jet flowfield, which often in multiple shock and shock/shear layer interactions, subson personic and separated flows, makes this flow interesting f fundamental fluid dynamics standpoint.

Impinging jet flows have been the focus of research fo three decades, where their fluid dynamic and acoustic pro have been carefully examined by a number of capable inv tors. Notable among the acoustic studies are those by Neuv Powell,[3] Tam and Ahuja,[4] Henderson and Powell,[5] and m cently Krothapalli et al.[1] One of the primary outcomes of aeroacoustic studies is that the highly unsteady, oscillatory of impinging jet, which is accompanied by discrete, high-amp acoustic tones, referred to as impingement tones, is cause feedback loop. The globally oscillatory behavior of the jet a resulting impingement tones have been explained well by a back mechanism derived from earlier work by Powell.[6] Re Krothapalli et al.[1] demonstrated that the feedback pheno might also be responsible for the lift loss, described earlier, th the generation of large-scale structures in the jet shear lay cause the focus of the present work is the mean behavior impinging jet, a more detailed discussion of the unsteady pro is outside the scope of this article. The interested reader is d to the references just cited. Suffice it to say that the fluid dy and acoustic properties of this flow appear to be intimately r

The structure and fluid dynamic properties of this flov also been investigated in a number of studies. In a classic Donaldson and Snedeker[7,8] examined the flowfield using sch

Presented as Paper 2000-2224 at Fluids 2000, Denver, CO, 19–22 June 2000; received 7 August 2000; revision received 24 July 2001; accepted for publication 20 September 2001.

*Associate Professor, Fluid Mechanics Research Laboratory, Department of Mechanical Engineering. Senior Member AIAA.
†Engineer/Scientist, Mailcode 1067126, P.O. Box 516. Member AIAA.
‡Boeing Technical Fellow, Mailcode 1067126, P.O. Box 516. Associate Fellow AIAA.

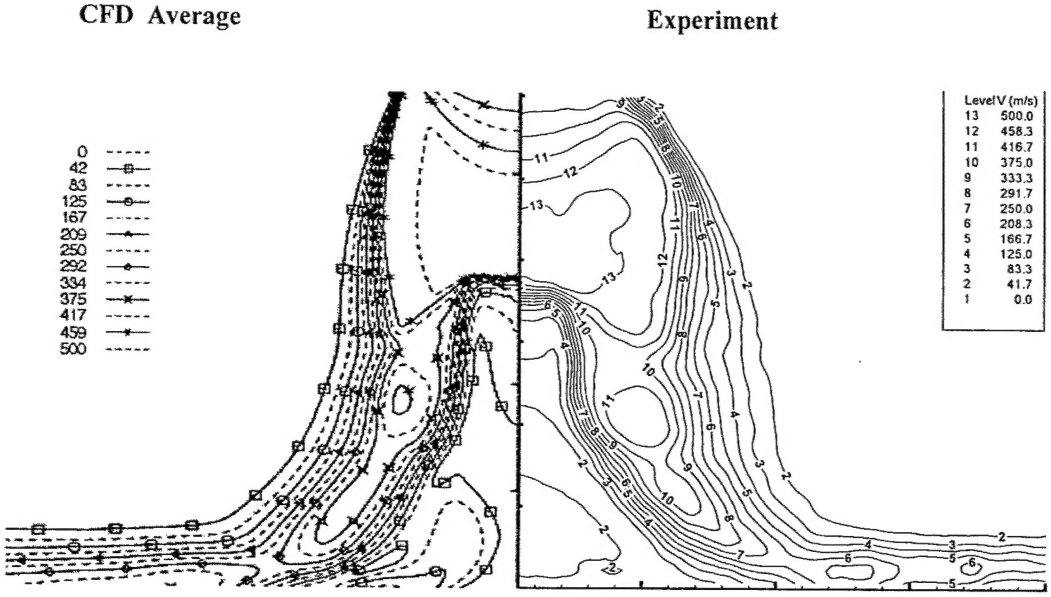

Fig. 8 Comparison of velocity contours from CFD and experimental PIV data: sonic nozzle, NPR = 5, $h/d = 3$.

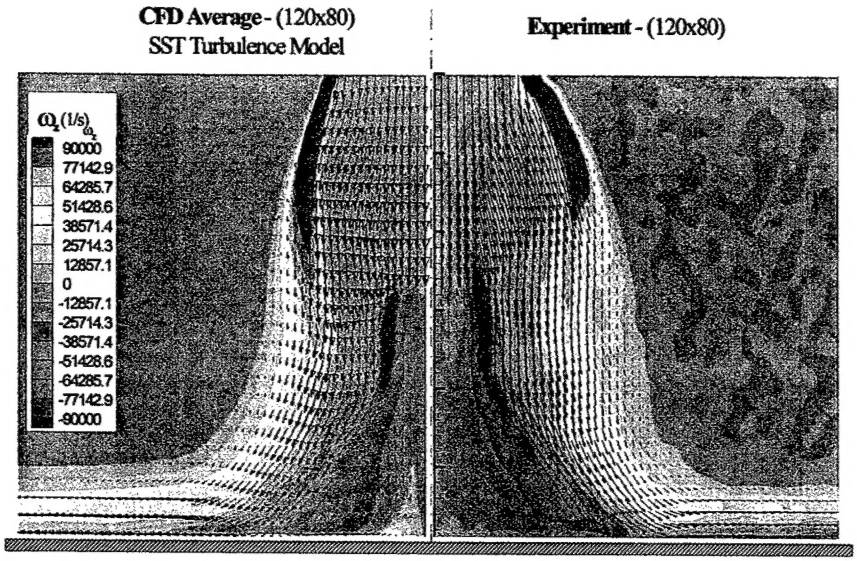

Fig. 9 Measured (PIV) and computed velocity vectors and vorticity contours: sonic nozzle, NPR = 5, $h/d = 3$.

comparison of the surface pressure distributions, presented earlier in Fig. 5. A comparison of the vorticity contours reveals the remarkable similarity in the shape and magnitude of the diffusing vorticity values between the computational and experimental results. It is clear that the vorticity field is well predicted by the computations indicating an accurate simulation of the strength and location of the primary jet shear layer, which is redirected into the wall-jet shear layer. As noted earlier, the inner shear layer that emanates from the triple point (Fig. 1b) is also extremely well predicted in terms of shape and vorticity levels.

A comparison of the predicted and measured ground plane surface-pressure distributions is shown in Fig. 5. Results from numerical solutions employing several turbulence models are included and compared to the experimental data. The dependent variable in this figure C_p represents the nondimensional surface-pressure coefficient, where $C_p = (P_s - P_\infty)/(P_0 - P_\infty)$ and P_s is the surface pressure. The x axis represents the radial location, nondimensionalized by the nozzle throat diameter, in this case same as the exit diameter d.

The overall pressure distribution with a low-pressure plateau and an annular peak is typical of an impingement flow with a recirculation bubble (Fig. 1) as discussed earlier. The pressure near the impingement point is well below the jet total pressure that is normally recovered for an ideally expanded nozzle without a separation bubble. The recirculating bubble divides the jet core and deflects it radially outward so that the peak pressure is lower than the stagnation pressure and occurs away from center of the interaction. In principle, the pressure peak should correspond to the location of the stagnation streamline in the inner shear layer, which divides the jet flow that is redirected into the wall jet from the fluid that is entrained into the recirculation bubble. This is the behavior observed in the present case where the pressure peak occurs roughly around $r/d = 1$, a location that corresponds to the impingement of the inner shear layer as seen in Fig. 9. The baseline Spalart model is seen to significantly overpredict the pressure throughout the impingement region, whereas the inclusion of the curvature formulation (SARC) produces a distribution in agreement with the SST model prediction and in much better agreement with the experimental results. A closer comparison of the SST or SARC results with the experimental data reveals that the greatest discrepancy between computational and the experimental data occurs in the central portion of the impingement zone. In this region (r/d roughly less than 0.4) both models overpredict the plateau pressure by as much as 30%. The overprediction of the pressure in this region is expected if one realizes that $r/d \leq 0.4$

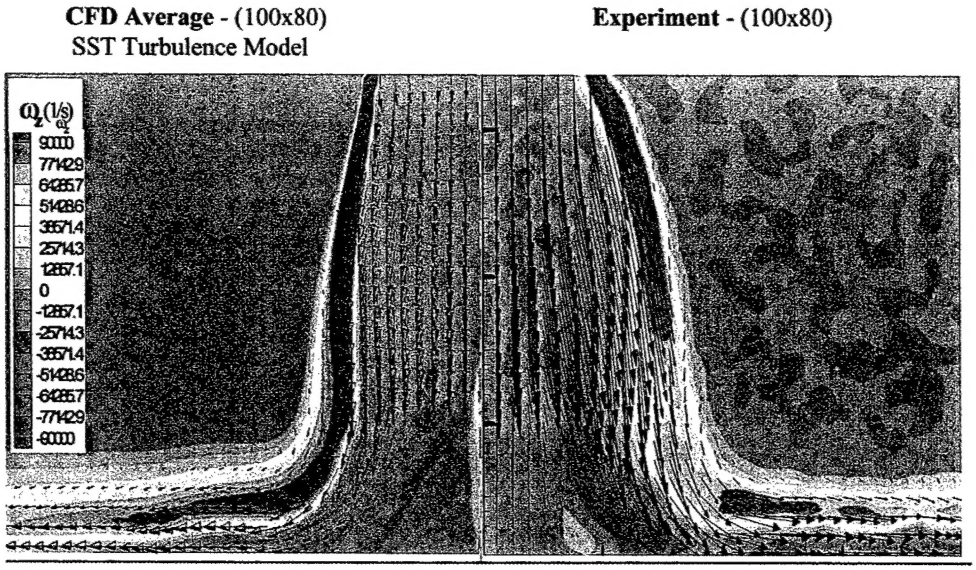

Fig. 12 Comparison of velocity vectors and vorticity contours from CFD and PIV: sonic nozzle, NPR = 5, $h/d = 1.6$.

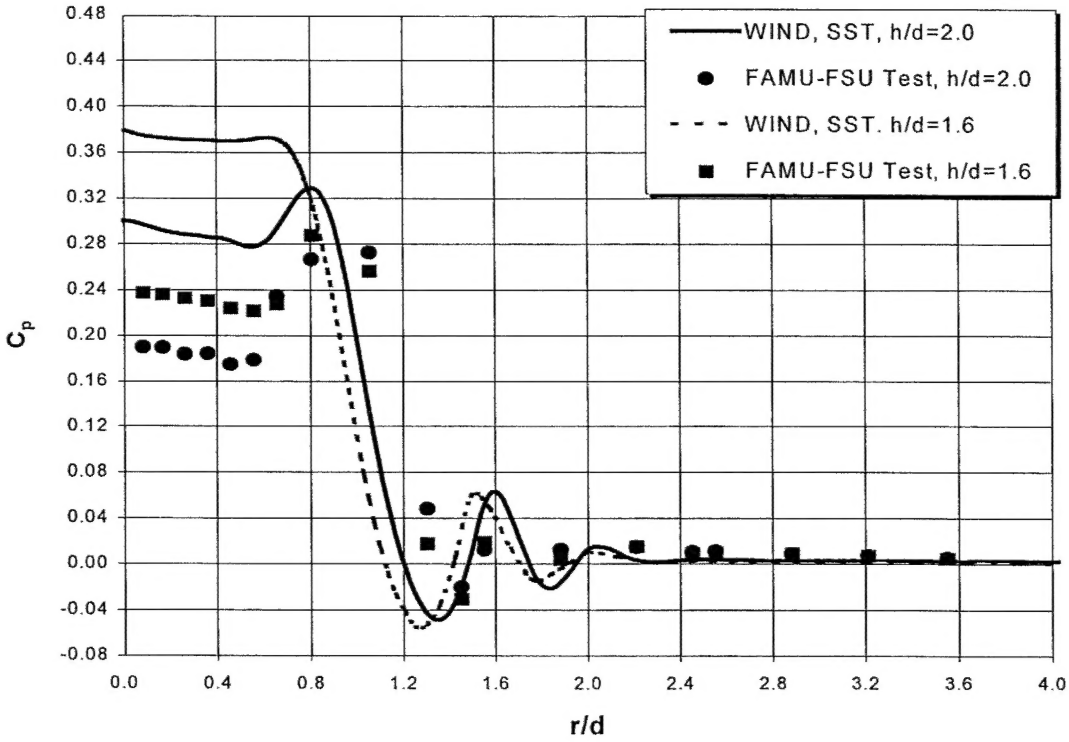

Fig. 13 Comparison of measured and computed surface-pressure distributions: sonic nozzle, NPR = 5, $h/d = 1.6$ and 2.

flow structure and the velocity field. As in the primary test case ($h/d = 3$), the Mach disk, triple point, and the inner shear layer are all captured by the computations. However, a closer look reveals that there is less diffusion of vorticity in the primary jet and wall-jet shear layer in the computed flow, where these shear layers appear more compact with higher vorticity values relative to the measured flowfield. Additionally, the triple point and the origin of the slip line (marked for clarity in Fig. 13) in the computed flowfield appears diffused, almost bifurcated, and the impingement location of the slip line is closer to the centerline than indicated by the PIV data.

As expected, these differences in the computed and measured velocity field translate into a discrepancy in the pressure distribution in Fig. 13. Although the computations reveal the presence of the stagnation bubble, indicated by the annular pressure peaks, the magnitude of the pressure in the impingement region downstream of the Mach disk is significantly overpredicted. This is presumably caused by an underprediction of the strength of the Mach disk for reasons similar to those outlined in our discussion of Figs. 5, 8, and 9 for the primary test case.

The comparison between CFD and PIV results for $h/d = 1.6$ shown in Fig. 12 follows the same trend as Fig. 11. Although overall there is good agreement between the computed and measured results, there are differences especially in the impingement region in the vicinity of the Mach disk. The triple point is much more diffused relative to the measured flow, even more so than that observed in Fig. 11. Similarly, there is a more significant difference between the experimental and computed pressure distributions (Fig. 13) in the impingement region. The computed flow for this case fails to capture the annular peak clearly present in the measured distribution.

In general, there is very good agreement between the computational results and the measured data, where the computations captured the essential features of the flow. However, it appears that, as the interaction strength increases, that is, as the nozzle to ground plane distance decreases, the differences between the two

[19]Ross, C., Lourenco, L., and Krothapalli, A., "PIV Measurements in a Shock-Containing Supersonic Flow," AIAA Paper 94-0047, Jan. 1994.

[20]Bush, R. H., "A Three Dimensional Zonal Navier Stokes Code for Subsonic Through Hypersonic Propulsion Flowfields," AIAA Paper 88-2830, July 1988.

[21]Cain, A. B., and Bush, R. H., "Numerical Wave Propagation Analysis for Stretched Grids," AIAA Paper 94-0172, Jan. 1994.

[22]Spalart, P. R., and Allmaras, S. R., "A One-Equation Turbulence Model for Aerodynamic Flows," AIAA Paper 92-0439, Jan. 1992.

[23]Menter, F. R., "Zonal Two Equation k–ω Turbulence Models for Aerodynamic Flows," AIAA Paper 93-2906, July 1993.

[24]Spalart, R. R., and Shur, M. L., "On the Sensitization of Turbulence Models to Rotation and Curvature," *Aerospace Science and Technology*, Vol. 1, No. 5, 1997, pp. 297–302.

[25]Launder, B. E., Priddin, C. H., and Sharma, B. I., "The Calculation of Turbulent Boundary Layers on Spinning and Curved Surfaces," *Journal of Fluids Engineering*, Vol. 99, No. 1, 1977, pp. 231–239.

[26]Park, S. V., and Chung, M. K., "Curvature-Dependent Two-Equation Model for Prediction of Turbulent Recirculating Flows," *AIAA Journal*, Vol. 27, No. 3, 1989, pp. 340–344.

[27]Mani, M., Ladd, J. A., and Bower, W. W., "An Assessment of Rotation and Curvature Correction to One- and Two-Equation Turbulence Models for Compressible Impinging Jet Flows," AIAA Paper 2000-2406, June 2000.

[28]Wilcox, D. C., "Reassessment of the Scale Determining Equation for Advanced Turbulence Models," *AIAA Journal*, Vol. 26, No. 11, 1988, pp. 1299–1310.

[29]Jones, W. P., and Launder, B. E., "The Calculation of Low-Reynolds-Number Phenomena with a Two-Equation Model of Turbulence," *International Journal of Heat and Mass Transfer*, Vol. 16, No. 6, 1973, pp. 1119–1130.

[30]Bradshaw, P., "Compressible Turbulent Shear Layers," *Annual Review of Fluid Mechanics*, Vol. 9, 1977, pp. 33–54.

[31]Kalghatgi, G. T., and Hunt, B. L., "The Occurrence of Stagnation Bubbles in Supersonic Jet Impingement Flows," *Aeronautical Quarterly*, Vol. 27, Aug. 1976, pp. 169–185.

[32]Alvi, F. S., Elavarasan, R., Shih, C., Garg, G., and Krothapalli, A., "Active Control of Supersonic Impinging Jets Using Microjets," AIAA Paper 2000-2236, June 2000.

[33]Kitamura, S., and Iwamoto, J., "Numerical Analysis of Supersonic Impinging Jet," *Transactions of the Japan Society for Aeronautical and Space Sciences*, Vol. 41, No. 132, 1998, pp. 57–64.

[34]"JSF Surface Erosion Materials Characterization Program Test Results," R.G.A. Angel, British Aerospace PLC, FAE-R-RES-4620, Issue 1, April 1999.

[35]Messersmith, N. L., and Murthy, S. N. B., "Thermal and Mechanical Loading on a Fire Protection Shield Due to a Combustor Burn-Through," *Propulsion and Energetics Panel (PEP) 88th Symposium*, CP-587, AGARD, 1996, pp. 22-1–22-13.

M. Sichel
Associate Editor